AD-A048 111 DAVID W TAYLOR NAVAL SHIP RESEARCH AND DEVELOPMENT CE--ETC F/G 20/4
STRUCTURAL DESIGN STUDY OF TAP-1 SUPERCAVITATING FOIL AND STRUT--ETC(U)
DEC 77 E D HOYT, J H MA, W H BUCKLEY

UNCLASSIFIED DTNSRDC-77-0094 NL

1 OF
AD
A048111

END
DATE FILMED
1 -78
DDC

DAVID W. TAYLOR NAVAL SHIP RESEARCH AND DEVELOPMENT CENTER

Bethesda, Md. 20084

STRUCTURAL DESIGN STUDY OF TAP-1 SUPERCAVITATING FOIL AND STRUT

by

Edgar D. Hoyt
James H. Ma
William H. Buckley
Garnett Ryland II

ADVANCED SHIP DIVISION
STRUCTURES DEPARTMENT

December 1977

Report 77-0084

STRUCTURAL DESIGN STUDY OF TAP-1 SUPERCAVITATING FOIL AND STRUT

Report 77-0084

MAJOR DTNSRDC ORGANIZATIONAL COMPONENTS

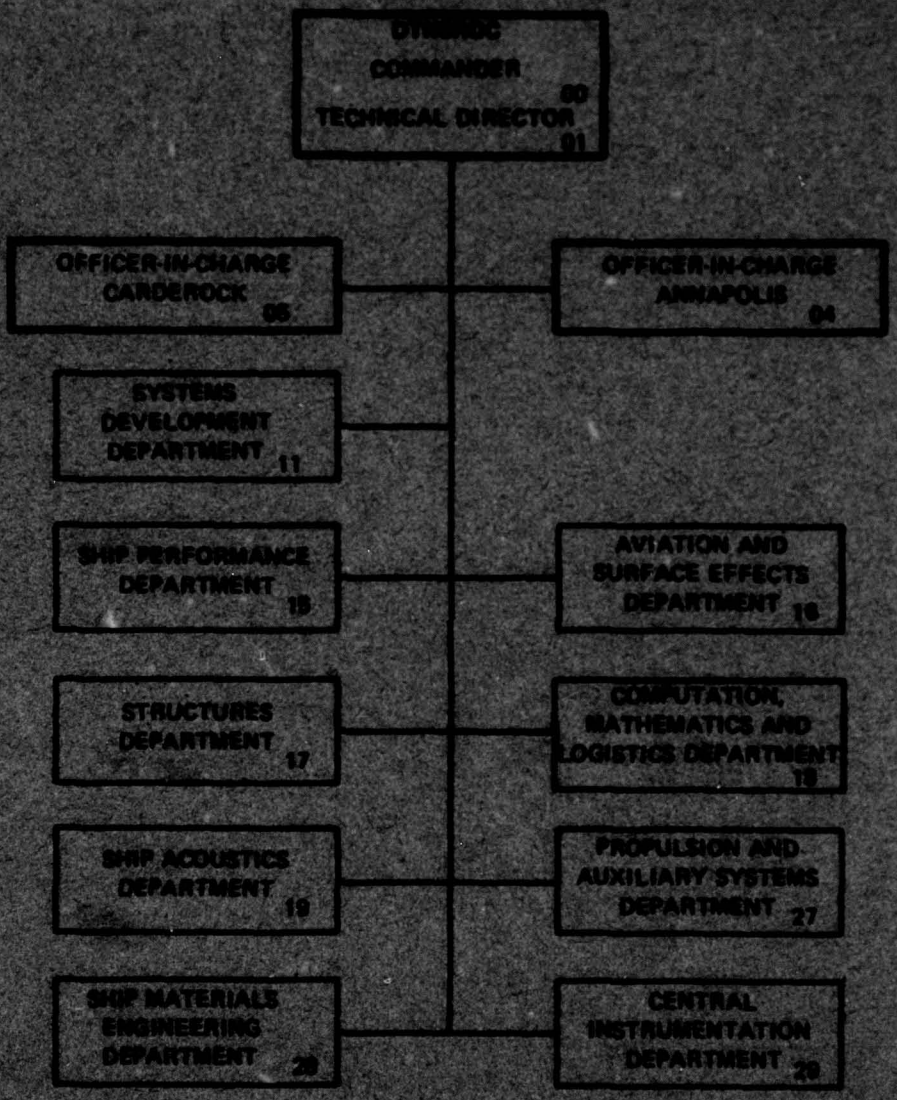

UNCLASSIFIED

SECURITY CLASSIFICATION OF THIS PAGE (When Data Entered)

REPORT DOCUMENTATION PAGE

READ INSTRUCTIONS BEFORE COMPLETING FORM

(14) DTNSRDC-77-0094

1. REPORT NUMBER

2. GOVT ACCESSION NO.

3. RECIPIENT'S CATALOG NUMBER

4. TITLE (and Subtitle)

(6) STRUCTURAL DESIGN STUDY OF TAP-1 SUPERCAVITATING FOIL AND STRUT

(9) Formal rept.

5. TYPE OF REPORT & PERIOD COVERED

6. PERFORMING ORG. REPORT NUMBER

7. AUTHOR(s)

(10) Edgar D. Hoyt, James H. Ma
William H. Buckley, Garnett Ryland II

8. CONTRACT OR GRANT NUMBER(s)

9. PERFORMING ORGANIZATION NAME AND ADDRESS

David W. Taylor Naval Ship Research and Development Center
Bethesda, Maryland 20084

10. PROGRAM ELEMENT, PROJECT, TASK AREA & WORK UNIT NUMBERS

Task Area ZF 43 421 001
Design Element 62754 N
Work Unit 1-1520-001

11. CONTROLLING OFFICE NAME AND ADDRESS

(16) F43421

12. REPORT DATE

(11) December 1977

13. NUMBER OF PAGES

88

14. MONITORING AGENCY NAME & ADDRESS (if different from Controlling Office)

(17) ZF43421001

15. SECURITY CLASS. (of this report)

UNCLASSIFIED

15a. DECLASSIFICATION/DOWNGRADING SCHEDULE

16. DISTRIBUTION STATEMENT (of this Report)

(12) 84p.

APPROVED FOR PUBLIC RELEASE: DISTRIBUTION UNLIMITED

17. DISTRIBUTION STATEMENT (of the abstract entered in Block 20, if different from Report)

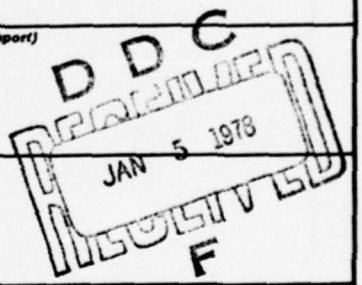

18. SUPPLEMENTARY NOTES

19. KEY WORDS (Continue on reverse side if necessary and identify by block number)

High Speed Strut/Foil System
Supercavitating Foil
Mixed Foil Parabolic Strut
Representative Hydrodynamic Loads
Structural Feasibility
Foil Principal Stresses
(Critical Loading Conditions)

20. ABSTRACT (Continue on reverse side if necessary and identify by block number)

A conceptual design study of a flapped, supercavitating foil has been performed in order to assess the structural feasibility of a configuration otherwise acceptable from a hydrodynamic point of view. Consideration has also been given to the design of a single, steerable strut as a supporting member for the foil. The study includes the establishment of a limit load criteria for structural design, a survey of hydrodynamic loading data for supercavitating struts and foils, calculation of design loads based upon these data for the critical loading conditions, the conceptual design of a flapped foil having a steady 1g loading of 60 tons, and a finite element stress analysis of a solid version of the foil for a more precise evaluation of leading edge and foil root bending stress than was available from simple beam calculations. A brief parametric analysis of foil bending stress trends with increased foil aspect ratio is also presented.

DD FORM 1 JAN 73 1473 EDITION OF 1 NOV 65 IS OBSOLETE
S/N 0102-LF-014-6601

UNCLASSIFIED

SECURITY CLASSIFICATION OF THIS PAGE (When Data Entered)

387682

4/B

TABLE OF CONTENTS

LIST OF FIGURES

LIST OF TABLES

NOMENCLATURE

A	Area of foil planform
AR	Aspect ratio
ΔA	Elemental area on bending section
b	Foil span
$\overline{BM}_\xi$	Bending moment, per unit width of strip, about lines of constant percent of chord
c	Chord length
C_D	Drag coefficient
$C_L = \frac{L}{1/2\,\rho\,V^2 A}$	Lift coefficient
$C_{L_\alpha} = \frac{\delta C_L}{\delta \alpha}$	Slope of the curve of lift vs angle of attack
C_m	Pitching moment coefficient
$C_{M_F} = \frac{M_F}{qAc}$	Flap hinge moment coefficient
$C_p = \frac{p}{q}$	Pressure coefficient
d	Submergence of foil below the surface
e	Base of Naperian logarithms
f	Flap chord length
F_Z, F'_Z	Axial force in strut – see Figure 15
g	Acceleration of gravity
H_W	Height of wave
I	Moment of inertia about neutral axis in bending
k_1	Non-dimensional spanwise center of lift
k_2	Non-dimensional chordwise center of lift
L	Lift
L_W	Length of wave
M	Bending moment acting on section
M_F	Flap hinge moment
M_X, M_Y	Bending moment, about an axis parallel to the X or Y axis respectively, on a cross section of the strut – see Figure 15

M'_X, M'_Y, M'_Z	Bending moment, about an axis parallel to the X', Y' or Z' axis respectively, on a cross section of the foil or strut – see Figures 14 and 15
M'_{Y1}	Spanwise distribution of the pitching moment, about Y' axis, due to normal loading on foil – see Figures 14 and 31
M'_{Y2}	Spanwise distribution of the pitching moment, about Y' axis, due to normal loading on flap
M_Z	Spanwise distribution of the yawing moment, about the Z axis, due to normal loading on the strut
o	Subscript designating initial value of quantity
p	Hydrodynamic pressure
p_a	Air pressure at the water surface
p_{amb}	Ambient or free-stream pressure at the depth of the foil
p_v	Vapor pressure of the water
$q = 1/2\,\rho\,V^2$	Stagnation pressure of the flow
s	Distance aft of leading edge
T_W	Wave period
T'_Y	Torsional moment about the Y' axis
T'_{Y1}	Torsional moment, about Y' axis, on a cross section of the foil due to loading on foil (excluding flap)
T'_{Y2}	Torsional moment, about Y' axis, on a cross section of the flap due to loading on flap only
V	Speed
T_Z	Torsional moment about the Z axis
Δv	Vertical falling velocity of foil
v_o	Wave orbital velocity (speed) at the water surface
v'_o	Wave orbital velocity at foil depth
V_W	Speed of wave
V_X, V_Y	Shear force, parallel to X or Y axis respectively, on a cross section of the strut – see Figure 15
V'_X, V'_Y, V'_Z	Shear force, parallel to X, Y, or Z axis respectively, on a cross section of the foil or strut – see Figure 14 and 15
W	Normal deflection of foil
w_f	Spanwise distribution of flap normal loading
w'_X	Spanwise distribution of the foil chordwise (tangential) loading
w_Y	Spanwise distribution of strut normal loading
w'_Z	Spanwise distribution of the foil normal loading

X, Y, Z	Orthogonal axes with origin on steering axis at top of strut – see Figures 2 and 15
X', Y', Z'	Orthogonal axes with origin in lower surface of foil – see Figures 2 and 15
y, z	Coordinate parallel to respective axis
α	Angle of attack
$\alpha_{\eta t}$	Angle of attack measured with respect to the line connecting the leading and trailing edges of the lower or pressure face of the foil
δ_f	Flap deflection angle
ζ	Distance from neutral axis to elemental area, or extreme fiber
λ	A scale ratio or factor
ρ	Mass density of water
σ	Maximum bending stress on cross section
σ_r	Radial stress, normal to lines of constant s/c
σ_{tu}	Ultimate stress in tension
σ_{ty}	Yield stress in tension
σ_v	Cavitation number based on vapor pressure of water
σ_{xt}	Chordwise normal stress, top* fiber (foil without annex)
σ^a_{xt}	Chordwise normal stress, top* fiber (foil with annex)
σ_y	Spanwise bending stress
σ_{yt}	Spanwise normal stress, top* fiber (foil without annex)
σ^a_{yt}	Spanwise normal stress, top* fiber (foil with annex)
$\tau_{xy,t}$	Shear stress, at foil top* surface
*	Subscript b, in place of t, indicates stress of bottom surface

ABSTRACT

A conceptual design study of a flapped, supercavitating foil has been performed in order to assess the structural feasibility of a configuration otherwise acceptable from a hydrodynamic point of view. Consideration has also been given to the design of a single, steerable strut as a supporting member for the foil. The study includes the establishment of a limit load criteria for structural design, a survey of hydrodynamic loading data for supercavitating struts and foils, calculation of design loads based upon these data for the critical loading conditions, the conceptual design of a flapped foil having a steady 1g loading of 60 tons, and a finite element stress analysis of a solid version of the foil for a more precise evaluation of leading edge and foil root bending stress than was available from simple beam calculations. A brief parametric analysis of foil bending stress trends with increased foil aspect ratio is also presented.

ADMINISTRATIVE INFORMATION

This project was authorized by the Naval Material Command (NAVMAT) and funded by High Speed Hydrofoil Struts and Foils Direct Laboratory Funding Project ZF 43 421 001, Program Element 62754N. Work was performed in the Ship Performance Department of the David W. Taylor Naval Ship Research and Development Center (DTNSRDC).

INTRODUCTION

A structural design study of the TAP-1 supercavitating foil and strut[22*] has been conducted in order to determine if structural difficulties were likely to exist in a design which was otherwise acceptable from a hydrodynamic point of view. Since emphasis was placed on feasibility as opposed to optimization, the structural evaluation did not include iterative design to minimize structural weight. Instead, if applied stresses were found to be less than the associated allowable stresses, the design was considered satisfactory from a feasibility point of view without further changes to reduce weight.

The immediate purpose of the feasibility study was to establish, for a representative strut/foil design employing the TAP-1 model configuration of Figure 1: a) its acceptability with respect to spanwise and chordwise bending stresses, particularly in the area of the leading edge,

*List of references page 72.

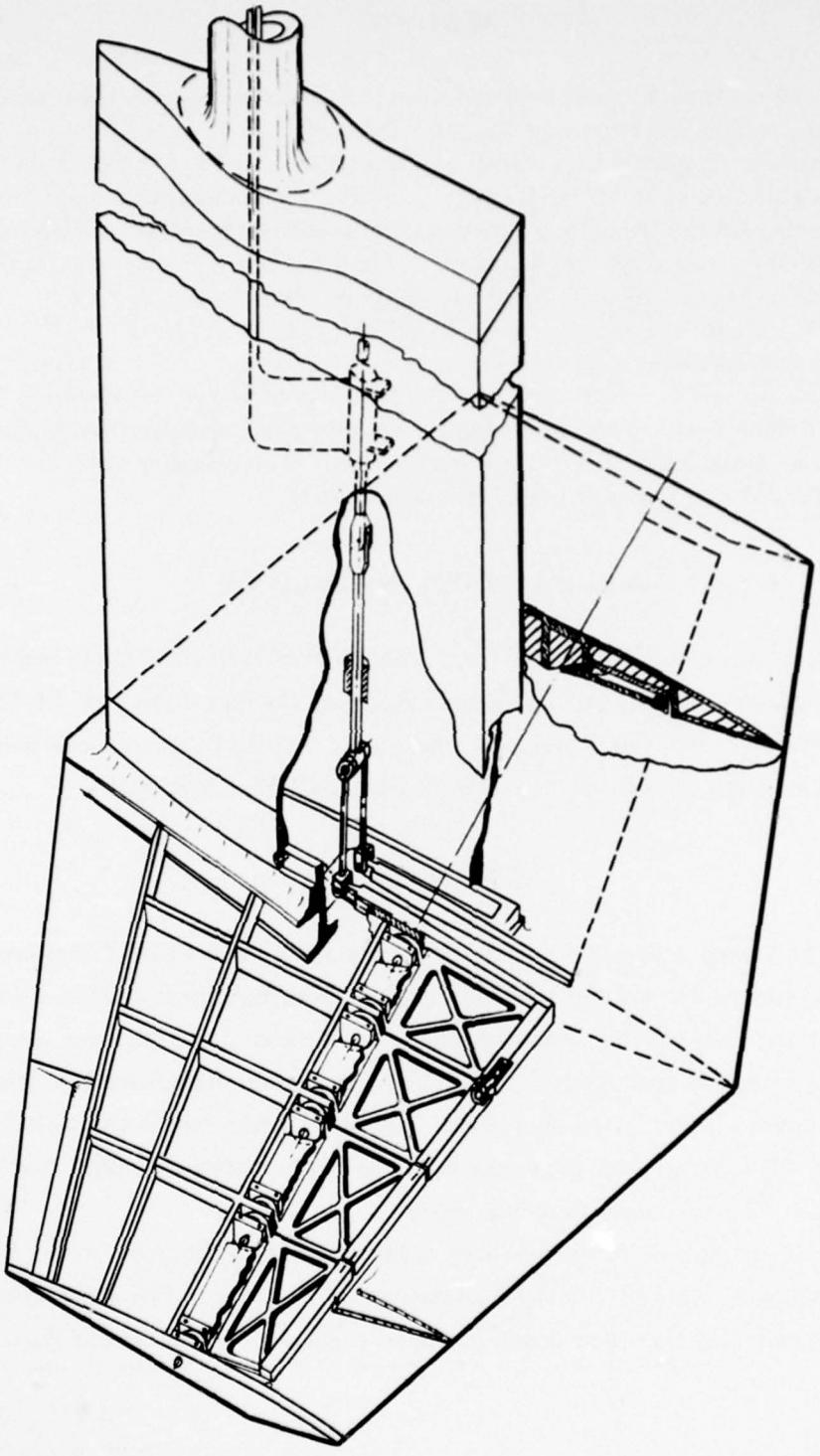

Figure 1 – Structural Design Concept, TAP-1 Hydrofoil

b) a representative flap design including an actuation linkage which would be contained entirely within the hydrodynamic contour, and c) structural proportions at the strut-to-foil attachment and at the upper end of the strut assuming that a steerable strut featuring a king post would be employed.

These particular areas of investigation were selected based upon the presumption that, if feasibility could be demonstrated for them, the entire design would be feasible.

APPROACH

The approach employed in this investigation consisted of four major steps: first the establishment of a basis for structural design, and within that context, the adoption of specific loading conditions which were believed critical for the particular strut and foil configuration under study; second the calculation of component design loads for the designated loading conditions; third the development of a structural configuration which would sustain the design loads when constructed of a material considered representative of current hydrofoil construction; and finally, in the case of the foil, having established a structural configuration based upon simplified stress calculations, a more exact analysis was performed utilizing finite element analysis techniques to verify the design in the leading edge and foil root areas.

The sizing of the foil was based upon an assumed steady lift loading of 60 long tons (out of a total ship weight of 200 tons) and a design lift coefficient of 0.136 at 80 knots. The reference lift area was thus

$$A = \frac{60 \times 2240}{0.136 \times 18,133} = 54.5 \text{ ft}^2$$

Principal strut and foil dimensions are shown in Figure 2.

With regard to the basis of strength design, the limit load approach presently employed in Navy hydrofoil ship design was utilized. In this procedure the critical loading conditions anticipated in service are specified following which detail loads are calculated corresponding to each of the loading conditions. The loads so determined are designated Limit Loads. These in turn are multiplied by specified factors of safety to obtain Yield Loads and Ultimate Loads which are then employed in establishing member sizes. In this investigation, Yield Loads correspond to Limit Loads multiplied by a Yield Factor of Safety of 1.20, while Ultimate Loads correspond to Limit Loads multiplied by an Ultimate Factor of Safety of 1.50. Under Yield Loads, the foil system must not deform elastically or permanently so as to interfere with the intended function of the foil system, while under Ultimate Loads the foil system must not collapse. In those cases in which buckling, crippling or other sources of

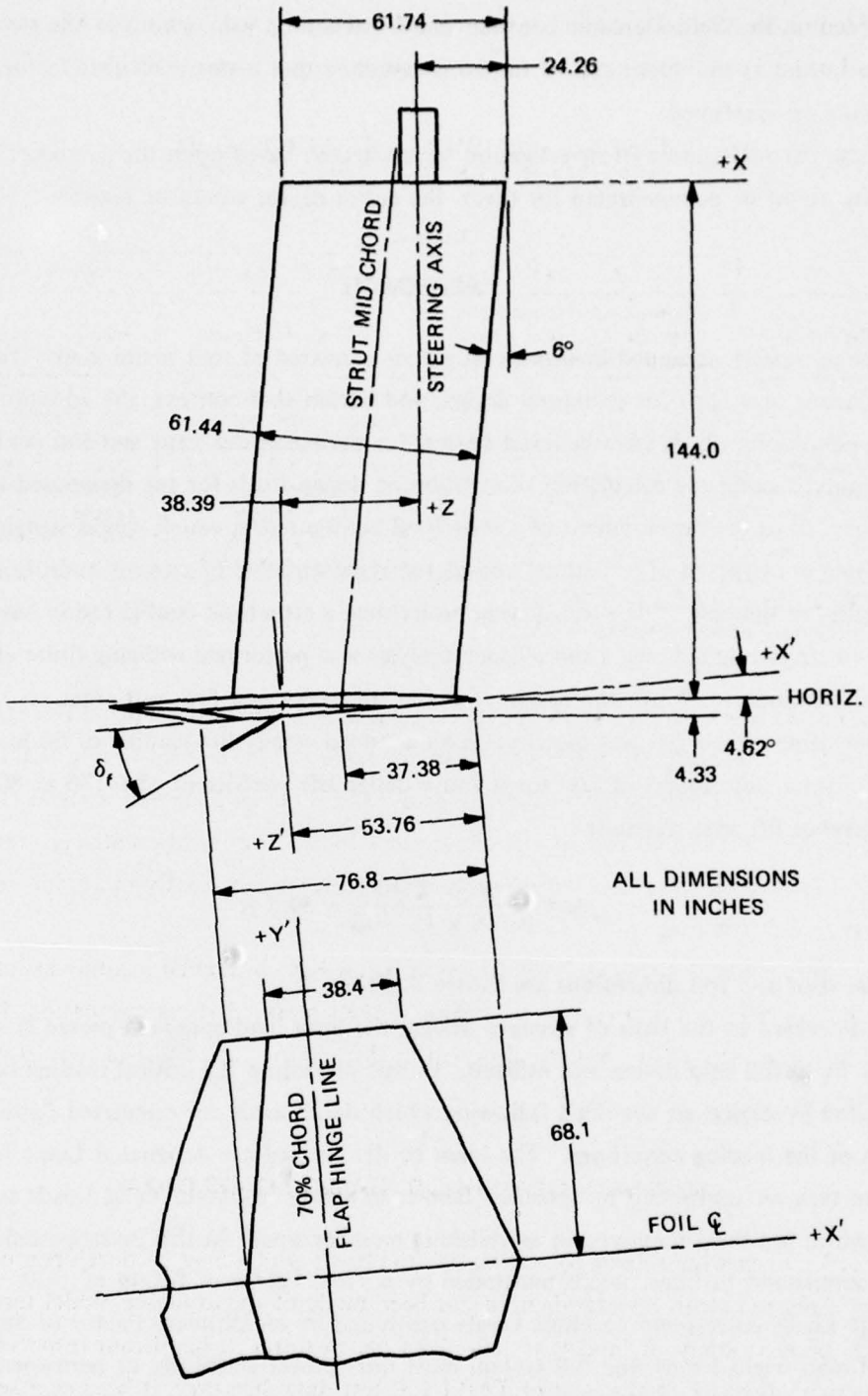

Figure 2 – Structural Geometry, TAP-1 Hydrofoil

elastic instability do not govern, it is usually required only that the material yield stress not be exceeded under Yield Loads and that material ultimate tensile stress not be exceeded under Ultimate Load. These basic strength requirements are summarized in Table 1.

TABLE 1 – ELEMENTS OF LIMIT LOAD APPROACH TO STRUCTURAL DESIGN

	Quantity		
	Limit Load	Yield Load	Ultimate Load
Definition	Maximum load anticipated in service for one or more structural components	1.20* x Limit Load	1.50* x Limit Load
Strength Requirement	(None)	Under Yield Loads the structure must not experience elastic or permanent deformation deleterious to its intended function. Material yield stress must not be exceeded	The structure must not collapse under ultimate loads. Material ultimate tensile stress must not be exceeded

*Yield Factor of Safety = 1.20
**Ultimate Factor of Safety = 1.50

The conceptual design of the strut/foil configuration, which is reported in detail in Reference 1, is essentially the result of proportioning member sizes by simple beam theory using the Yield and Ultimate Loads derived below and material allowable stresses (F_{ty} = 130,000 psi, F_{tu} = 145,000 psi) corresponding to HY-130 steel or alternatively precipitation hardened 17-4 PH stainless steel. Both of these materials are currently in service in subcavitating foil systems.

The finite element stress analysis discussed below has considered a solid version of the foil (in the interests of economy) to determine if the simplified stress calculations have in fact resulted in a satisfactory structural design in the leading edge and foil root attachment areas which are locally solid.

SUMMARY OF HYDRODYNAMIC LOADS DATA

In order to provide a basis for estimating the loads which may be developed on super-cavitating foils and struts an examination has been made of the available model test data. There has been a variety of models tested, all of which differ in significant respects from the TAP-1 design. Because of the lack of TAP-1 foil test data, however, it became essential that a review be made of available hydrodynamic test data which might be used to estimate structural design loads.

The most extensively tested foil, and one of the few tested on a blunt based strut, is the BUSHIPS (supercavitating) Parent Foil. These tests have provided the principal basis for estimating the hydrodynamic loading characteristics of the TAP-1 foil.

The BUSHIPS Parent Foil was designed for use in comparative tests at different test facilities. It has a rectangular plan form with an aspect ratio of 3. The section has a little more camber than the TAP-1 foil and a thickness-to-chord ratio of 0.1308 compared with 0.0868 for the TAP-1 foil at the trailing edge of the lower face. The Parent Foil was mounted on a single blunt based, parabolic strut with a chord equal to the foil chord and a thickness-to-chord ratio of 0.15.

The Parent Foil has been the subject of extensive testing at:

DTNSRDC - Carderock, Carriage 5

DTNSRDC - Langley, Tank No. 1 and the High-Speed Hydrodynamics Facility, (HSHF)

Hydronautics, Inc. - Variable Pressure Channel

General Dynamics/Convair - Model Basin

Lockheed - Underwater Missile Facility (LUMF), Variable Pressure

Grumman - Whirling Tank

These facilities encompass a wide variety of capabilities and procedures, which are summarized in Table 2, taken from Reference 2. In addition to tests of the basic foil at all of these facilities, tests were made at Hydronautics and at Convair with flaps of a different configuration.

TABLE 2 – FACILITIES AND CONDITIONS FOR PARENT HYDROFOIL PROGRAMS

	FACILITY							
	LUMF	Hydronautics		Grumman	Convair	Langley	DTMB	Langley
Data Reference	2	11	12	13	5	3	3	4
Type of Facility	Controlled Pressure Towing Tank	Controlled Pressure Water Channel		Whirling Tank	Towing Tank	Towing Tank #1	Towing Tank	High Speed Facility
Water Temperature - deg F	50 to 55	80 to 100	65 to 100	–	56	–*	–	76 to 84
Velocities Tested - fps	15 to 41	24 to 39	39 to 42	68 to 135	50 to 80	35 to 100	35 to 100	67 to 127
Model Chord - inch	5	5	2.5	1.66	3	5	5	5
Reynolds Number x 10^{-6}	0.5 to 1.2	1.1 to 2.0	0.9 to 1.1	0.7 to 1.5	0.9 to 1.4	–	–	
Froude Number	4 to 11	6 to 11	15 to 16		18 to 28	10 to 27	10 to 27	19 to 36
Angle of-Attack - deg (relative to reference line)	2 to 14.5	0 to 10	0 to 10	-1 to 9	11.7 to 15.5	2.3 to 12.3	10.3	-1.0 to 10
Submergence Ratio	0.5 to 1.5	0.5 to 1.0	0.5 to 1.0	0.75 to 1.25	0.33 to 1.0	0.5 to 2.0	0.5 to 1.0	0.5 to 1.5
Ambient Pressure - atm	1 to 0.05	1 to 0.1	1 to 0.1	1	1	1	1	1
Vapor Cavitation Number	9.6 to 0.06	2.3 to 0.07	1.4 to 0.08	0.05 to 0.08	0.9 to 0.3	2 to 0.25	2 to 0.25	0.46 to 0.13

*Dilute Salt Water

FOIL LIFT

The lift developed by a supercavitating hydrofoil, when expressed in terms of the lift coefficient, is markedly effected by the location and extent of the cavity formed. The extent to which atmospheric air is able to penetrate the cavity also has an important influence. These flow characteristics are determined by the angle of attack*, the speed and the ambient pressure at the depth of the foil. The depth of submergence, usually expressed as a multiple of the foil chord, is also an important parameter. The speed and pressure are customarily combined to give the vapor cavitation number, defined as

$$\sigma_v = \frac{p_{amb} - p_v}{q}$$

where $p_{amb} = p_a + \rho gh$

p_a is the air pressure at the surface

p_v is the vapor pressure of the water

ρgh is the increase of pressure due to submergence

$q = 1/2\,\rho V^2$ is the stagnation pressure of the flow

V is the speed

In dealing with cavity flows about submerged bodies it has long been considered that the vapor cavitation number was an adequate scaling parameter for establishing valid model test conditions. Accordingly it has been customary to conduct model tests either at full scale speeds (with a slight adjustment to account for the differences in submergence) or to reduce the air pressure above the water - in a variable pressure channel or tank - and to operate at the speed required to provide the desired cavitation number. There is now substantial evidence that, to achieve similarity of flow over supercavitating foils mounted on blunt based, surface piercing struts which cause ventilation of the foil cavity, the surface air pressure should be reduced in the model test to maintain the full scale ratio of atmospheric pressure to free stream pressure at the foil depth. To accomplish this, while maintaining constant vapor cavitation number, requires equality of the Froude number in model and full scale. This can only be achieved in a variable pressure facility such as the LUMF or the Hydronautics channel. A further difficulty, in tests of the Parent Foil, is that the size of the full scale foil was not established. A complete model test program would have to include tests over a range of Froude number for each value of the cavitation number.

*The angle of attack, $\alpha_{\eta t}$, is measured with respect to the line connecting the nose and tail edges of the lower or pressure face of the foil.

It is not certain that variations of viscous and surface tension effects, which would require equality of Reynolds number and Weber number, can be neglected in model tests involving ventilated cavity flows. The ratio of air density to water density may also be important as well as the concentration of dissolved air in the water.

Tests of the Parent Foil in the several facilities reveal noticeable differences in the character of the flow and in the lift developed when tested at the same vapor cavitation number. As a result, the performance to be expected in full scale is uncertain especially in certain speed ranges.

Because they encompass the largest range of angle of attack and of speed, the results of DTNSRDC tests will be presented first. Comparisons will then be given with some of the other test results.

The lift developed by the basic Parent Foil with no flap, as determined by tests at DTNSRDC-Langley, Tank 1, is presented in Reference 3 in the form of plots of the lift coefficient as a function of the vapor cavitation number for constant angle of attack. Separate plots are shown for each angle of attack from 4.67 degrees to 14.67 degrees, in one degree increments, of which seven are shown as examples in Figure 3. All are for a depth-to-chord ratio of 1.0.

These data have been transformed to plots of lift coefficient versus speed, for a full scale depth of 5 feet which is one chord length for the TAP-1 prototype, as shown in Figure 4. This transformation was accomplished by means of the cross plot in Figure 5. In addition to the curves for constant vapor cavitation numbers of 0, 0.15, 0.2, 0.4, 0.6 and 0.8, this figure includes auxiliary curves whose significance will be pointed out later.

Curves are shown in Figure 4 for constant angles of attack of 9, 12 and 15 degrees. Contours have also been drawn for constant values of loading, L/A, in pounds per square foot. Certain limit curves are also shown which will be described below.

At angles of attack of about 5½ degrees or less both the top and bottom surfaces of the foil are wetted at all speeds. (Some cavitation was observed on the lower surface near the leading edge for angles of attack less than 4 degrees in tests at Hydronautics, which has the only facility permitting continuous observation of the lower surface). For any speed above about 20 knots a cavity exists in the wake of the foil, which is termed a base cavity. A cavity also occurs behind the blunt base of the strut so that the foil base cavity is ventilated with atmospheric air. This flow regime is referred to here as *base vented* when the vented base cavity exists behind the foil in the absence of foil surface cavitation.

Figure 3 – BUSHIPS Parent Foil: Variation of Lift Coefficient with Cavitation Number

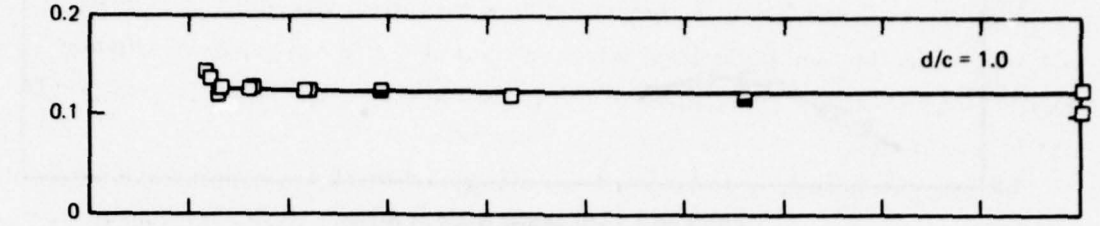

Figure 3a – 4.67 Degree Angle of Attack

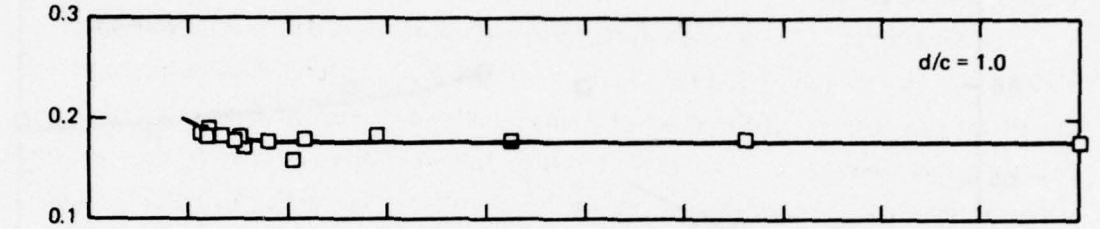

Figure 3b – 5.67 Degree Angle of Attack

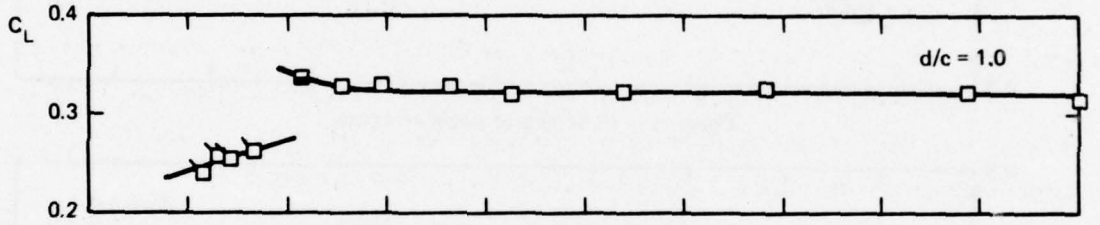

Figure 3c – 8.67 Degree Angle of Attack

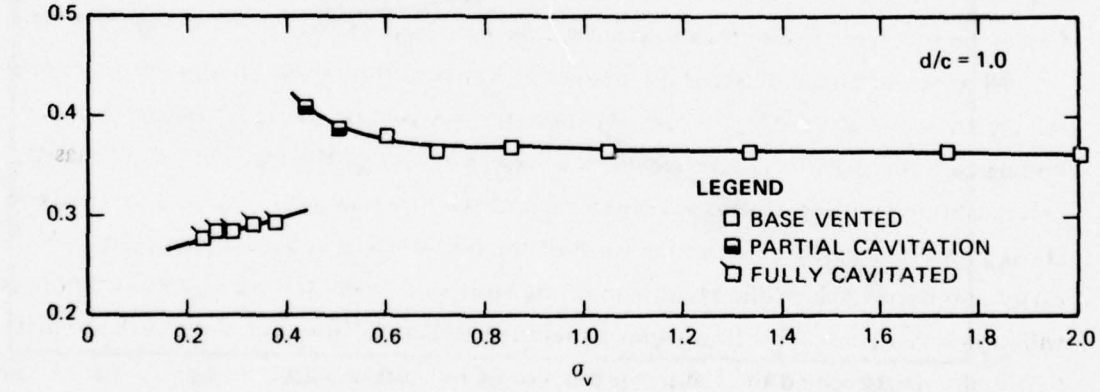

Figure 3d – 9.67 Degree Angle of Attack

Figure 3 – Continued

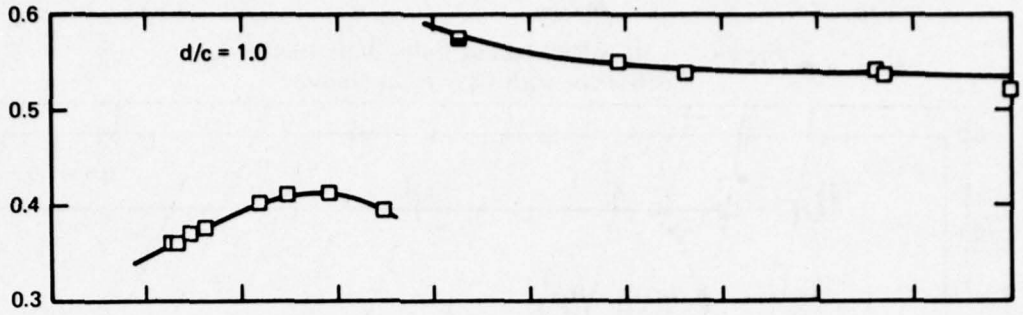

Figure 3e – 12.67 Degree Angle of Attack

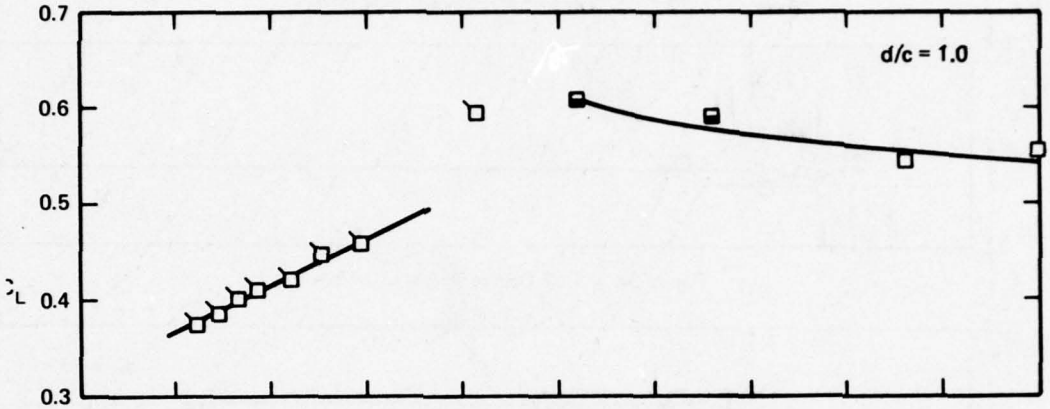

Figure 3f – 13.67 Degree Angle of Attack

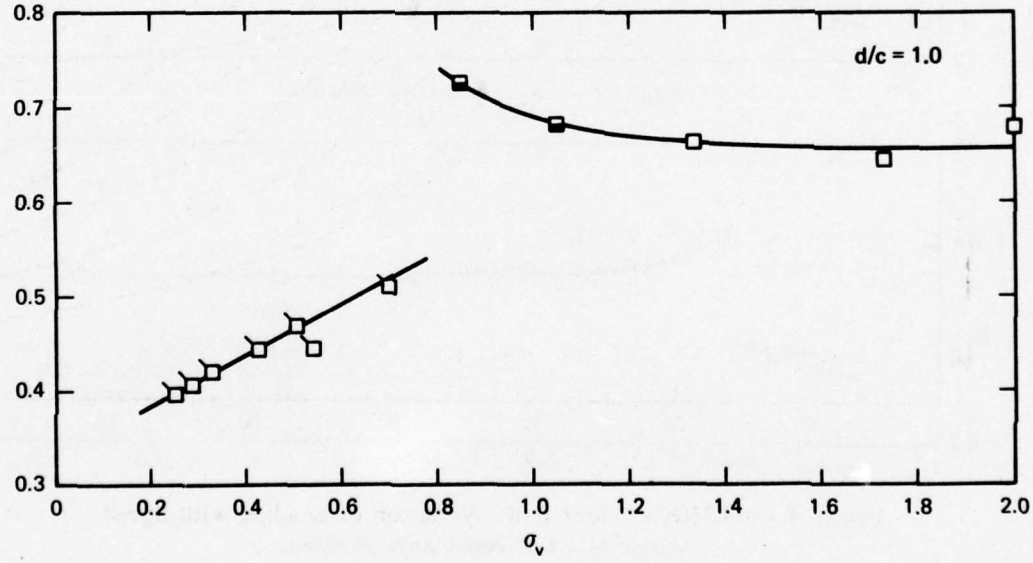

Figure 3g – 14.67 Degree Angle of Attack

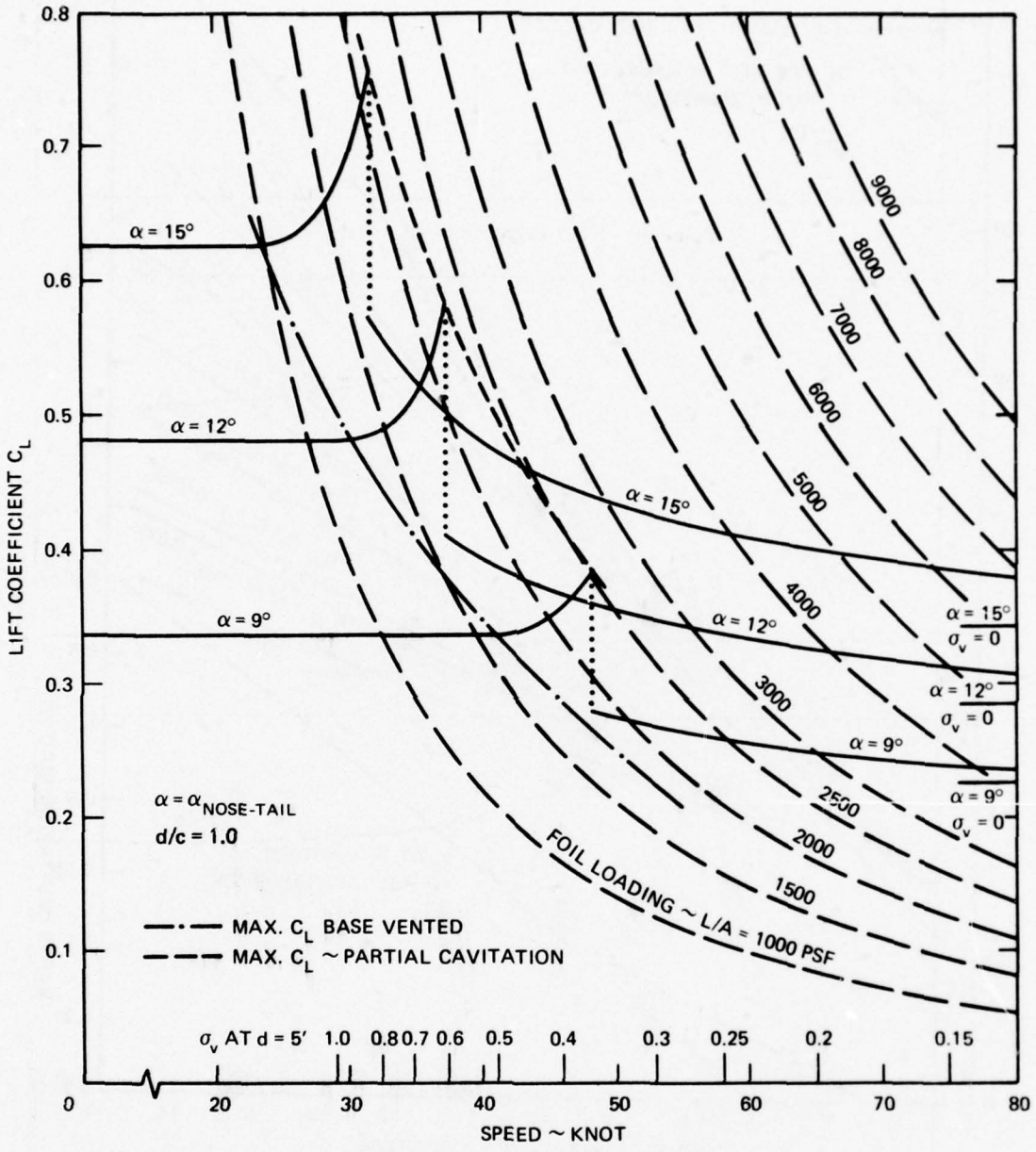

Figure 4 – BUSHIPS Parent Foil: Variation of Loading with Speed

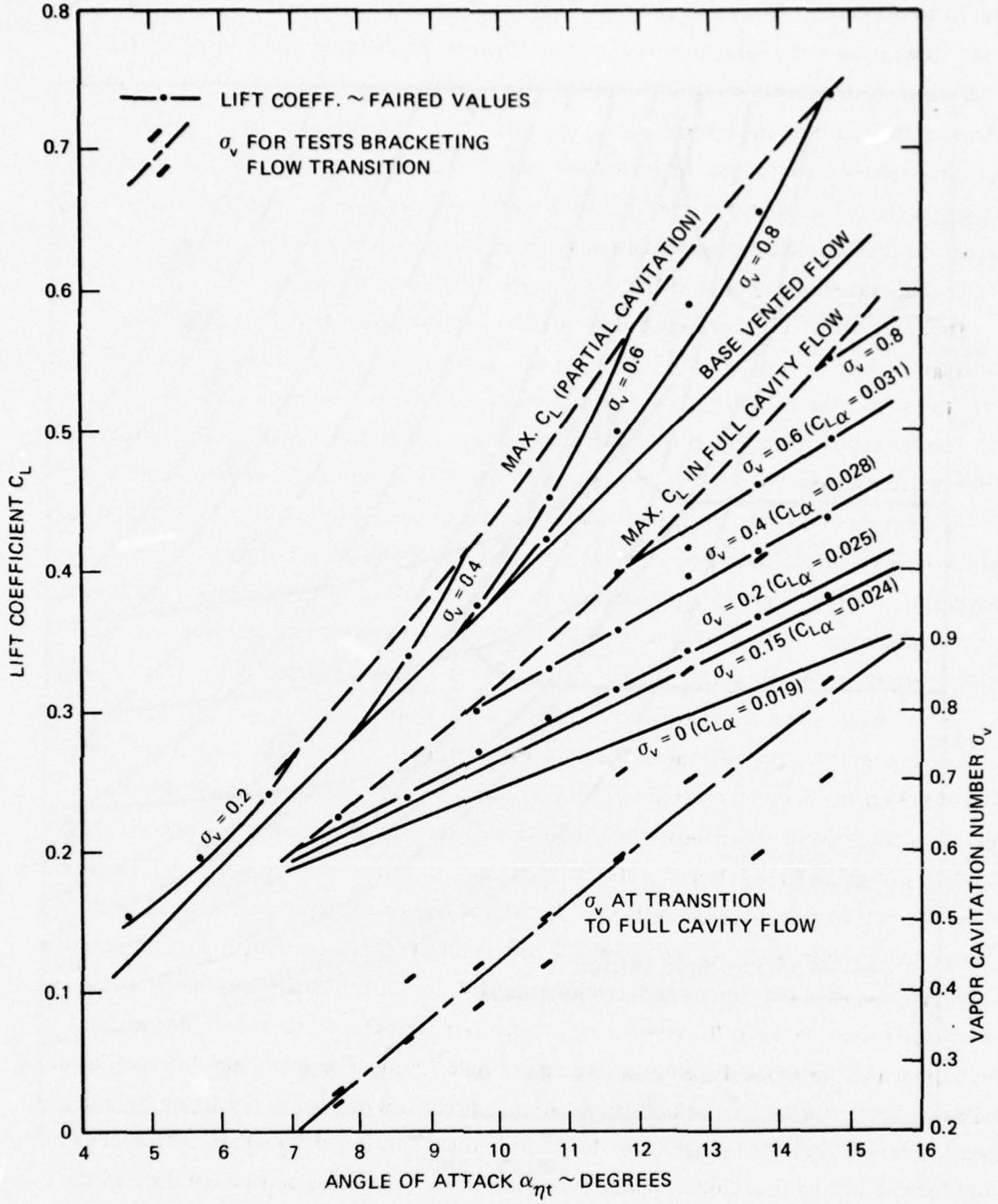

Figure 5 – BUSHIPS Parent Foil: Variation of Lift Coefficient with Angle of Attack

Base vented flow can occur at angles of attack up to 10 or 12 degrees at speeds less than 20 to 30 knots. The limiting value of lift coefficient as a function of speed, with base vented flow, is shown by the dot-dash curve in Figure 4 for a depth-to-chord ratio of 1.0.

With increasing angle of attack or speed, vapor filled cavities are formed on the upper surface of the foil near the leading edge. Tip vortex cavitation also occurs in many cases. This flow regime is termed *partial cavitation* when the leading edge cavity is not connected to the base cavity. It is characterized by unsteadiness of cavity size and of lift and drag forces. The lift coefficient increases with increasing speed, for a given angle of attack, as is indicated by the solid curves of Figure 4 in the speed range from 23 to 48 knots.

The increases of lift coefficient with increasing speed under partial cavitation are accompanied by an increase in the length of the upper surface vapor cavity. Ultimately this cavity joins with the base cavity and the foil becomes *fully cavitated.*

The transition from partial cavitation to fully cavitated flow is poorly defined for several angles of attack – see Figure 3f for example. In part this is due to the limited number of tests in this neighborhood, but it may also be caused by instability of the flow. Indeed the tests at Hydronautics, Reference 4, indicate that, in a speed interval in the neighborhood of the transition, either type of flow may be observed. This kind of hysteresis has not been experienced in any of the other test facilities. On the other hand only the Hydronautics facility permits a slow reduction of speed after the establishment of full cavity flow.

To establish consistent values for the speed at transition, as a function of angle of attack, the dot-dash curve at the bottom of Figure 5 was constructed. This was done by plotting (heavy dashes) the vapor cavitation number, σ_v, for the points shown in Figure 3 with the highest σ_v for fully cavitated flow and the lowest σ_v for partial cavitation. The curve was drawn to just exceed the lower σ_v value at each angle of attack, except at $\alpha_{\eta t}$ = 12.67 degrees where the data appear anomalous Figure 3e. The curves of Figure 3 were entered at the corresponding values of σ_v to determine the maximum lift coefficients with partial cavitation and with fully cavitated flow, which are used to plot the broken curves on Figure 5. From these the limiting values of lift coefficient at angles of attack of 9, 12 and 15 degrees are determined and plotted in Figure 4 at the appropriate speed. The maximum lift coefficient attainable in the Partial Cavitation regime, at any speed, is indicated in the figure by a heavy dashed line over the speed range from 30 to 50 knots. This upper boundary corresponds to a foil loading of just over 2000 pounds per square foot. There is a substantial drop in the lift coefficient on establishment of full cavity flow, compared with the maximum values obtained under partial cavitation conditions, as indicated by the dotted lines in Figure 4.

At the minimum speed for full cavity flow, closure of the cavity near the foil produces a reentrant jet which is projected forward to impinge on the foil, resulting in considerable fluctuation of lift and drag. At higher speeds the cavity is steady over the foil and steady loads result, which is the intended mode of operation of supercavitating foils.

In full cavity flow over the Parent Foil, the cavity is ventilated by air flowing down the base of the strut. This air flow path is, however, restricted in size by closure of the strutbase cavity a short distance downstream. Thus the pressure in the strut ventilated foil cavity is below the pressure at the water surface, hence below ambient, in most cases and some lift is developed on the upper surface of the foil. The pressure reduction on the foil upper surface, when measured in terms of the stagnation pressure of the flow, becomes less important with increasing speed and the lift coefficient decreases as shown by the solid lines in Figure 4, approaching a minimum value for each angle of attack, as indicated in the margin.

In spite of this decrease of lift coefficient, the quadratic increase of stagnation pressure with speed results in a corresponding increase of maximum loading with increase of speed. Very high loadings are indicated, at larger angles of attack, and there is no reason to believe that the attainable loading will not continue to increase as the speed is increased above 80 knots. Moreover there is no indication that the loading will not continue to increase with increasing angle of attack.

A quite different flow regime is occasionally observed on the Parent Foil when the cavity breaks the surface at its downstream end and closure of the strut-base cavity is eliminated. The top surface of the cavity becomes more sharply inclined upward and the regime is very stable. This generally provides such a large path for atmospheric air that the cavity pressure is substantially atmospheric. The increase of cavity pressure to atmospheric causes a reduction of the lift coefficient essentially to that indicated for the $\sigma_v = 0$ condition in Figure 4. Such *fully ventilated* or *planing* cavities were observed, but not consistently, in tests in the Langley Tank No. 1 at a submergence of ½ chord and at speeds of 38 knots and above. In tests of the Parent Foil in the High-Speed Hydrodynamics Facility at Langley fully ventilated cavities were obtained at intermediate speeds but never at the highest speeds. Apparently the high accelerations at the start of the high speed runs caused an initial formation of a low pressure cavity which was unable to reach the surface (Reference 5).

The lift coefficient for the Parent Foil as a function of the angle of attack, at a vapor cavitation number corresponding to a speed of about 58 knots and a depth of 5.0 feet or one chord of the 60 ton prototype, is shown in Figure 6 from Reference 2. Test results from five facilities are compared. The higher lift coefficient obtained at Langley, Tank 1, is thought to be due to the lower cavity pressure relative to the surface air pressure. On the other hand

the apparent correlation of the LUMF results with those from Convair, where the cavity pressure is known to be low, cannot be explained. It is suggested in Reference 2 that the results from tests of the 2.5 inch chord model at Hydronautics are indicative of model errors. The investigators believe that differences between the results obtained at DTNSRDC (on carriage 5) and in Tank 1 at the Langley are due to differences in the water in the two basins, Reference 3. In any event, a lift curve slope of about C_{L_α} = 0.018/deg is indicated for conditions of nearly complete ventilation (cavity pressure close to surface pressure) at this vapor cavitation number. The Langley Tank 1 data give a lift curve slope of 0.025/degree.

Figure 7 (from Reference 2) shows the lift coefficient for the Parent Foil as a function of the angle of attack at a vapor cavitation number corresponding to a speed of about 92 knots and a depth of 5.0 feet or one chord of the 60 ton prototype. Results of tests at 5 laboratories are compared. Three points from Reference 5 have been added to this plot, from tests of the Parent Foil in the High-Speed Hydrodynamic Facility at Langely (HSHF) which were not available when Reference 2 was written. Reasonable agreement is indicated except for the Hydronautics 2.5 inch chord model and the Langley HSHF tests. As shown in Reference 5, the latter tests consistently produced a lift above that obtained in Tank 1 except when a planning cavity was obtained. The high Froude number of these tests may be a factor in the results. A lift curve slope of C_{L_α} = 0.020/degree is indicated by the Langley HSHF tests, while the LUMF tests give a value of 0.018/degree.

In calculations in the following section, a lift curve slope of 0.023/degrees was used as shown in Figures 6 and 7. This value was derived from an examination of the Langley Tank 1 results for the Parent Foil, see Figure 5, and is appropriate to a cavitation number of about 0.13, corresponding to a full scale speed of about 80 knots.

FLAP EFFECTIVENESS

The Parent Foil was tested at Convair (Reference 6) with split flaps over a range of chordwise and spanwise dimensions. Results for full span flaps of 30 percent chord ratio, estimated by extrapolation of test results from a maximum span ratio of 0.9, are shown in Figure 8 for a vapor cavitation number of 0.4 corresponding approximately to the maximum speed of the tests. The tests were conducted at depth-to-chord ratios of 1/3, 2/3 and 1.0, at angles of 11.7, 13.8 and 15.5 degree (measured with respect to the foil design reference line) and with flap deflections of 0, 5 and 10 degree. Under these conditions the foil is *fully cavitated,* with a cavity pressure of about 1/2 atmosphere, except at a depth-to-chord ratio of 1/3 when *fully ventilated, planing* cavities were observed.

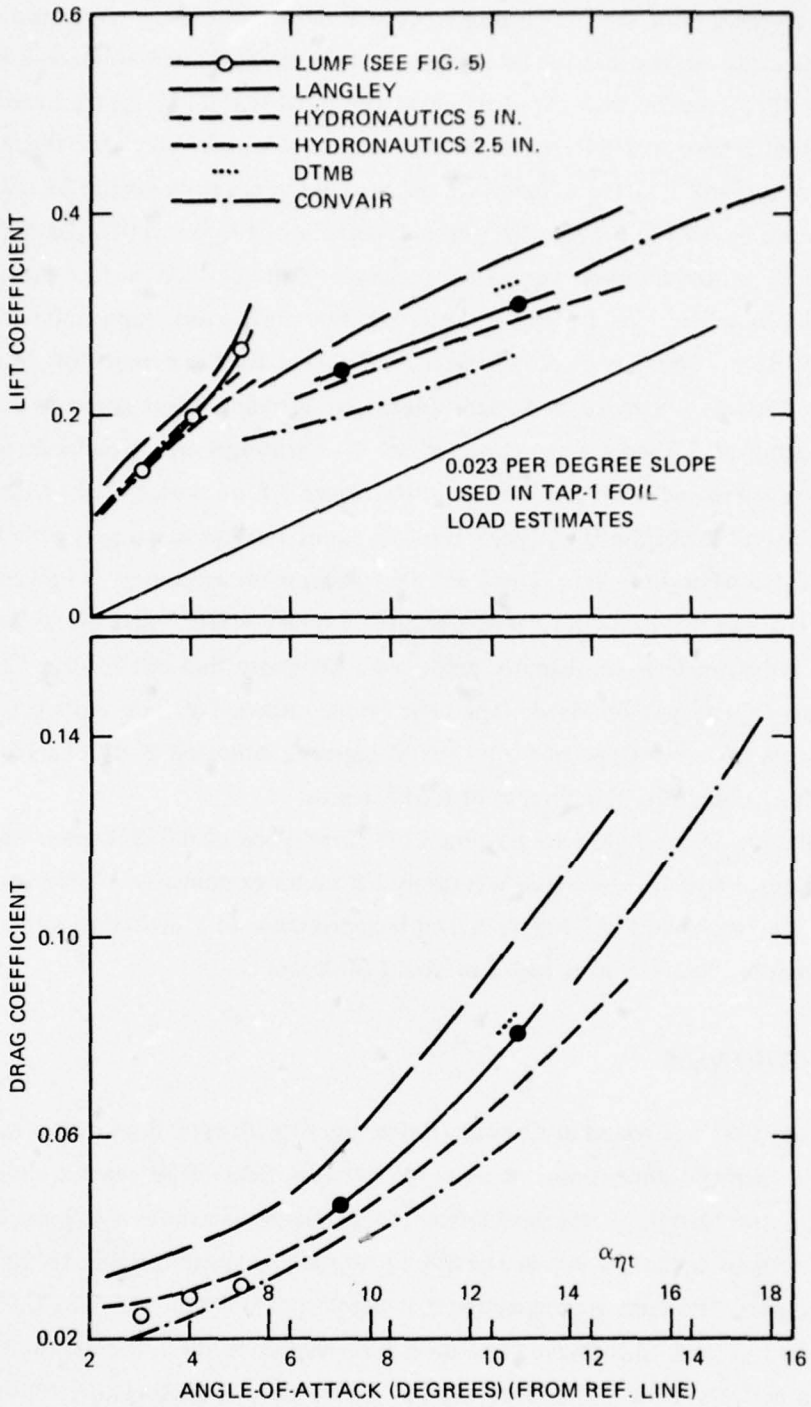

Figure 6 – BUSHIPS Parent Foil: Facility Comparison of Lift and Drag Coefficients for d/c = 1.0 at a Vapor Cavitation Number of 0.25

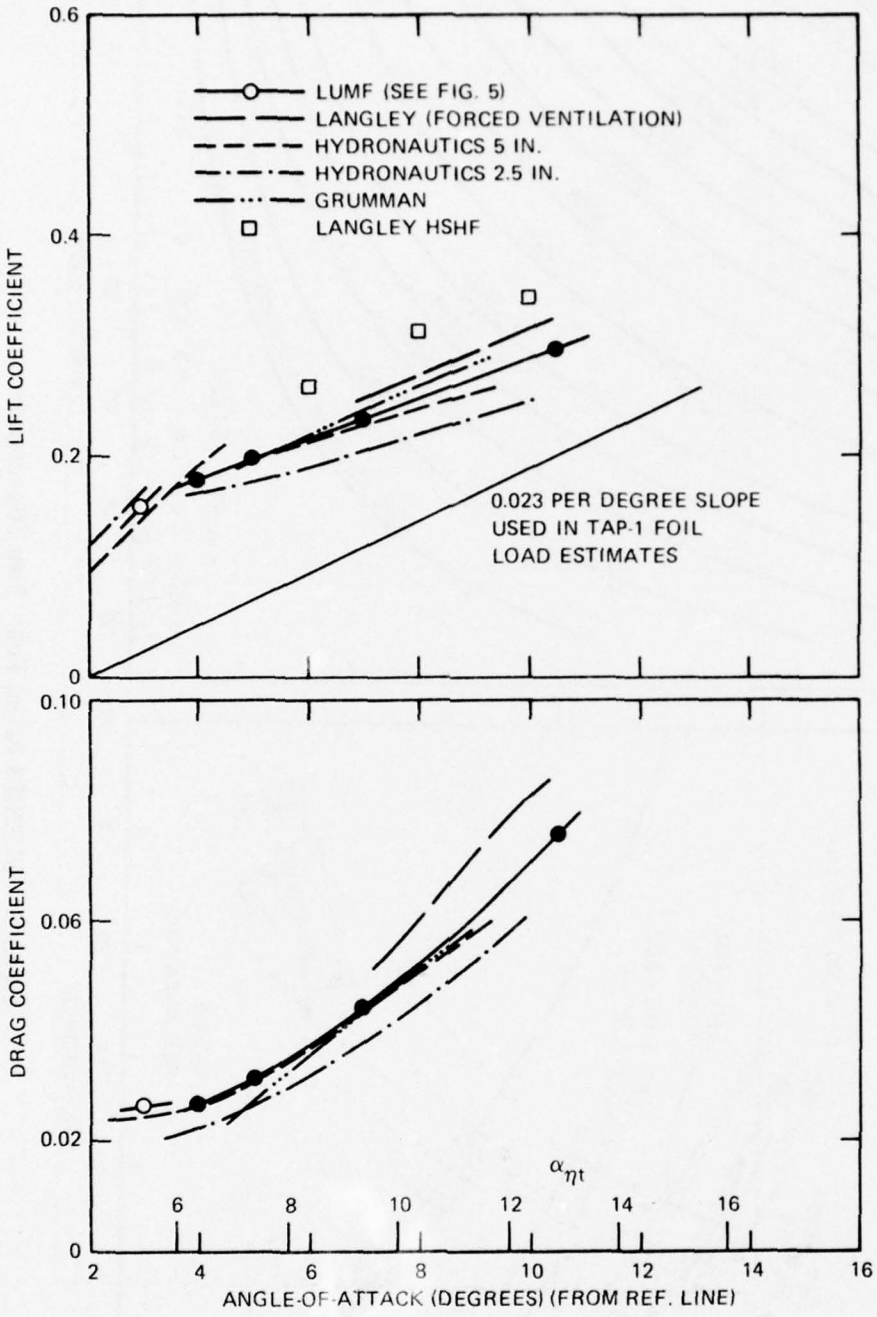

Figure 7 – BUSHIPS Parent Foil: Facility Comparison of Lift and Drag Coefficients for d/c = 1.0 at a Vapor Cavitation Number of Approximately 0.10

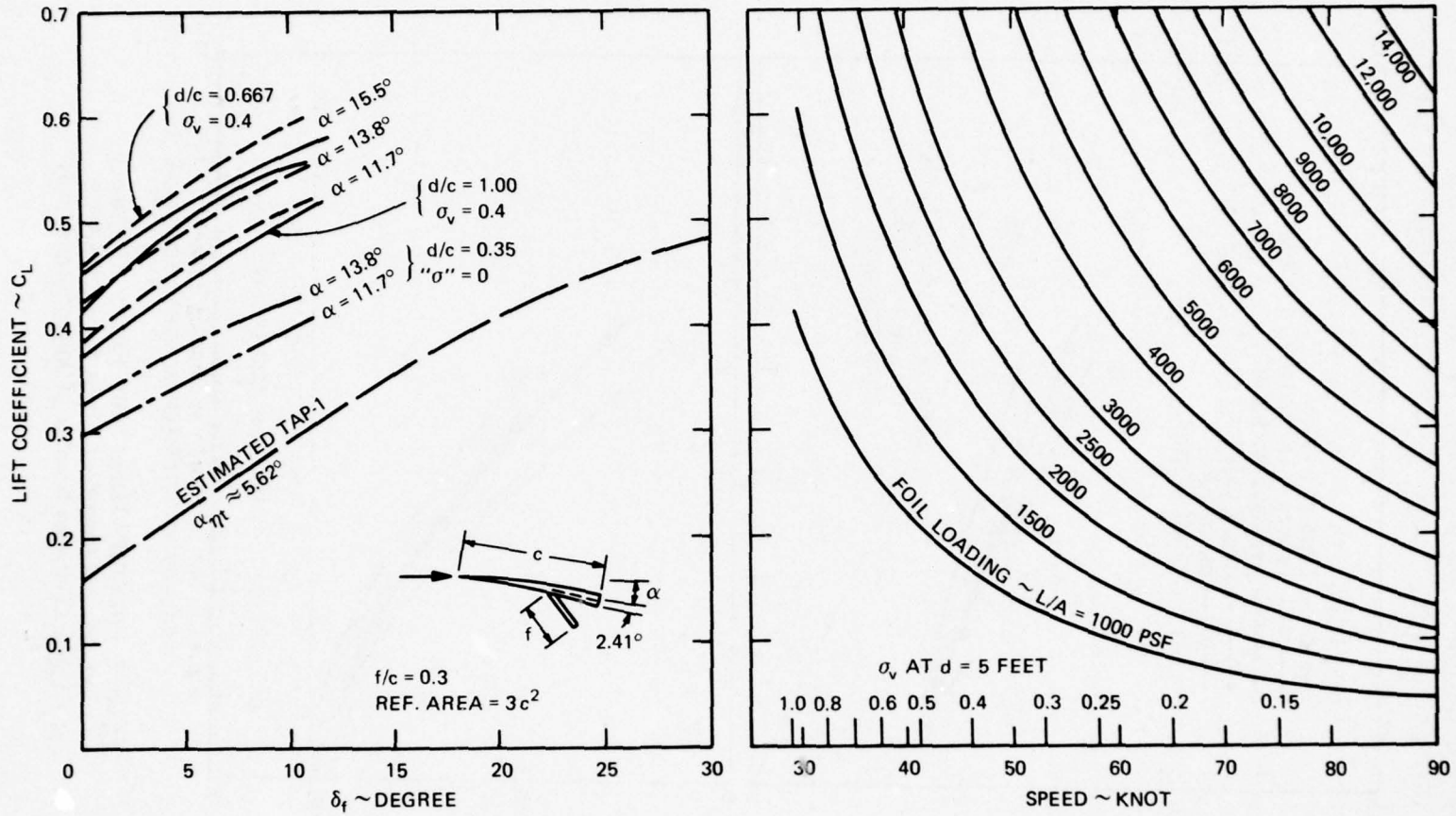

Figure 8 – BUSHIPS Parent Foil: Flap Effectiveness

The experimental curves of Figure 8 show some decrease in flap effectiveness at higher flap deflections but are essentially linear in the 0 to 10 degree range. The average slope of the curve is little affected by variations in depth of submergence or foil angle of attack. Variations of lift coefficient with angle of attack and depth of submergence for zero flap deflection are consistent with the results of tests in other facilities.

An estimate was made of the variation of lift coefficient with flap deflection for the TAP-1 foil over a range of flap deflection from zero to 30 degrees, using as guidance the slope and curvature of the Convair results for small flap deflections and using the curves in Figure 23 as guidance for larger flap deflections. The result, shown in Figure 8 is assumed to be valid over the range of speed from 50 to 80 knots.

An indication of the effect of flap deflection on total foil lift can be obtained from the curves of constant loading shown in the right-hand portion of Figure 8.

FLAP HINGE MOMENTS

Flap hinge moments were measured in the Parent Foil model tests at Convair, Reference 6. Some of these results, for a submergence of one chord and a flap chord ratio of 0.3, are plotted in Figure 9 in the form of hinge moment coefficient versus lift coefficient for a range of angles of attack and flap deflection. Predictions based on Auslaender's theoretical formulation of flap effectiveness, Reference 7, are also shown.

In the determination of TAP-1 flap hinge moments in the sections which follow, integrated two dimensional flap test data have been employed to assure consistency between hinge moments and flap lift loads.

STRUT SIDE FORCE DATA

A number of model tests have been made on a blunt-based strut similar in many respects to the TAP-1 strut. These provide the basis for estimating the side load to be expected on the TAP-1 strut.

The blunt-based strut No. 2 was created by cutting off the rear 50 percent of a streamlined strut, designated strut No. 2 in Reference 8, and leaving an almost semi-elliptic section with a 24 percent thickness ratio. Tests of this model were conducted at DTNSRDC in the High Speed Basin, Reference 9, and on the Rotating Arm, Reference 10, and also at the Lockheed Underwater Missile Facility, Reference 11.

A typical curve showing the variation of strut side force with side slip angle is presented in Figure 10. At any constant speed the side force increases almost linearly with side slip

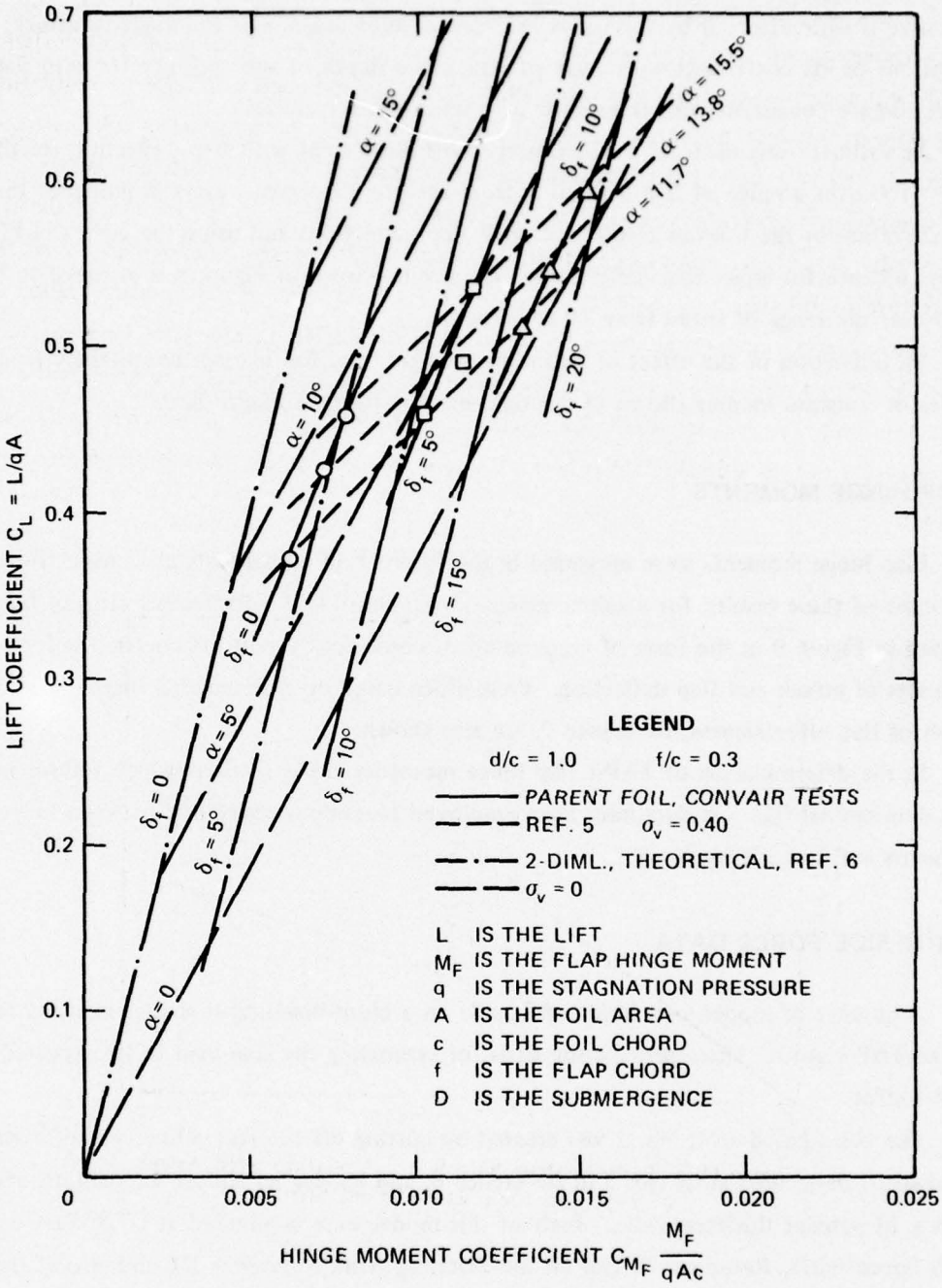

Figure 9 – Variation of Lift Coefficient with Flap Hinge Moment

angle until a maximum is reached just before ventilation of the flow occurs. The effect of ventilation is a drastic reduction of the strut side force. With further increase in side slip angle a recovery of side force takes place. However, tests have not been made to a sufficiently large side slip angle to achieve a side force larger than that obtained just prior to ventilation. Since it appears unlikely that such a large side slip angle would be achieved in full scale ship operation, it will be assumed the side force would not exceed the preventilation value.

The maximum preventilation side force is shown in Figure 11, as a function of the speed. Values are given for three values of strut tip immersion. For design purposes in the sections which follow a limit side force loading of 1800 psf has been used, as indicated in Figure 11. The somewhat larger loading indicated by the tests in the LUMF facility have been discounted because the tests were conducted at less than full-scale Froude number. The tests in the LUMF show that, at any given cavitation number, an increase of Froude number results in ventilation at a smaller side slip angle, hence reducing the maximum preventilation side force coefficient.

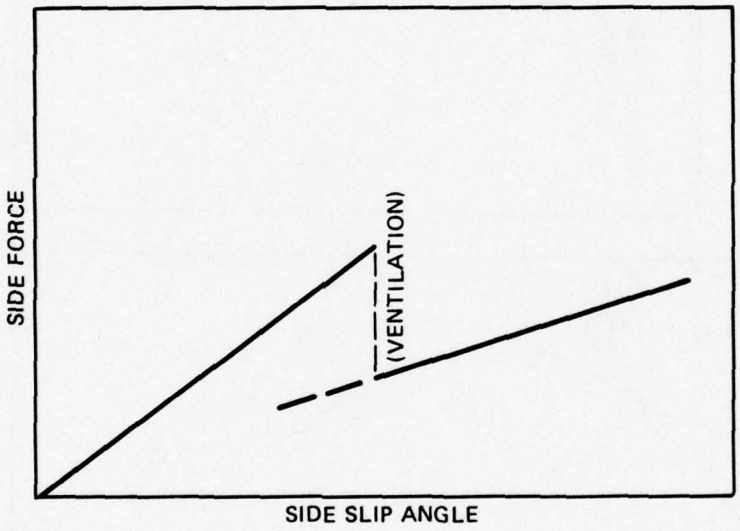

Figure 10 – Typical Strut Side Force Variation with Angle of Side Slip for a Blunt-Based Strut

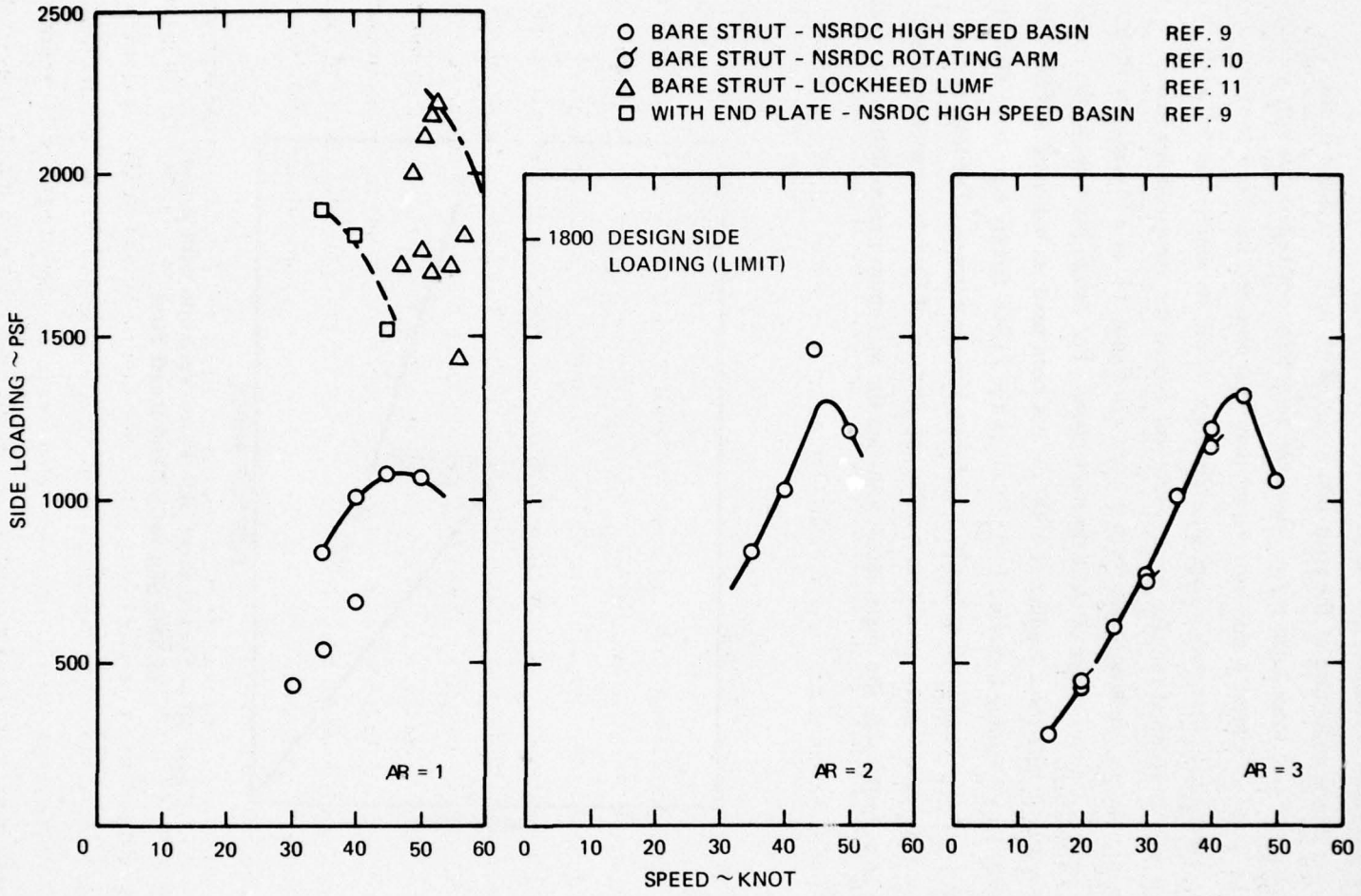

Figure 11 – Blunt-Based Strut No. 2: Variation of Ventilation Limited Side Force with Speed

STRUCTURAL LOAD CRITERIA

The selection of structural load criteria employed in this study has been influenced strongly by the type of loading conditions known to be critical for the forward foil systems of conventional (subcavitating) canard configuration hydrofoil ships. While no attempt has been made here to provide for all types of loads in the criteria (e.g. debris impact loads), the critical loading conditions specified are intended to cover those few loading situations which typically have the greatest influence on strut and foil member sizes.

These have been taken as:

a) a maximum lift condition

b) a maximum strut side force condition

c) a maximum asymmetric foil lift condition (This is usually also a maximum strut torsion condition due to the associated asymmetric foil drag).

These general loading conditions have been developed into four critical design cases for the TAP-1 supercavitating strut/foil configuration on the basis of the following rationale.

MAXIMUM LIFT CONDITIONS

The maximum lift load to be considered in design could conceivably be based upon the maximum attainable lift at any speed up to the highest value considered in the design of the TAP-1 foil, namely 80 knots. The data of Figure 4, however, have already suggested that this is impractical because once fully cavitating flow has been established lift coefficient tends to become constant with increasing speed, with the result that the attainable lift load at any given angle of attack increases with the free stream dynamic pressure without apparent limit. In order to avoid design for unrealistically high loads at 80 knots, a maximum load equal to 2.5 times the normal 1g lift has been selected based upon subcavitating foil experience which has shown that lift loads of this magnitude are seldom if ever required for control of the ship. The 2.5 factor lift load is also approximately equal to the maximum attainable lift from a typical subcavitating foil at full flap deflection.

The selection of a particular value of maximum lift for foil structural design represents a departure from the rationale employed in structural design of subcavitating foils. In general, where flap deflections are governed by an Automatic Control System (ACS) having no limits on flap deflections, other than mechanical stops, structural design for full flap deflection at all foil borne speeds has been considered essential. With supercavitating foils this approach can clearly result in excessive loads and specific provisions for restricting flap deflections (such as hinge moment limiting) are believed necessary and should be considered in ACS design.

Having selected a maximum lift load it was believed appropriate to establish two loading conditions for detail design. The first of these corresponds to a foil lift load distribution which results in maximum loading on the foil leading edge while the second results in maximum load on the flaps. In either case the total lift load will correspond to 2.5 factors of lift. The first case has been designated Condition I Maximum Lift at Maximum Speed while the second has been designated as Condition II Maximum Lift at Maximum Elevator Deflection.

The maximum speed has already been established as 80 knots and therefore the primary question for Condition I concerns the particular angle of attack and flap deflection associated with 2.5 factors of lift at 80 knots, while for Condition II the major unknowns are the speed and foil angle of attack which, at a full flap deflection of 30 degrees, will result in 2.5 factors of lift (tentatively assumed to be 60 knots). In order to quantify these unknowns the critical loading circumstance in each case will be assumed to correspond to a broach recovery in rough water during head sea operation. The angle of attack of the foil in each case will be assumed to equal the sum of the 1g trim angle, an incremented angle due to wave orbital velocity, and an incremental angle due to the pitch/heave velocity resulting from broaching. For simplicity the wave conditions will additionally be assumed the same at each speed.

The incremented angles of attack associated with wave orbital velocities at foil reentry have been calculated based upon the following assumptions:

Wave height, H_W = 12 ft

Wave length, L_W = 120 ft

Instantaneous foil depth = 5 ft

The speed of the wave is $V_W = 2.26 \sqrt{L_W}$

$= 2.26 \sqrt{120} = 24.8$ ft/sec

and the period is, $T_W = \frac{120}{24.8} = 4.84$ sec

The peak vertical velocity of the wave orbital motion is,

$$v_o = \frac{\pi H_W}{T_W} = \frac{\pi \times 12}{4.84} = 7.79 \text{ ft/sec}$$

At an assumed foil depth of 5 ft this is reduced to

$$v_o' = v_o \times e^{-\frac{2\pi h}{L_W}} = 7.79 \times e^{-\frac{10\pi}{120}} = 6.0 \text{ ft/sec}$$

At a ship speed of 60 knots this results in an incremented angle of attack of $\frac{6 \times 57.3}{101.4} = 3.39$ degrees while at 80 knots it becomes $\frac{6 \times 57.3}{135} = 2.55$ degrees.

The incremental angles of attack associated with ship pitch/heave following forward foil loss of lift will be estimated assuming that the reduction in lift persists for about one third of the wave encounter period and that the average acceleration during this interval is about -10 ft/sec^2. Based upon these assumptions, the vertical velocity of descent of the foil at water entry is $\Delta v \approx 10 \times \frac{120}{101.4 + 24.8} \times \frac{1}{3} = 3.15$ ft/sec at 60 knots, and $\Delta v \approx 10 \times \frac{120}{135 + 24.8} \times \frac{1}{3} = 2.50$ ft/sec at 80 knots. At a ship speed of 60 knots the incremental angle of attack due to pitch/heave is thus $\frac{3.17}{101.4} \times 57.3 = 1.79$ degrees while at 80 knots it is $\frac{2.5}{135} \times 57.3 = 1.06$ degrees.

The resulting foil lift loads, angles of attack, and flap deflections are summarized for Design Conditions I and II in Figures 12 and 13, respectively. In Condition I Maximum Lift at Maximum Speed, the total angle of attack is 8.18 degrees with a flap deflection of 8.25 degrees, while in Condition II the total angle of attack is 10 degrees with a flap deflection of 30 degrees.

MAXIMUM STRUT SIDE FORCE CONDITION

Experience with fully submerged subcavitating foil systems suggests that steerable strut side loads approaching maximum attainable side force can be experienced while maneuvering in rough seas. Moreover, lift loads acting concurrently on the foil can be asymmetrically distributed and momentarily in excess of the steady 1g value. A maximum strut side force condition has therefore been established as Design Condition III Maneuvering in High Seas which consists of the maximum preventilation loading of 1800 psf (see Figure 11) acting in combination with 1.5 factors of lift having a 60-40 percent spanwise distribution such that strut lateral bending is increased over that due to side force alone. For purposes of this study it has been considered adequate to proportion the foil lift loads of Condition II to achieve a load level corresponding to 1.5 factors of lift in order to obtain detailed foil loads. For full flap deflection, it will be noted that the speed corresponding to 1.5 factors of lift would be roughly

$$V = 60 \times \sqrt{\frac{1.5}{2.5}} = 46.5 \text{ knots}$$

which is in the general speed range of maximum attainable (preventilation) strut side force as shown in Figure 11.

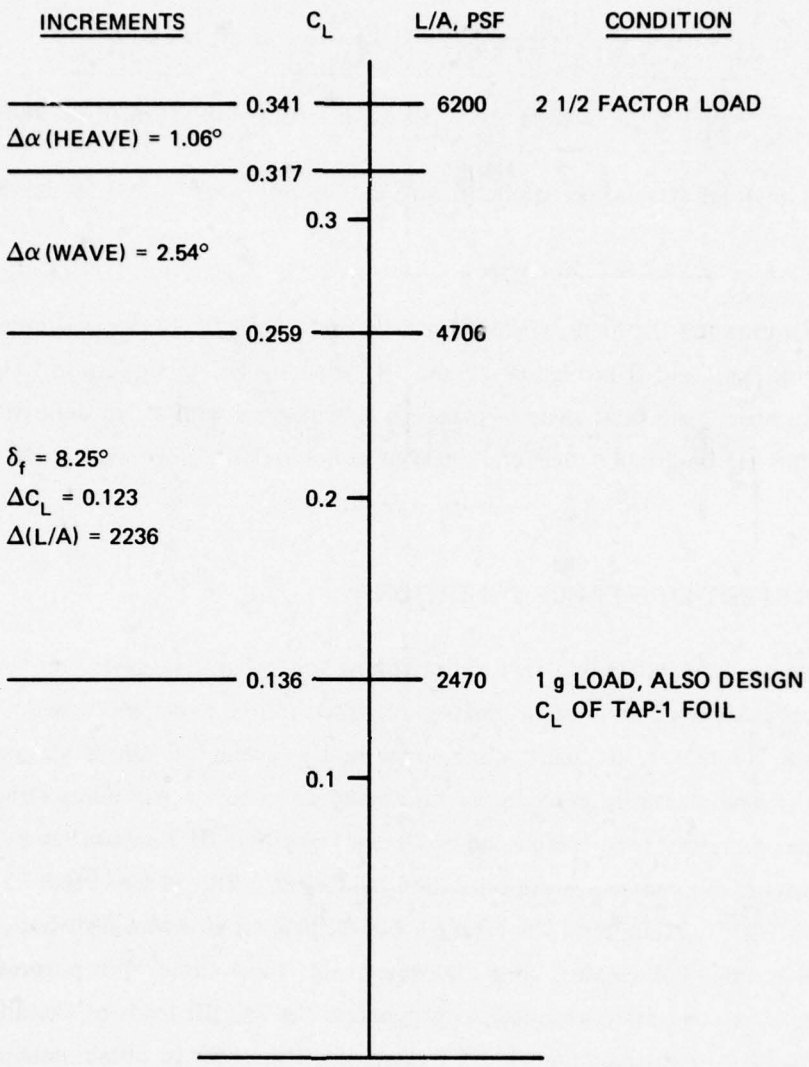

Figure 12 – Composition of Limit Load, 80 Knot Broach (Design Condition I)

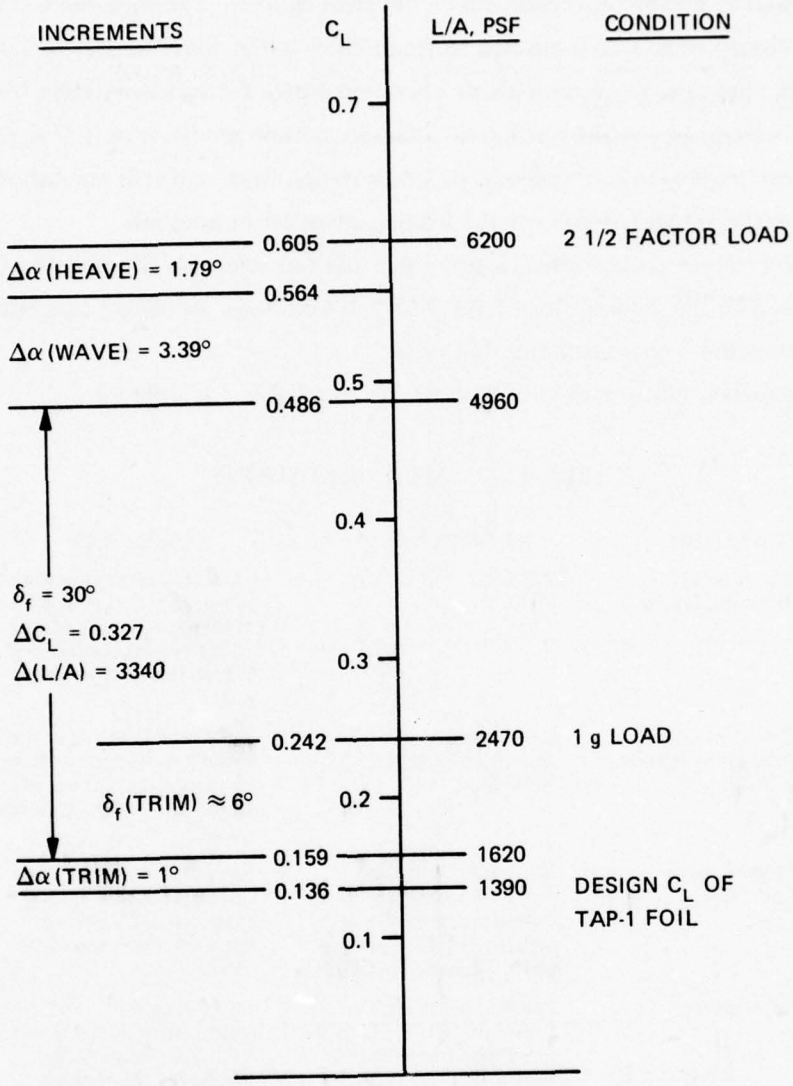

Figure 13 – Composition of Limit Load, 60 Knot Broach (Design Condition II)

MAXIMUM ASYMMETRIC FOIL LIFT CONDITION

The fourth design condition considered in this study is an extreme asymmetric lift loading which tends to result in maximum lateral bending moment at the strut-to-foil attachment as well as maximum torsion about the steering axis. The total loading in this case is somewhat arbitrary since it is presumed to result from initial water impact following a broach in rough water and since no trials or operational data for supercavitating foils is available for this situation. A lift loading of 2 factors on one semispan only (for a net lift of 1 factor) has been employed in the design of subcavitating foils, and it is employed here for lack of a more rational load criteria for the loading situation in question.

In order to produce critical strut torsion loads the foil semispan lift and drag loads have been proportioned to the 2 factor load level from the Condition II loading case which features full flap deflection and hence maximum foil drag.

The four design conditions discussed above are summarized in Table 3.

TABLE 3 – DESIGN CONDITIONS

CONDITION	LIMIT LOADS	REMARKS
I. Maximum Lift at Maximum Speed	2.5 Factors of Lift at 80 knots	Flap deflection as required to produce designated lift at 80 knots at an angle of attack corresponding to a broach recovery in rough water.
II. Maximum Lift at Maximum Elevator Deflection	2.5 Factors of Lift at Maximum Elevator Deflection	Full flap deflection at the speed required to produce the designated lift during a broach recovery in rough water.
III. Maneuvering in High Seas	Maximum Strut Side Force of 1800 PSF Combined with 60 - 40 percent Lift Distribution at 1.5 Factors, Total Lift	Foil lift to correspond to Condition II foil loads proportioned down to designated semispan lift loads.
IV. Foil Reentry	2.0 Factor Lift on One Semi-Span Only, (Total Lift Corresponds to 1.0 Factor Lift for Two Semispans)	Foil semispan lift and drag loads proportioned down from 2.5 factors to 2.0 factors on one semispan.

STRUCTURAL DESIGN LOADS

The conditions under which the maximum, i.e. limit, loads are to be expected on the strut and foil are described and their overall magnitudes established above. To carry out the structural design it is necessary, in addition, to know the distribution of the external loadings. In this section estimates are derived for the external load distribution following which the necessary integrations are carried out to provide limit shears, bending moments and torques on any cross section of the foil and for the upper and lower ends of the strut. These load components are shown in Figures 14 and 15.

FOIL LOWER SURFACE LOAD DISTRIBUTION

Since the supercavitating foil is loaded only on the lower surface at high speeds, the forces are derived by consideration of the pressure and shear (drag) forces on the bottom of the foil. Allowance is made for the design angle of attack, Figure 2, by requiring the total force normal to the bottom to be $\frac{L}{\cos 4.62^\circ}$, where L is the lift associated with a particular design condition. The effect of ship pitch angle on the relation between lift and normal force has been ignored.

Spanwise Load Distribution

The TAP-1 foil has been twisted in an attempt to maintain a constant section lift coefficient along the span, when the foil is at its design lift coefficient. In the structural design, the foil has been assumed to be untwisted, for simplicity, but the load distribution used is that appropriate to the twisted foil.

The distribution of added load due to the increased angle of attack shown in Figures 12 and 13 is assumed to be the same as it would be for a wing in air, which can be approximated by the method of Reference 12. An examination of the results, in Reference 13, of such calculations shows that, with a taper ratio of 0.50 and a quarter-chord sweep angle of only 11 degrees, there is very little variation of the section lift coefficient along the span except for the inevitable drop to zero at the tip. For purposes of estimating spanwise lift, it is assumed that the full-span, constant percent-of-chord flaps will produce a spanwise distribution of added load essentially the same as that produced by increased angle of attack.

On the basis of the above considerations, and for ease of computation, it has been assumed that, under all loading conditions, the spanwise load distribution corresponds to a

constant section lift coefficient from midspan out to 90 percent of the semispan with a linear reduction from there to the tip. The overall foil lift coefficient is then approximately 0.95 times the "constant" local lift coefficient. The corresponding spanwise distribution of the foil normal load is shown in Figure 16 for Design Condition I and II. These distributions include the component normal to the foil plane of the loading on the flap. The latter is given in Figure 17.

The spanwise distribution of loading in the 'X' direction, tangent to the foil lower surface, is shown in Figure 18 for Design Condition I and Figure 19 for Design Condition II. These loadings result from fluid friction and from the appropriate component of the flap normal loading, Figure 17.

The fluid friction is assumed uniformly distributed over the foil and flap lower surfaces. The average skin friction coefficient has been estimated from Figure 5, Chapter 2 of Reference 14, which shows that, at Reynold's numbers of 4×10^7 to 5.3×10^7 (corresponding to speeds of 60 and 80 knots respectively) the friction drag coefficient will be approximately 0.0025 for fully turbulent flow. This was increased by 50 percent to allow for roughness, resulting in an average skin friction coefficient of 0.00375.

Chordwise Load Distribution

Derivation of the chordwise pressure distribution is based on two fundamental assumptions:

1. Chordwise pressure is a constant function of the percent-of-chord for all spanwise positions from midspan out to 90 percent of the semispan, which will be termed the basic pressure distribution for a particular design condition. Beyond this point the pressures decrease linearly to zero at the foil tip.

2. The chordwise pressure distribution can be adequately approximated by that on a plane foil in two-dimensional flow with the same flap deflection and at the same section lift coefficient. This assumption has been made to permit the use of available pressure distribution data.

For Design Condition I, with a 2.5 load factor, the required lift coefficient is 0.341 as shown in Figure 12. The corresponding basic pressure distribution must then be based upon a section normal force coefficient of $0.341 \div (0.95 \cos 4.65)$ or 0.360. A flap deflection of 8.25 degrees has been estimated. The local angle of attack required to produce this normal force coefficient on the flat-faced foil will be determined in the course of the pressure distribution calculatio.

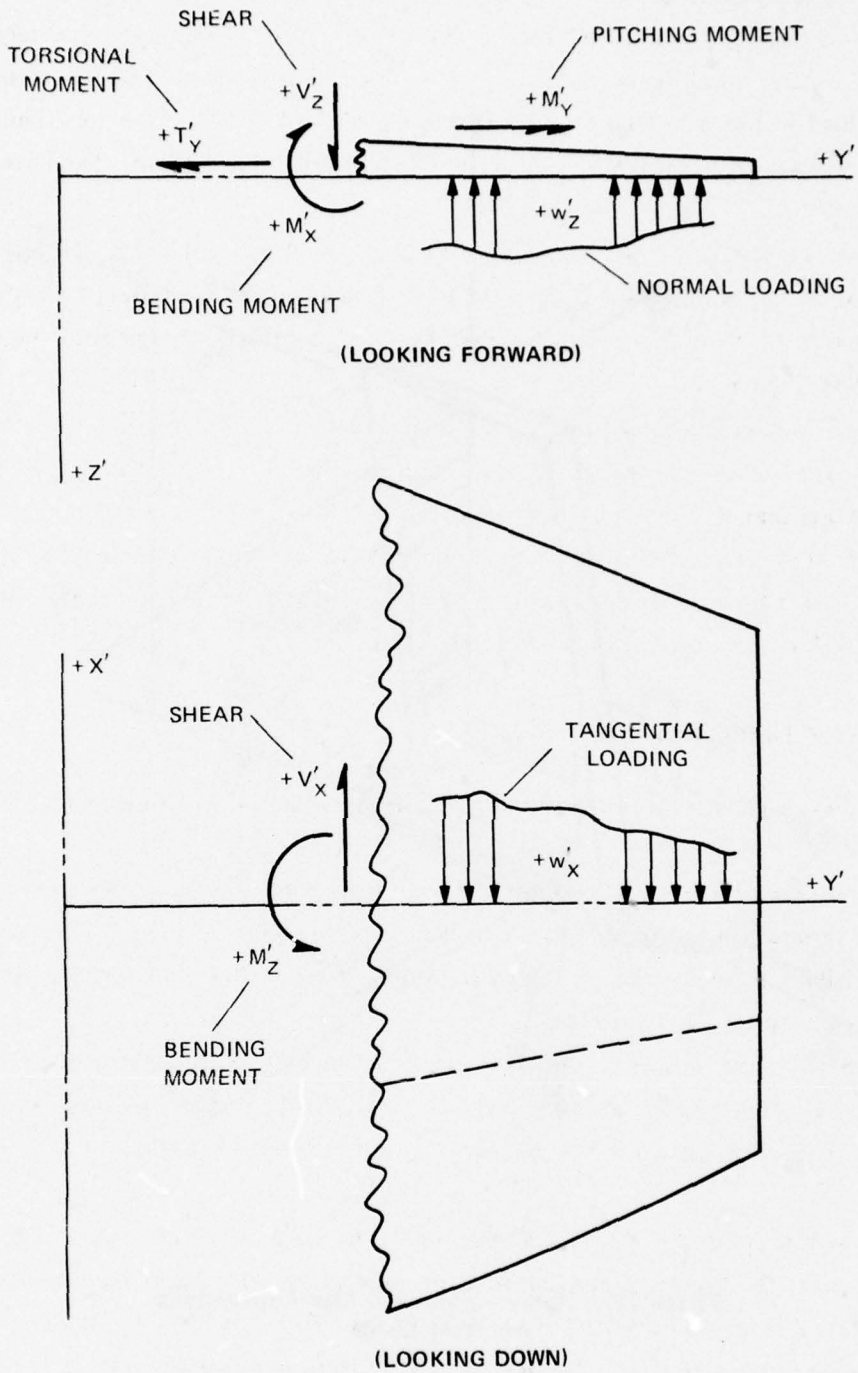

Figure 14 – Nomenclature and Sign Conventions for Foil Loads

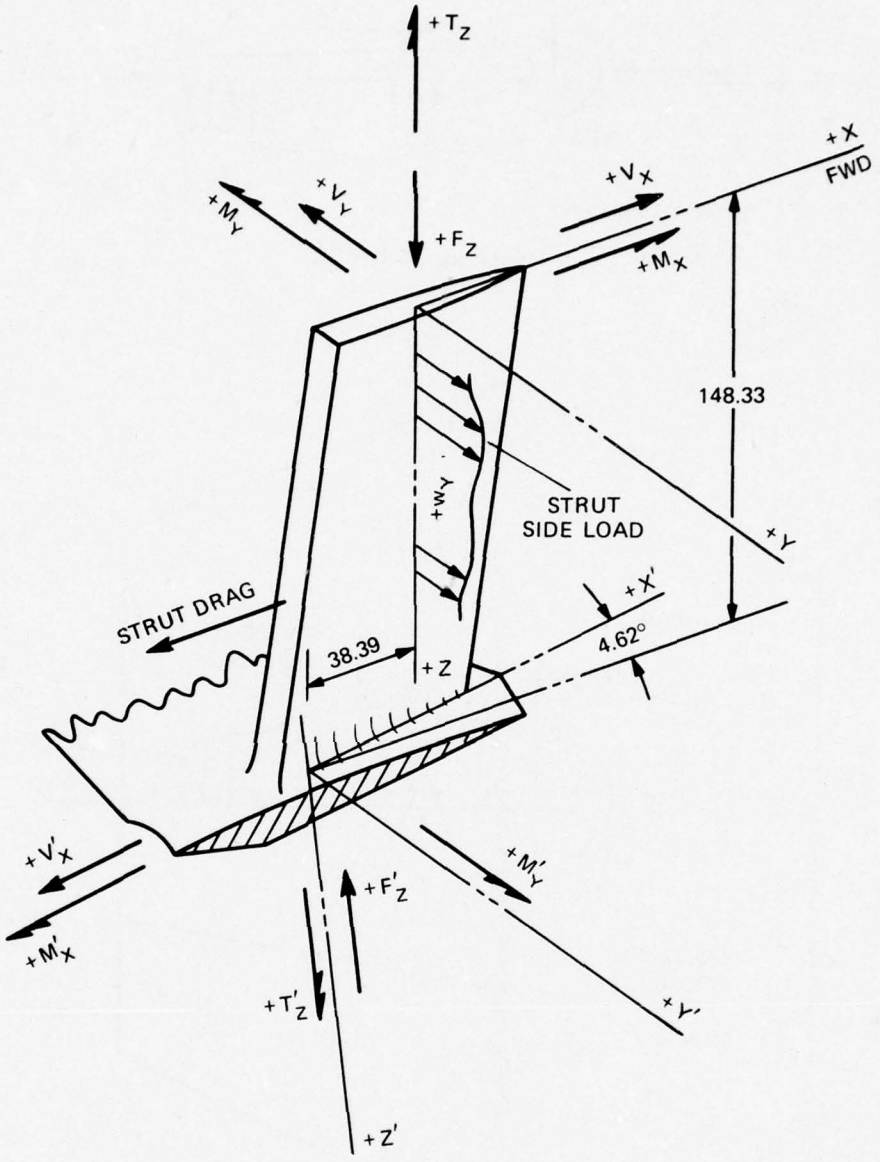

Figure 15 – Nomenclature and Sign Conventions for Strut Loads

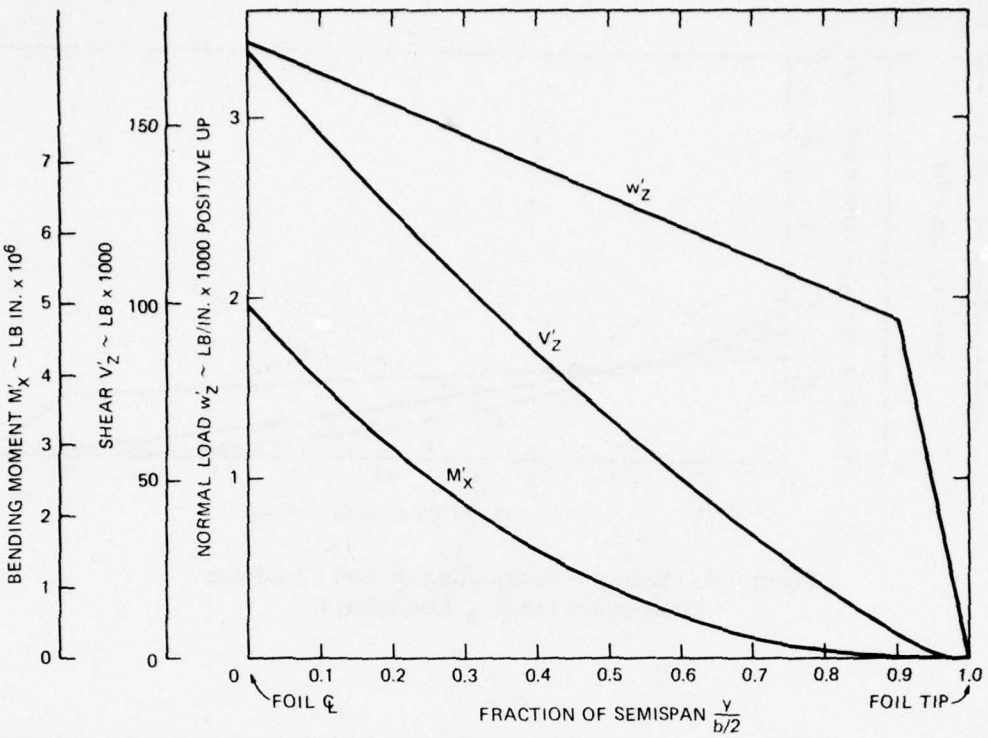

Figure 16 – Spanwise Distribution of Foil Normal Loading, Conditions I and II

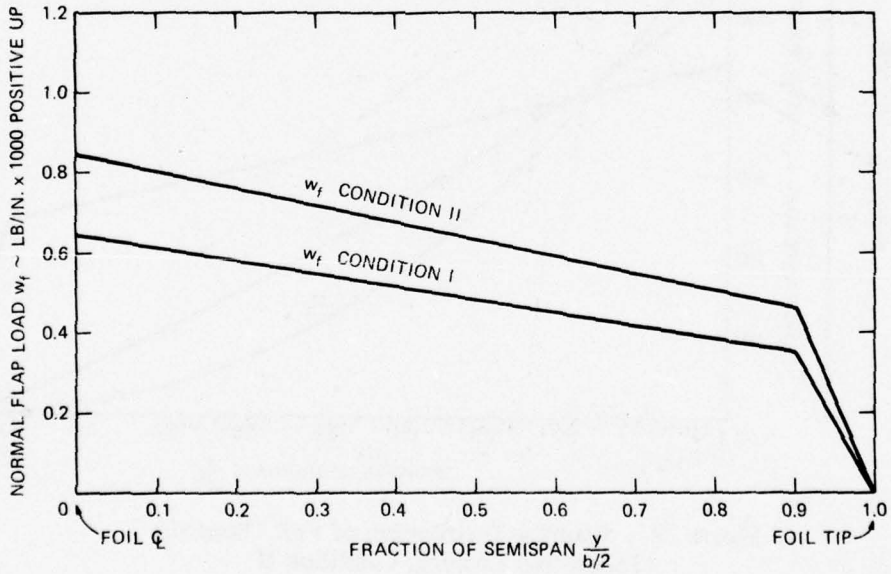

Figure 17 – Spanwise Distribution of Flap Normal Loading

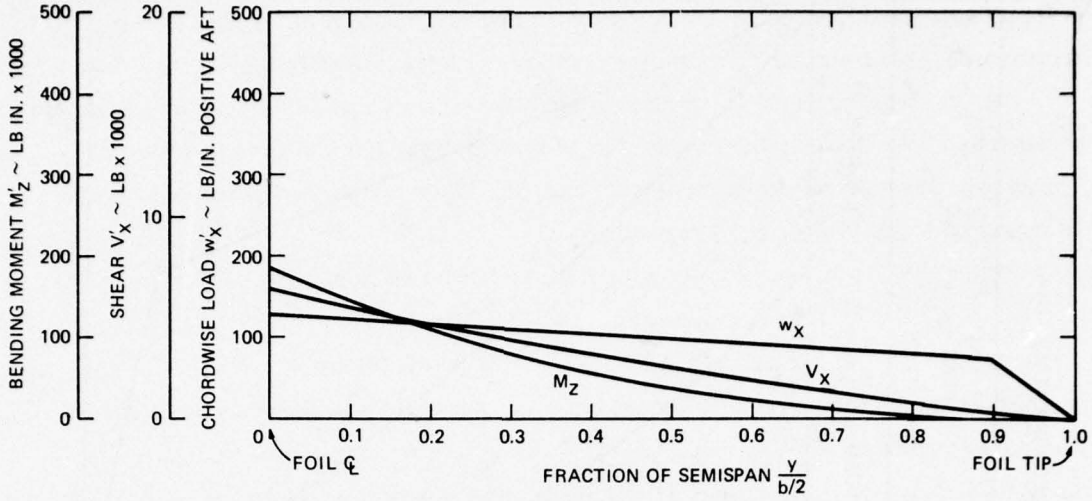

Figure 18 – Spanwise Distribution of Foil Chordwise (Tangential) Loading, Condition I

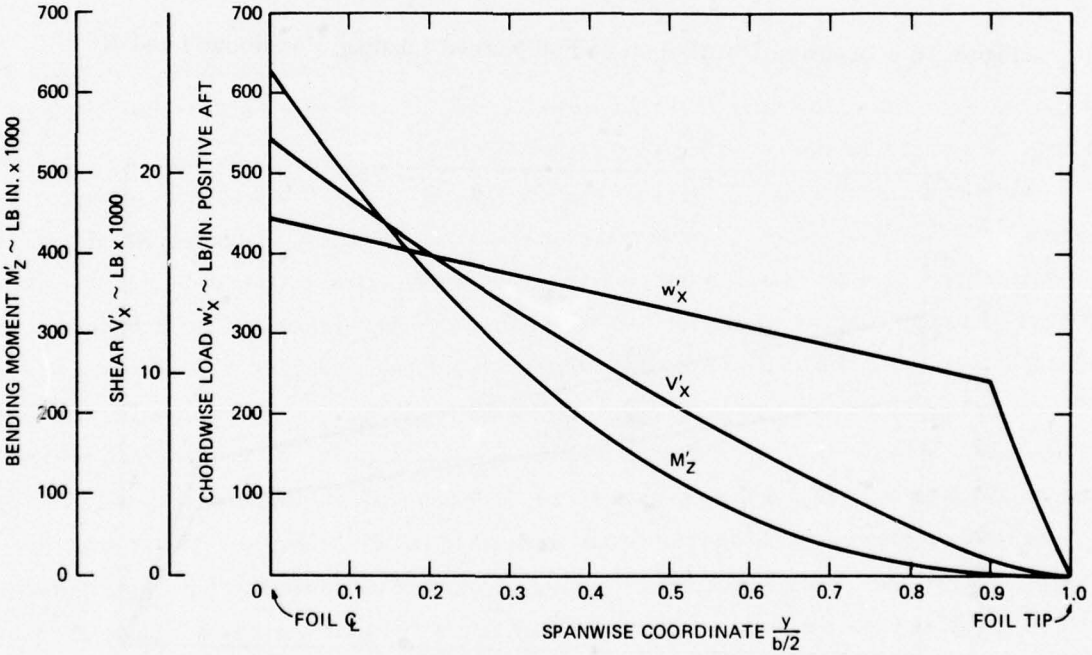

Figure 19 – Spanwise Distribution of Foil Chordwise (Tangential) Loading, Condition II

For Design Condition II, at 60 knots with a 2.5 factor load, the required lift coefficient is 0.605 with an estimated flap deflection of 30 degrees as shown in Figure 13. The corresponding basic section normal force coefficient is approximately 0.640.

The chordwise pressure distribution is calculated from the results of theoretical developments which were confirmed by experimental work done at the California Institute of Technology and reported in References 15 and 16. These results were presented for the following values of the pertinent parameters:

Angle of attack, α = 10 and 20 deg

Flap chord ratio, f/c = 0.2, 0.4, 0.6

Flap deflection, δ_f = 0, 20, 40, 60 deg

In addition, the experiments were carried out for a range of cavitation numbers from 0 to 1. Theoretical curves are given for two values of the cavitation number in all but one case. Since the design cavitation number for the TAP-1 foil is very low, the lower cavitation number data were used in each case.

Since the values of the parameters for which data are given do not include those applicable to the TAP-1 foil, it was necessary to carry out extensive graphical interpolations to obtain the applicable distributions. Figure 20 shows the theoretical distributions from Reference 16 for α = 10 deg and δ_f = 20 deg over the whole range of flap-to-chord ratio. Figure 21 contains cross curves of pressure coefficient versus flap chord ratio constructed from Figure 20 for 9 constant values of the fraction-of-chord, s/c. From these the dashed curve in Figure 20 was constructed for a flap chord ratio, f/c = 0.3.

Unfortunately the range of flap chord ratios was covered only for 0 and 20 degree flap deflection. The full range of flap deflections was covered only for a 0.2 flap chord ratio. Therefore the curves of Figure 22 were used to construct the cross curves of Figure 23 showing the pressure coefficient versus flap deflection, δ_f, for 9 constant values of the fraction-of-chord, s/c and for a flap chord ratio f/c = 0.2. Corresponding curves for an 0.3 flap chord ratio were then constructed on Figure 23, using values for 0 and 20 degree flap deflection from Figure 20 and using the 0.2 flap chord ratio curves as a guide. From these the curve in Figure 24 for an 8.25 degree flap deflection and 10 degree angle of attack was constructed.

A similar procedure was followed for an angle of attack of 20 degrees. Thus Figure 25 shows curves of the pressure coefficient C_p versus fraction-of-chord s/c for flap chord ratios of 0, 0.2, 0.4, and 0.6 and for a 20 degree flap deflection. The cross curves in Figure 26 then permit construction of the dashed curve in Figure 25 for a flap chord ratio of 0.3. From the curves of Figure 27, all for α = 20 degrees and f/c = 0.2, the cross curves of Figure 28 are constructed, for f/c = 0.2, and used as guides for similar cross curves for f/c = 0.3, based on

values at $\delta_f = 0$ and $\delta_f = 20$ degrees from Figure 25. From Figure 28 values were read at a flap deflection δ_f of 8.25 degrees and plotted on Figure 24 to give the curve for 20 degree angle of attack.

Using the data of Figure 24, linear interpolation/extrapolation provides the curve of Figure 29 for an angle of attack of 8.18 degrees. The resulting normal force coefficient of 0.357 is essentially that required for a 2.5 factor load at 80 knots in Design Condition I. The loading curve for Design Condition I is presented in Figure 30. Some adjustment of the theoretical data was made in the vicinity of the flap hinge, at s/c = 0.7, where the experimental results indicated a failure to reach the stagnation pressure.

To determine the chordwise pressure distribution for Design Condition II, the pressure coefficient is read from the cross curves of Figure 23 for a flap deflection δ_f of 30 degrees, flap chord ratio f/c of 0.3, and an angle of attack of 10 degrees. The results are plotted in Figure 29. With some adjustment in the vicinity of the flap hinge, at s/c = 0.7, and multiplication by the stagnation pressure, q = 69.44 psi, the results provide the loading curve for Design Condition II in Figure 30. The total loading, when integrated, was found to be approximately 5 percent less than the desired 6500 lbs/ft^2. This was considered sufficiently close to the desired value for the purposes of this study.

FOIL SHEAR, BENDING AND TORSION LOADS

Spanwise Bending and Shear

The foil is considered cut by a plane parallel to the X′-Z′ coordinate plane. The internal loads are considered shear forces in the X′ and Z′ directions and two moments as shows in Figure 14.

The shear V'_Z and bending moment M'_X derived by integration of the foil normal loading density w'_Z are shown in Figure 16 which applies to Design Conditions I and II. Corresponding loads for Design Conditions III and IV can be derived by applying the factors given below to the values in Figure 16.

	FACTOR	
DESIGN CONDITION	STARBOARD SEMISPAN	PORT SEMISPAN
III	0.72	0.48
IV	0.80	0

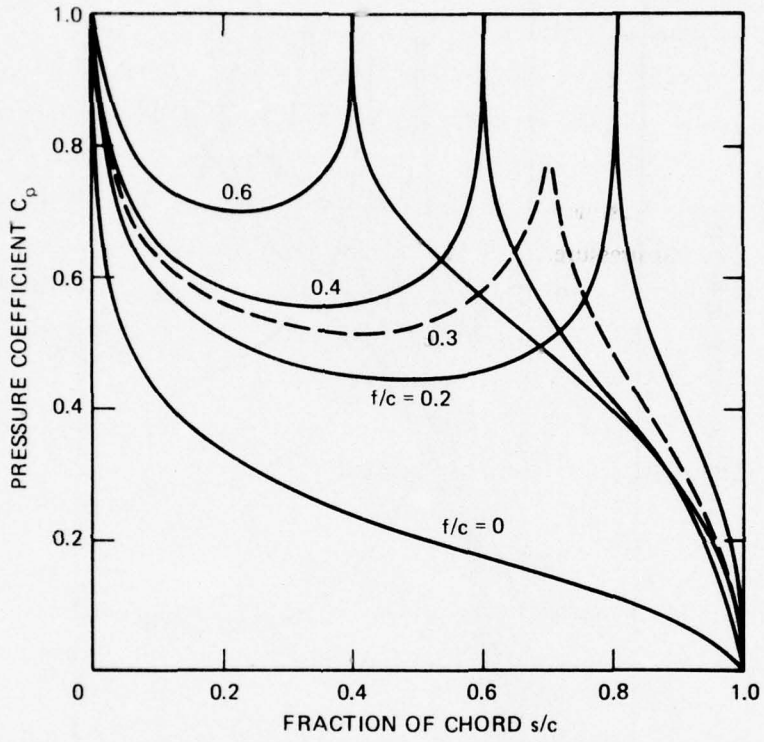

Figure 20 – Chordwise Pressure Distributions for Flat Plate with Flap; $\alpha = 10°$, $\delta_f = 20°$, f/c as a Parameter

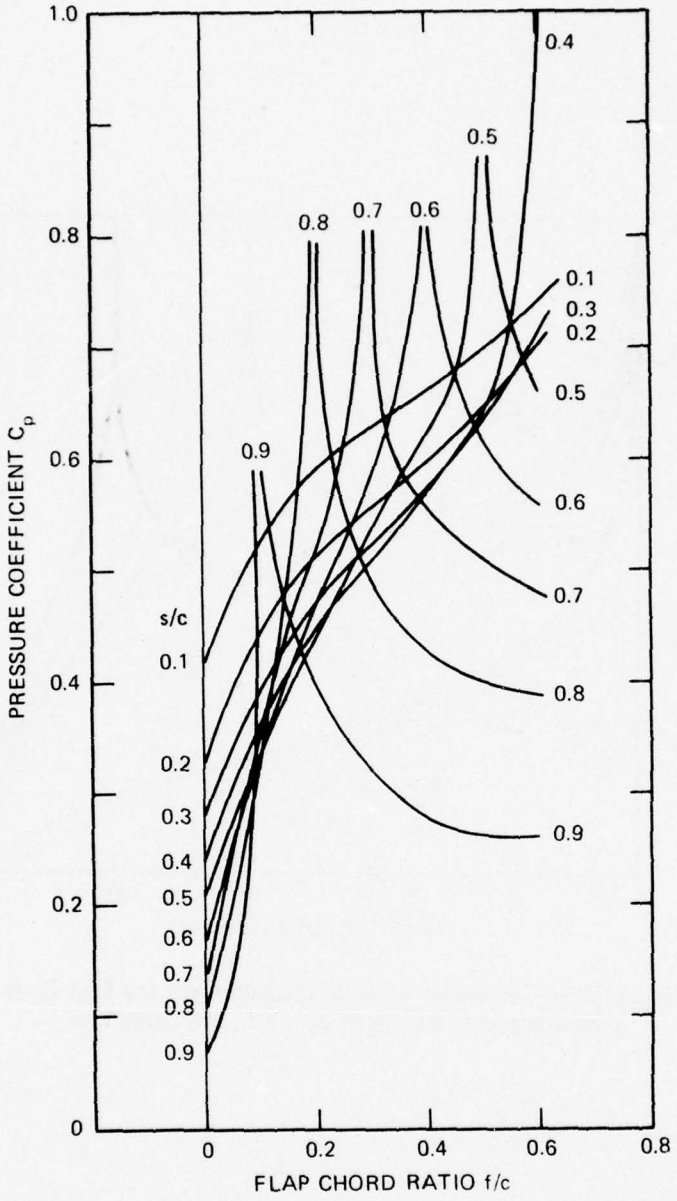

Figure 21 – Cross Curves of Pressure Coefficient Against f/c with s/c as a Parameter; $\alpha = 10^\circ$, $\delta_f = 20^\circ$

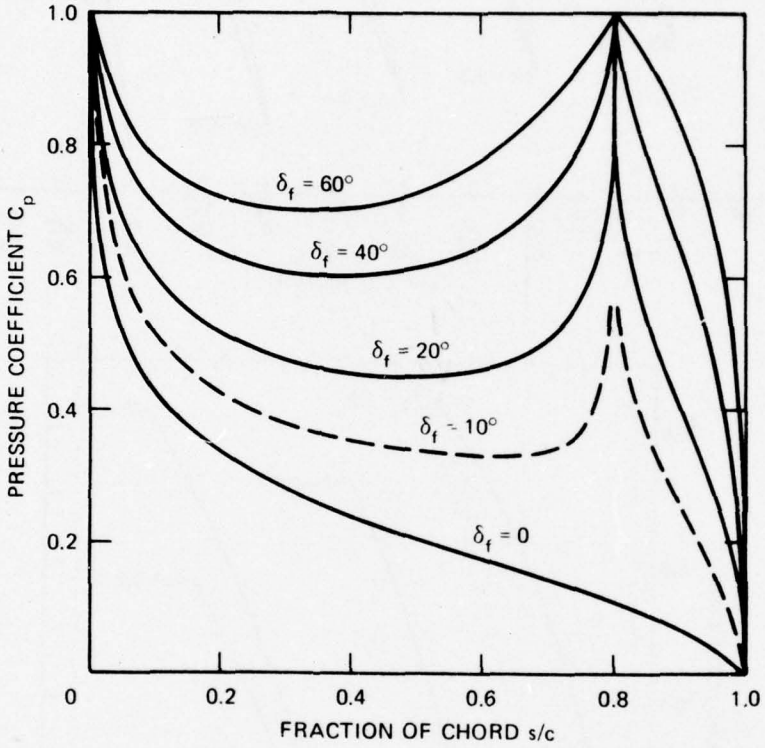

Figure 22 – Chordwise Pressure Distributions for Flat Plate with Flap; $\alpha = 10°$, f/c = 0.2, δ_f as a Parameter

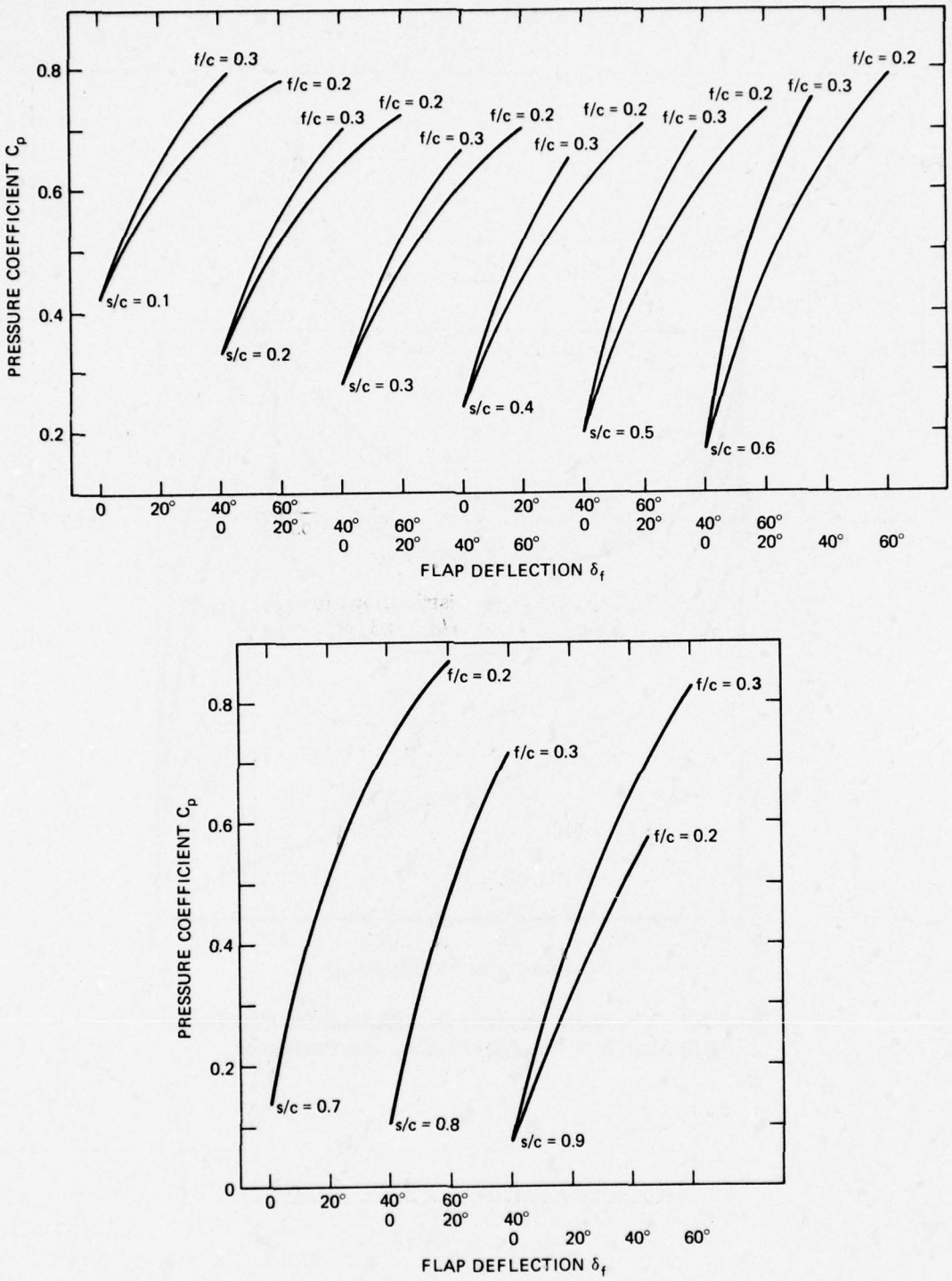

Figure 23 – Cross Curves of Pressure Coefficient Against δ_f with s/c as a Parameter; $\alpha = 10°$, f/c = 0.2 and 0.3

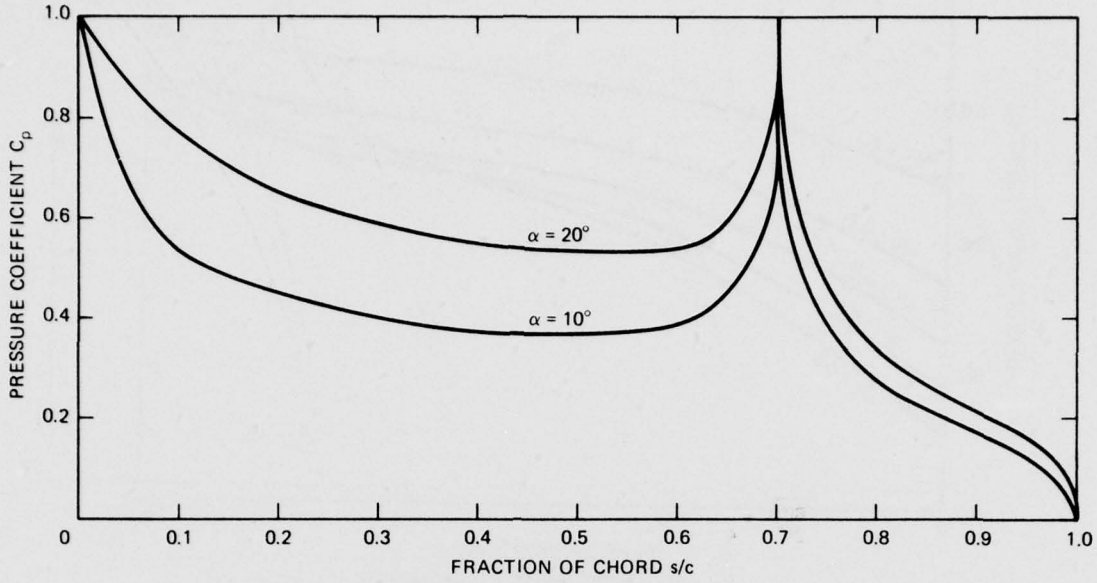

Figure 24 – Chordwise Pressure Distributions for Flat Plate with Flap; $\alpha = 10°$ and $20°$, f/c = 0.3, $\delta_f = 8.25°$

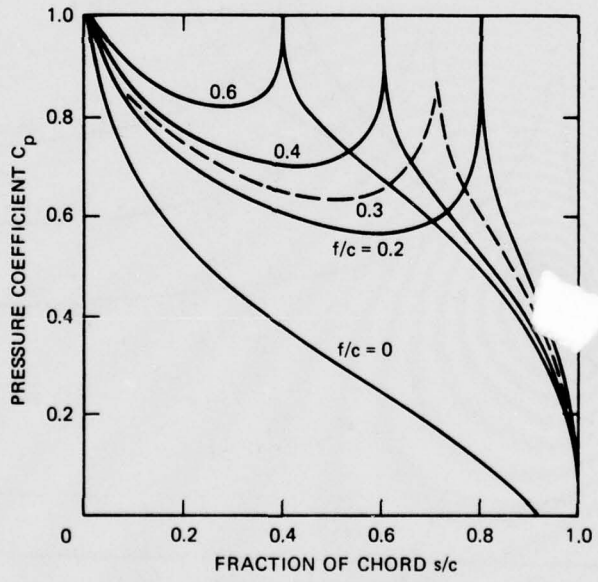

Figure 25 – Chordwise Pressure Distributions for Flat Plate with Flap; $\alpha = 20°$, $\delta_f = 20°$, f/c as a Parameter

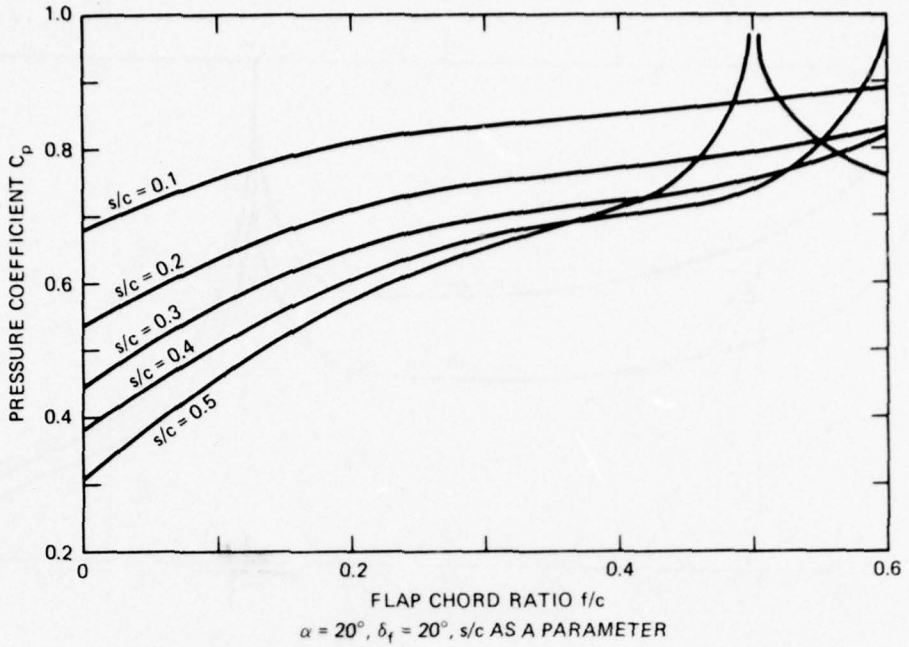

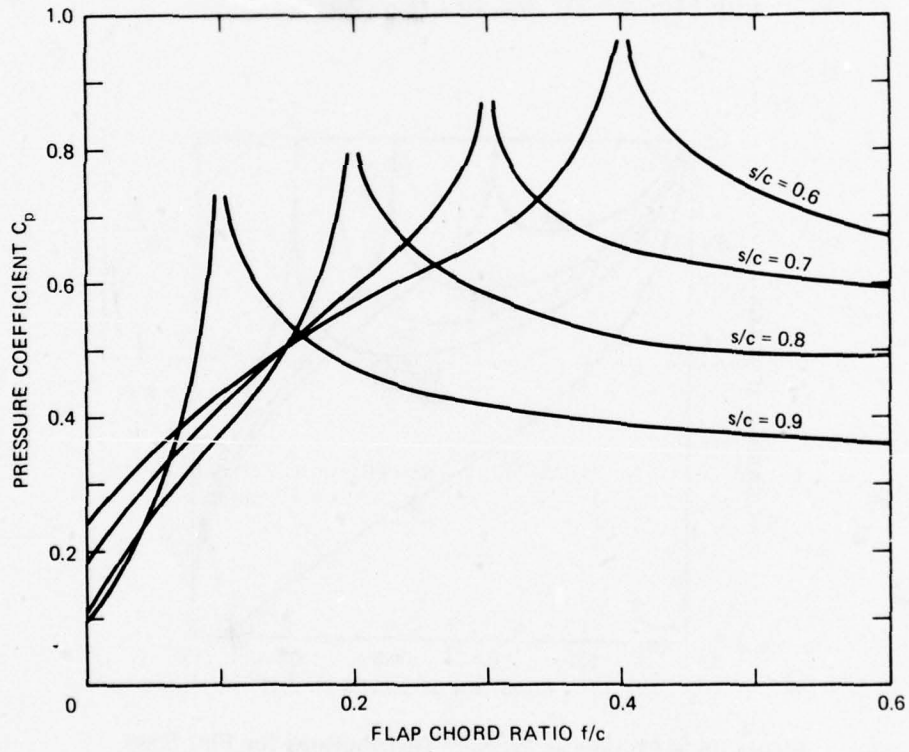

Figure 26 – Cross Curves of Pressure Coefficient Against f/c with s/c as a Parameter; $\alpha = 20°$, $\delta_f = 20°$

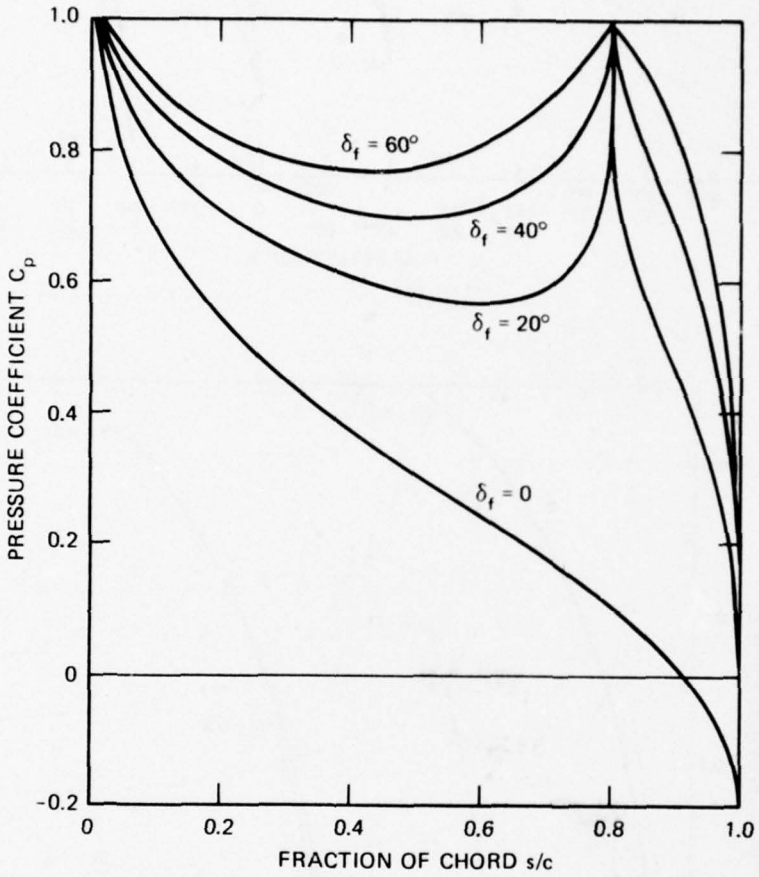

Figure 27 – Chordwise Pressure Distributions for Flat Plate with Flap; $\alpha = 20°$, f/c = 0.2, δ_f as a Parameter

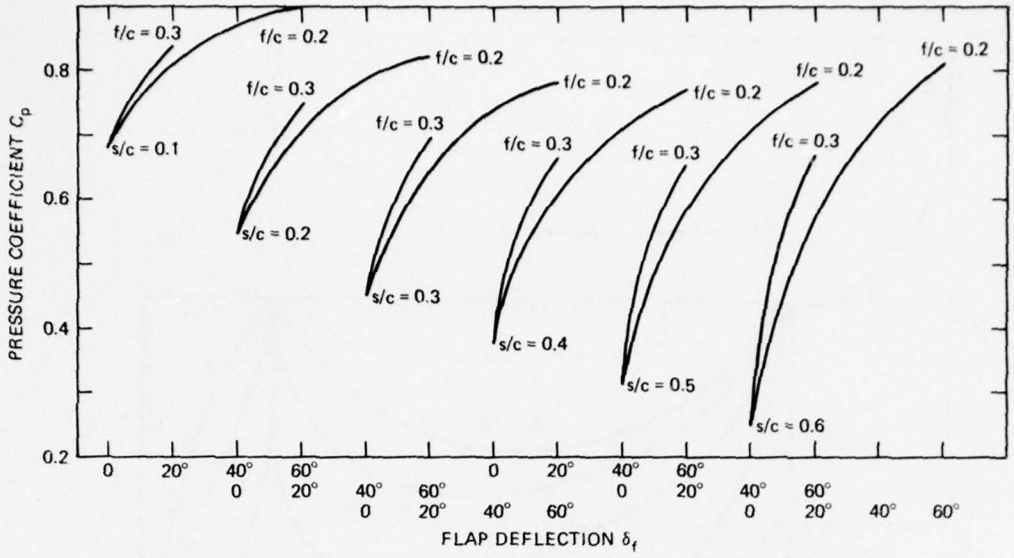

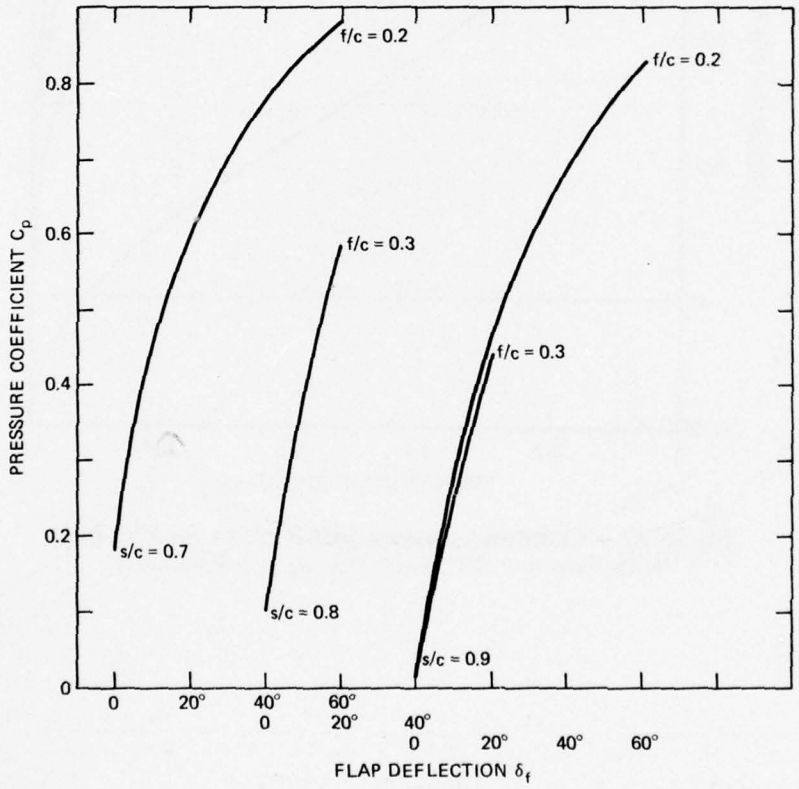

Figure 28 – Cross Curves of Pressure Coefficient Against δ_f with s/c as a Parameter; $\alpha = 20°$, f/c = 0.2 and 0.3

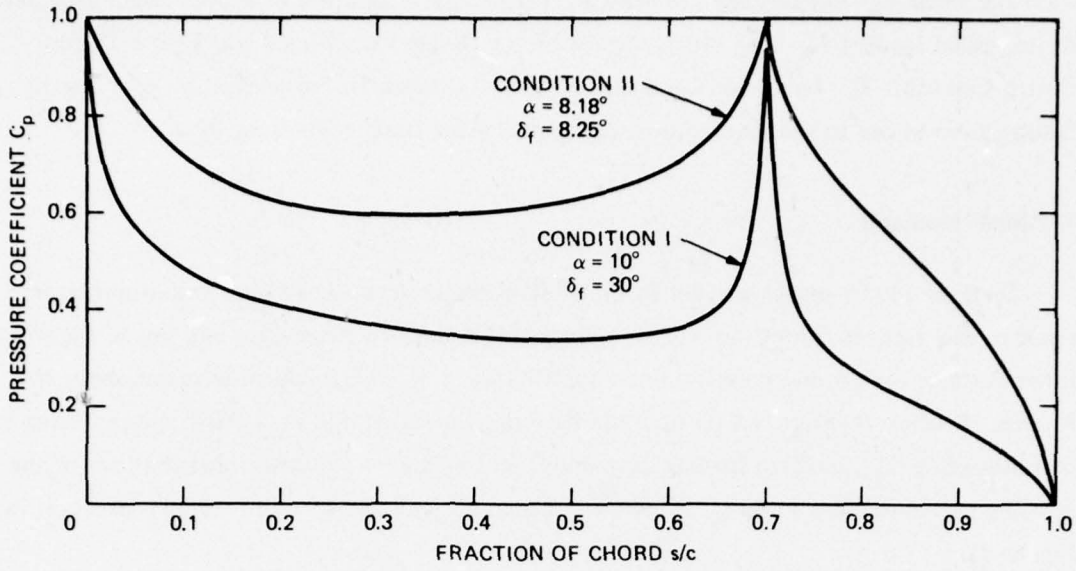

Figure 29 – Chordwise Pressure Distributions for Flat Plate with Flap; f/c = 0.3, Design Conditions I and II

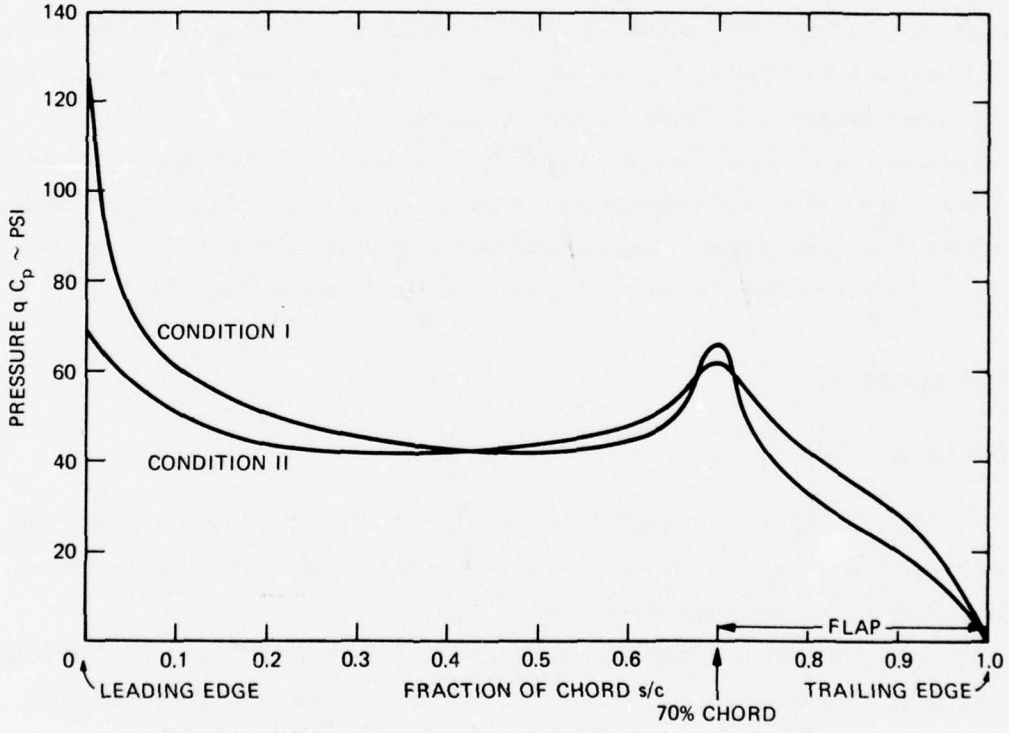

Figure 30 – Basic Chordwise Pressure Distributions

The shear V'_X and bending moment M'_Z derived by integration of the spanwise distribution of tangential loading w'_X is shown in Figure 18 for Design Condition I and Figure 19 for Design Condition II. Loads for Condition III and Condition IV are derived by applying the factors given above to the loads shown in Figure 19 for Design Condition II.

Torsional Moments

Sections cut by planes parallel to the X'-Z' plane are considered here and attention is given to the moment about the Y' axis. Since this is the flap hinge axis, and lies in the foil lower surface, the normal pressure alone contributes to T'_Y the torsional moment about the Y' axis. Because it is not certain how the flap hinge moment will be carried, the moments of foil loading T'_{Y1} and flap loading T'_{Y2}, are given separately. Spanwise distributions of the pitching moments M'_{Y1} and M'_{Y2} are given in Figure 31 and the section torsional moments in Figure 32.

Chordwise Bending Moments

Because of the thinness of the foil at and near the leading edge, and the occurrence of peak pressure loading at the leading edge, there is concern for the adequacy of the bending strength of the foil in this region. The foil is considered cut by normal planes intersecting the foil plane along lines of constant percent of chord.

Chordwise moments of the external loading about lines of constant percent of chord have been calculated for chordwise strips of unit width. Because of the assumed variation of chordwise pressure distribution along the span of the foil it has been possible to express the chordwise bending moment on all strips of unit width as shown in Figure 33.

STRUT LOADING

Design Loads

The strut is subjected to local loads applied at its lower end, at the foil attachment, and to hydrodynamic pressure and friction forces over its submerged length. The former are derived from the foil loads data given above.

The strut side loading is taken as zero for Design Conditions I, II, and IV. For Design Condition III an average strut side loading of 1800 psf is applied as discussed previously.

The strut side loading is taken acting to starboard so that the resulting bending moment at the top of the strut is added to that resulting from the asymmetric foil loading. A trapezoidal variation of the side load is assumed, as shown in Figure 34, which puts the center of side load 55 percent of the wetted length below the water surface. The chordwise center of pressure is assumed to be at 25 percent of the chord from the leading edge of the strut.

For Design Conditions I, II and IV the strut drag force lies in the plane of symmetry (X-Z plane). A drag coefficient of 0.02 (based on "planform area") was taken from Figure 18 of Reference 9 for zero side slip. The drag is assumed to be uniformly distributed along the submerged length of the strut, giving a resultant drag force applied 5.0 feet below the water surface. Total strut drag is 18,600 pounds in Design Condition I and 10,500 pounds in Design Condition II and IV.

In Design Condition III the strut is assumed to be operating with a side slip angle just sufficient to produce the maximum attainable preventilation side force. From the reference cited above it appears that the corresponding drag coefficient may be substantially higher. Resolution of forces into the plane of the strut indicates that the component of force in the X direction will be not much greater than the drag in Design Condition II. Consequently an X force of 10,500 pounds was used for Design Condition III.

Strut Shear, Bending and Torsion Loads

The loads at the upper and lower ends of the strut are summarized in Table 4. Their derivation is discussed in the following.

Loads at the bottom of the strut are referred to a primed frame of reference with origin in the plane of the foil lower surface at the 70 percent chord line on the centerline. The X axis is the intersection of the plane of symmetry with the foil lower surface, the Y axis is along the 70 percent chord line of the foil and the Z axis is normal to the foil lower surface. See Figures 2 and 15.

Loads at the top of the strut are referred to a frame of reference with the origin at the top of the strut and on the axis of the king post. These are "ship axes" with the X axis parallel to the keel, positive forward, and the Z axis positive downward. At the lower end of the strut the dominant load is the rolling moment M'_X due to unsymmetrical foil loading in Design Condition IV. As noted earlier this is 0.8 times the maximum foil root bending moment which occurs in Design Conditions I and II. Along with this bending moment there is a yawing moment or torque Q'_Z equal to 0.8 times the corresponding moment M'_Z for Design Condition II given in Figure 19. The pitching moment M'_Y, while large in Design Condition I is not expected to present any serious design problems.

TABLE 4 – SUMMARY OF STRUT ATTACHMENT LOADS (LIMIT)

LOCATION	CONDITION	V_X (LB)	V_Y (LB)	F_Z (LB)	M_X (IN. LB)	M_Y (IN. LB)	T_Z (IN. LB)
UPPER END OF STRUT (KING POST)	I	58,880	0	335,871	0	14,780,000	0
	II	81,180	0	333,400	0	19,300,000	0
	III	52,970	94,200	200,200	9,638,000	11,930,000	92,720
	IV	17,450	0	133,400	3,917,000	7,330,000	506,100
		V'_X * (LB)	V'_Y (LB)	F'_Z (LB)	M'_X (IN. LB)	M'_Y (IN. LB)	T'_Z (IN. LB)
LOWER END OF STRUT (FOIL ATTACHMENT)	I	12,800	0	338,000	0	5,550,000	0
	II	43,600	0	338,000	0	4,770,000	0
	III	26,200	0	203,000	1,170,000	2,860,000	152,000
	IV	17,450	0	134,400	3,917,000	1,910,000	506,100

*Loads at lower end of strut are referenced to axes in the foil chord plane with the origin at the intersection of the foil centerline and the 70 percent chord line. See Figure 15.

Maximum lateral bending over the lower 74 inches of the strut occurs in Design Condition IV and is constant over that length. For the upper 70 inches of the strut the maximum bending moment M_X results from the combination of asymmetric foil loading and strut side loading in Design Condition III. The corresponding load, shear and bending moment are shown in Figure 34.

Figure 35 shows the spanwise distribution of the torque Q_Z of the strut side load about the king post axis. The resulting internal torque Q_Z on any section of the strut is also shown in this figure.

The maximum bending moment at the top of the strut occurs in Design Condition II, principally because of the high drag in this condition and the more rearward center of lift due to the large flap deflection.

In Design Condition III the combined bending moment, resulting from simultaneous pitching and rolling moments, is 15,300,000 pound-inches. The associated shear of 108,000 pounds is a maximum.

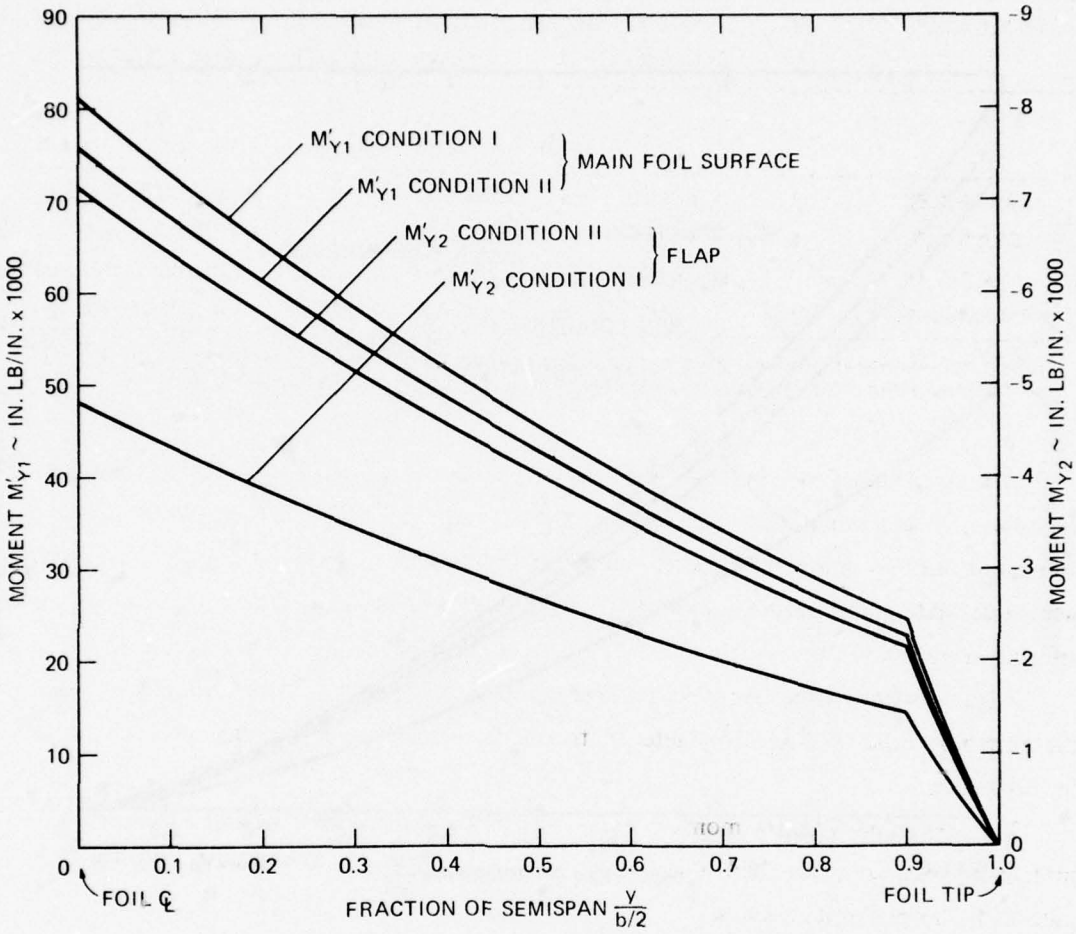

Figure 31 – Spanwise Distributions of Foil and Flap Pitching Moments

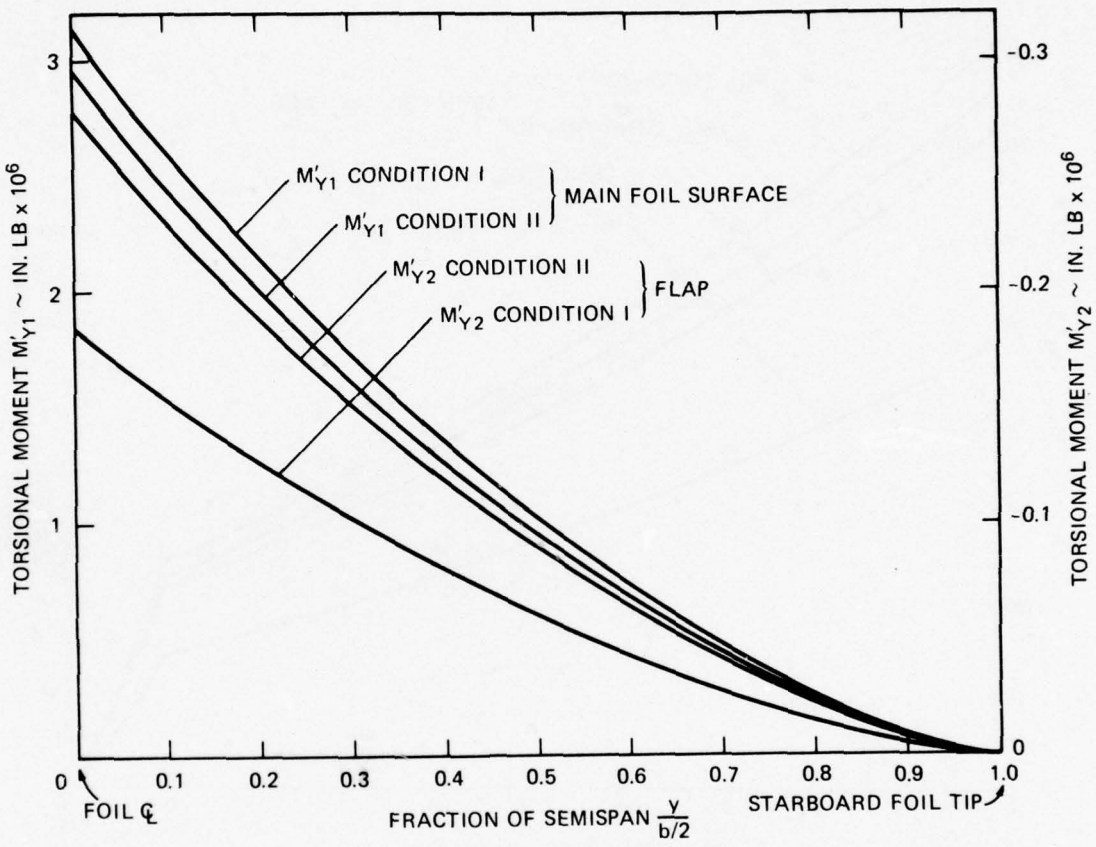

Figure 32 – Foil and Flap Torsional Moments

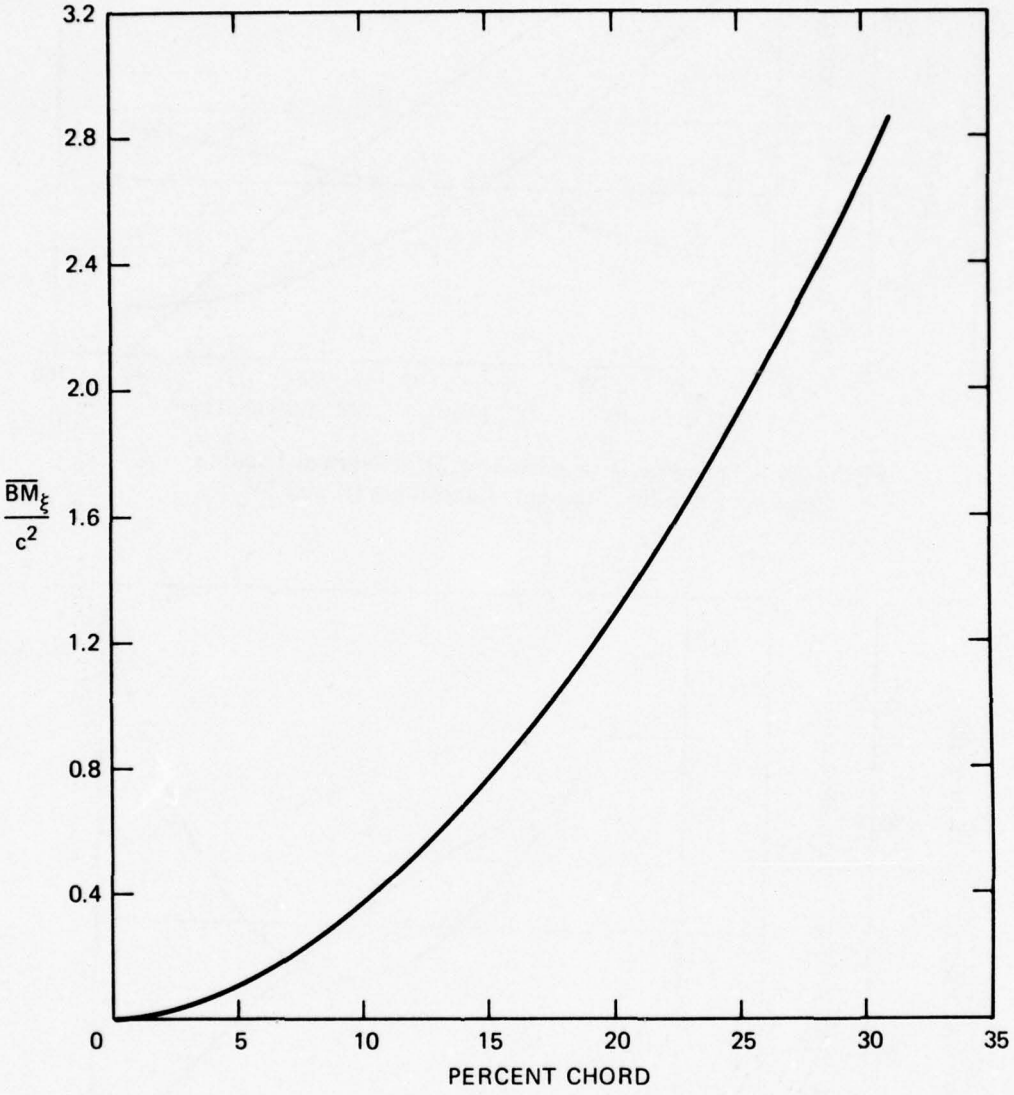

Figure 33 – Foil Chordwise Bending Moment

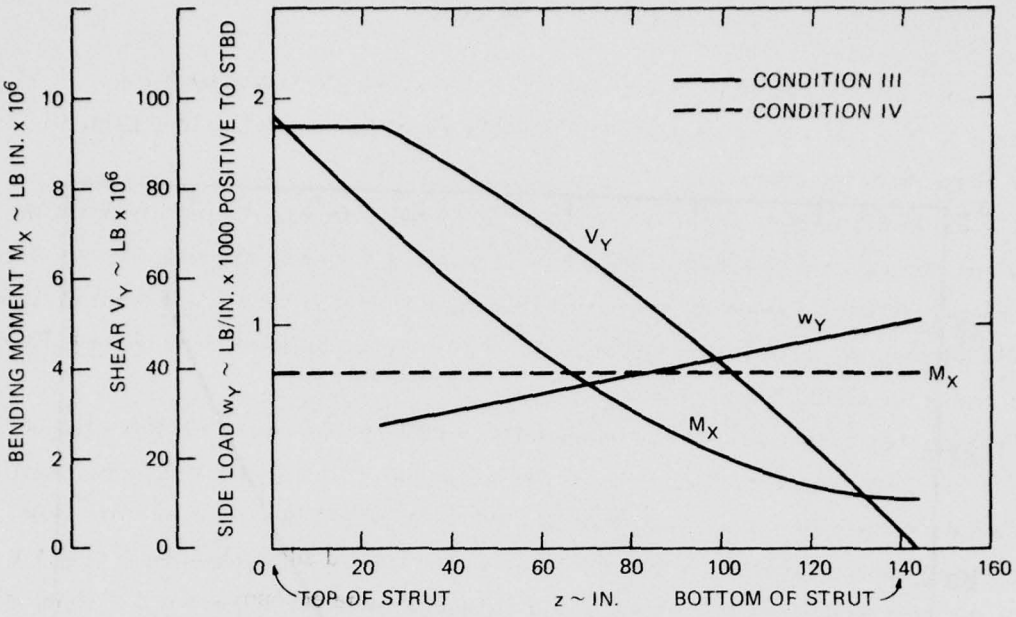

Figure 34 – Spanwise Distribution of Strut Normal Loading, Shear and Bending Moment, Conditions III and IV

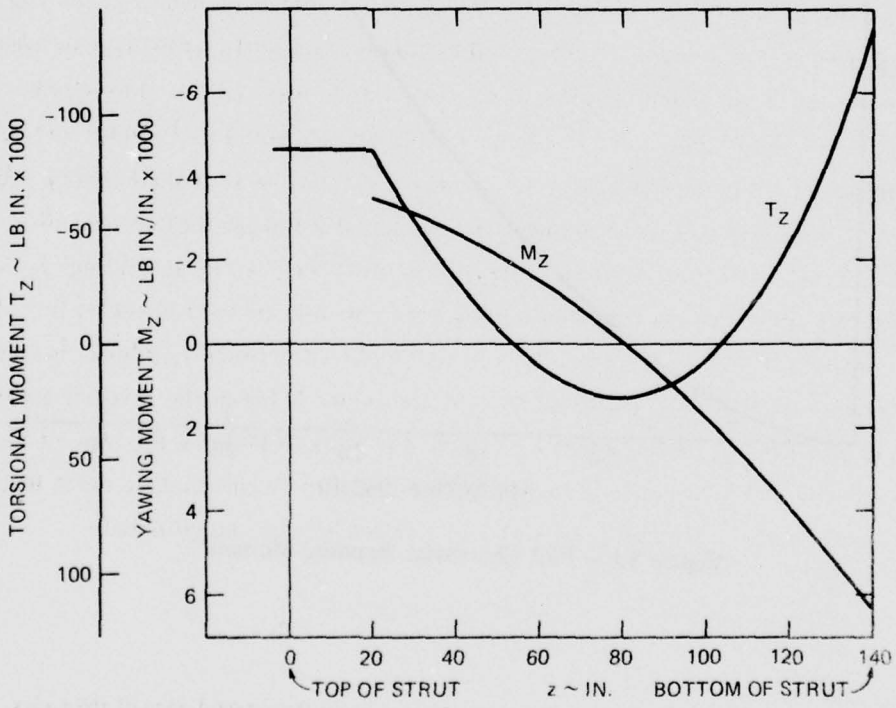

Figure 35 – Spanwise Distribution of Strut Torsion Loading, Condition III

CONCEPT DESIGN

The conceptual design of the TAP-1 foil and strut (see Figure 1) is described in Reference 1. The following is a summary of the findings of Reference 1 as they apply to critical elements of the design.

The foil leading edge structure is solid from the leading edge back to approximately the 30 percent chord point*. Because of the relatively thin foil section in this area, use of a solid section was considered reasonable from a structural weight point of view. As a result of using a locally solid section no difficulty was experienced in carrying chordwise bending loads back to the main structural box.

Spanwise bending stresses are maximum immediately outboard of the machined forging which forms the center of the foil. A simple beam bending stress estimate which conservatively neglected the contribution to spanwise bending strength of all but the center box structure resulted in an applied stress which was well below the designated allowable stress. As in the case of the leading edge structure no significant difficulties were encountered in withstanding the applied loads with reasonable structural proportions.

The most challenging design problem was found to be associated with the flaps both in terms of their own structure and in terms of their influence on foil structure. The flaps were originally conceived as being supported by a torque tube running the length of the foil semispan. However, the available depth of foil section was found to be inadequate for this purpose; moreover the torsional wind-up of the torque tube was considered excessive. The final conceptual design as illustrated in Figure 1 featured segmented flap elements (to prevent binding due to foil deflections) which were connected by shear pins at their trailing edges for purposes of transmitting flap hinge moments to the actuator linkage located near the center-line of the foil. The foil itself features heavy ribs between the flap hinge bearings to carry chordwise shears and moments from the trailing edge structure to the foil center box structure. While not apparent in Figure 1, plate segments are employed between flap hinge bearings on the lower surface to provide at least intermittent continuity between the cover plates of the foil ahead of and behind the flap hinge line. This was done to preserve the over-all torsional rigidity of the foil and help preclude flutter. (Note: no flutter checks were made in this particular design study). See Figures 4 and 5 of Reference 1 for design details.

*The reference chord in this study extends from the leading edge to the forward edge of the annex. The over-all chord is therefore greater than the reference chord.

The foil-to-strut attachment was accomplished using tension bolts which join the foil centerline forging to locally thickened skin at the lower end of the strut. As shown in Figure 7 of Reference 1, shear bolts were also examined as an alternative method of joining the strut and foil.

The conceptual design of the flap actuation linkage is shown in Figure 1. In this case no substantial problems were encountered in withstanding design flap hinge moments.

The king post at the upper end of the strut was found to require a relatively large diameter (14.5 inch O.D.) for the size of strut involved. This was due primarily to the large drag bending moments associated with the flap loads of Design Condition II Maximum Lift at Maximum Elevator Deflection. Based upon this result it was concluded that particular attention would have to be given to providing structural continuity between the king post and the strut proper if a steerable strut were to be employed in an actual design.

Table 5 presents a brief summary of the design loading conditions which were found to be critical for the structural elements discussed above. It will be noted that Design Condition III Maneuvering in High Seas was not a governing design condition for the structural elements considered. If the conceptual design study had included the strut itself, this, of course, would not have been the case. In view of experience with subcavitating foil designs, it was considered unusual that the king post bending moments associated with Condition II were significantly larger than those associated with Condition III. This result is due to the large drag loads associated with a supercavitating foil system in Condition II as well as to the reduced lateral bending moments resulting from asymmetric lift on a low aspect ratio foil in Condition III.

TABLE 5 – SUMMARY OF CRITICAL LOADING CONDITIONS FOR STRUCTURAL ELEMENTS

Structural Element	Critical Loading Condition	Remarks
Foil Leading Edge	Condition I: Maximum Lift at Maximum Speed	High lift at low flap deflection results in highest hydrodynamic loading on foil leading edge.
Foil at Strut Junction	Condition II: Maximum Lift at Maximum Elevator Deflection	Maximum lift same as Condition I. Chordwise loading larger for Condition II.
Flaps and Flap Actuation Linkage	Condition II	Maximum loading on flaps
Lower End of Strut	Condition IV: Foil Reentry	Maximum lateral bending moment - due to extreme asymmetric lift.
King Post	Condition II	Maximum bending moment - due to large drag loads.

FINITE ELEMENT STRESS ANALYSIS OF SOLID FOIL

A solid section, supercavitating foil has been analyzed in the present study. It has been noted in an earlier report (Reference 17) that conventional beam theory is inadequate for predicting the stress-distribution in a supercavitating blade. The application of classical plate and shell theories did not, in general, yield satisfactory results (Reference 18*); some irregular behavior in the computed stress near the leading edge and near the trailing edge remained unexplained. Recently, superior results on stress prediction for supercavitating propellers (References 19 and 20) were obtained by a numerical procedure developed by Ma (Reference 21). The procedure utilizing a finite element displacement model in conjunction with compatible solid elements in their general form is capable of simulating faithfully the correct response of a complex cantilevered blade or foil. Convergence to the true solution is guaranteed. This curved three dimensional finite element program was employed for the present analyses.

The TAP-1 foil has a typical wedge shaped chord section and a chord length which tapers linearly toward the tip.** At its center line the foil receives its support from a generously proportioned strut. The foil and its support are represented by 43 curved solid elements (Figure 36). In the case where the foil annex is included, 49 finite elements are employed. A fine element mesh is adopted at the leading edge and also along the fillet area near the foil/strut interface so that a clear picture of the stress distribution at those structurally critical regions can be observed. Because the actual foil is solid in the areas of greatest interest, to expedite the analysis the foil has been treated as a solid elastic body.

The nodal coordinates for the top and bottom faces of the foil are derived from the structural design layout for the TAP-1 Hydrofoil, supplied by the DTNSRDC Design Engineering Division, Code 294. The X′Y′ plane of the global coordinate system corresponds to the reference foil chord plane with center of the coordinate system located at the 0.7 chord point on the foil center line (see Figure 36). There are a total of 421-X′Y′Z′ coordinate points used in the finite element mesh to model the foil including annex.

Design Condition I, which corresponds to the maximum lift at a speed of 80 knots has been studied because it results in maximum foil bending moments as well as maximum loading on the foil leading edge. The pressure distribution of Figure 37 is input to the program in a linear piecewise fashion over each element surface. An equivalent set of nodal load vectors

*The computer program is based on a helicoidal shell with shallow camber.
**Twist of foil has been removed for structural load and stress analysis purposes.

(having 178 loading points) is generated where equivalence is based on work done through elastic deformation. A condition of support is realized by imposing a set of displacement constraints placed over elements No. 39 thru No. 43, for the basic foil configuration. Applying the principle of minimum potential energy, a system of equilibrium equations (1263 - 78 = 1185 equations) was set up and solved for displacements. Stresses referenced to the global coordinate direction (X'Y'Z') and the local surface coordinate (i.e. parallel and normal to constant-percentage chordlines) as well as principle stresses are subsequently calculated at 45 distinct positions in each element space. (Note: computation time on the CDC 6600 machine for the basic foil configuration is a little over 5 minutes (CPA - 320 sec).)

A maximum vertical deflection of 0.57-in. takes place at the leading edge of the foil tip. (See Figure 38). As expected, maximum deflections in the X' and Y' direction are smaller and on the order of 0.03 in. and 0.02 in. respectively. Some typical foil stress distributions at 25, 51 and 80 percent of semispan (measured along the Y' axis) are shown in Figures 39, 40 and 41.

For locations at 50 percent of the semispan and beyond, chordwise bending plays a major role. The chordwise bending stress begins to flatten out and actually decreases slightly at sections toward the center of foil, whereas the spanwise bending rises sharply. (See Figures 42 and 43). The peak spanwise stress occurs, at about 0.7 chord length instead of the trailing edge where the chord section has its maximum thickness. Some locally high stresses occur in the neighborhood of 0.3 chord length of the foil area close to the fillet interfacing with the strut (for instance at element no. 28). The inclusion of the foil annex generally lowers the foil stress, particularly the stress in the spanwise direction. Reduction in foil deflection (about 10 percent) is also observed (see Figure 38).

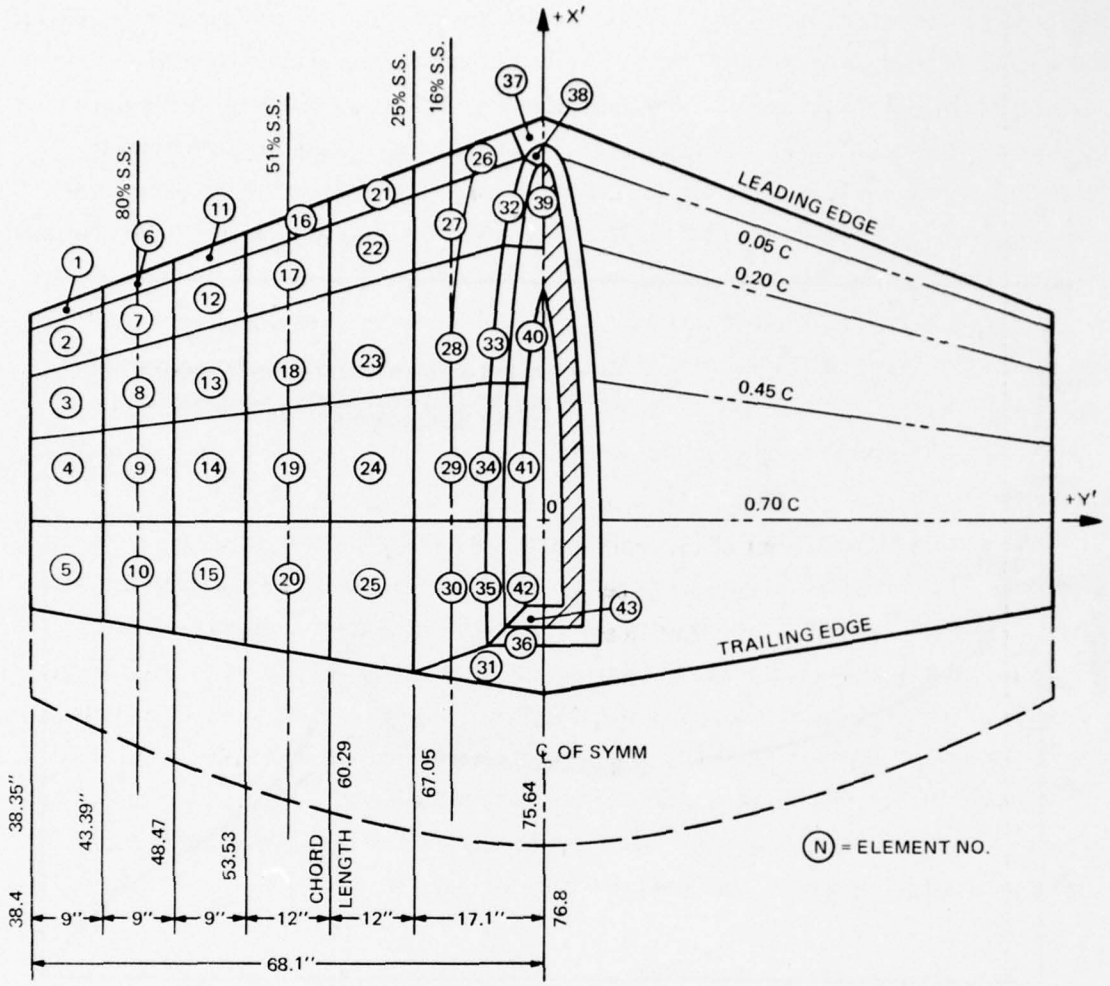

BASIC FOIL CONFIGURATION

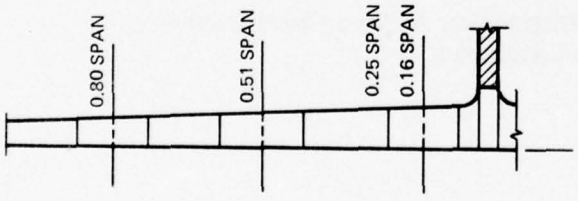

SEMISPAN SECTION ALONG OY-AXIS

Figure 36 – Finite Element Mesh for TAP-1 Foil and Strut

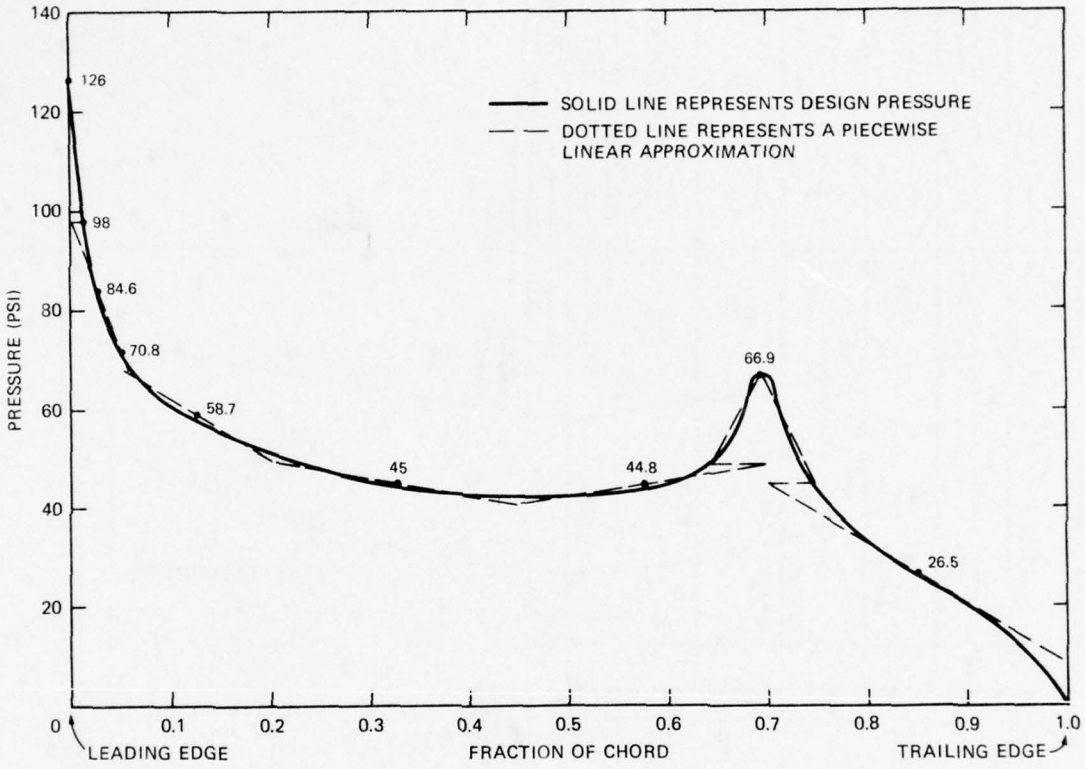

Figure 37 – Typical Pressure Distribution Across a Chord Section, Design Condition I

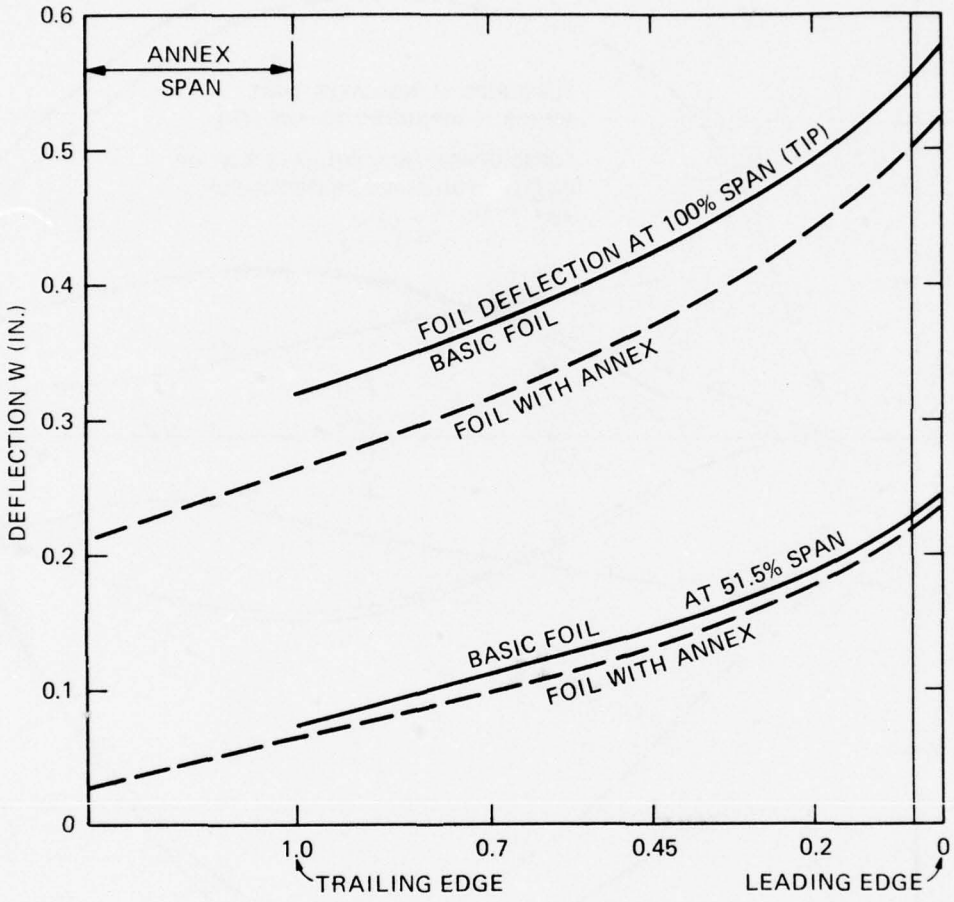

Figure 38 – Vertical Deflection of Solid Foil Span for Load Condition I

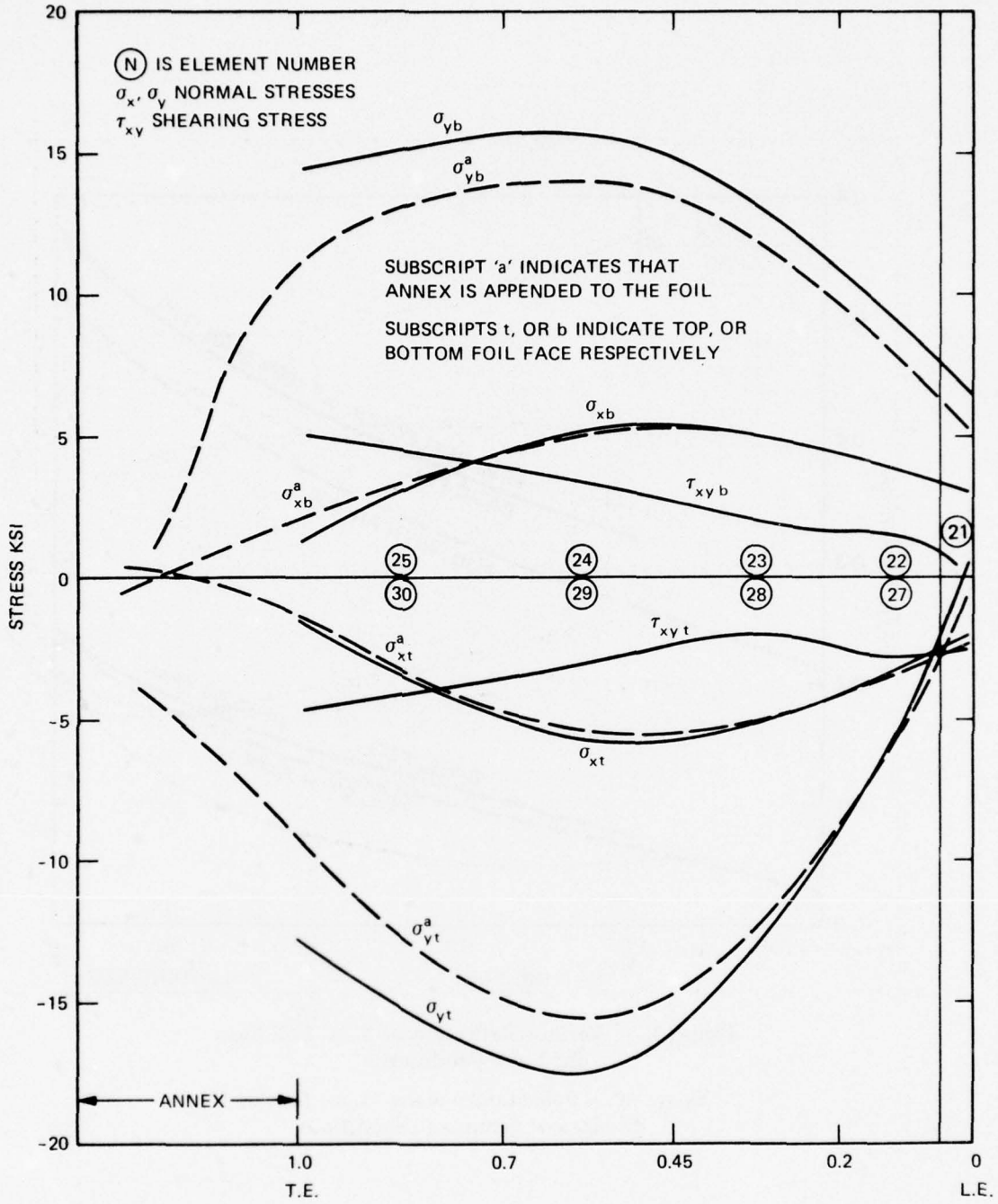

Figure 39 – Foil Stresses along Chord Section, 25 Percent Semispan, Top and Bottom Faces (Solid Foil)

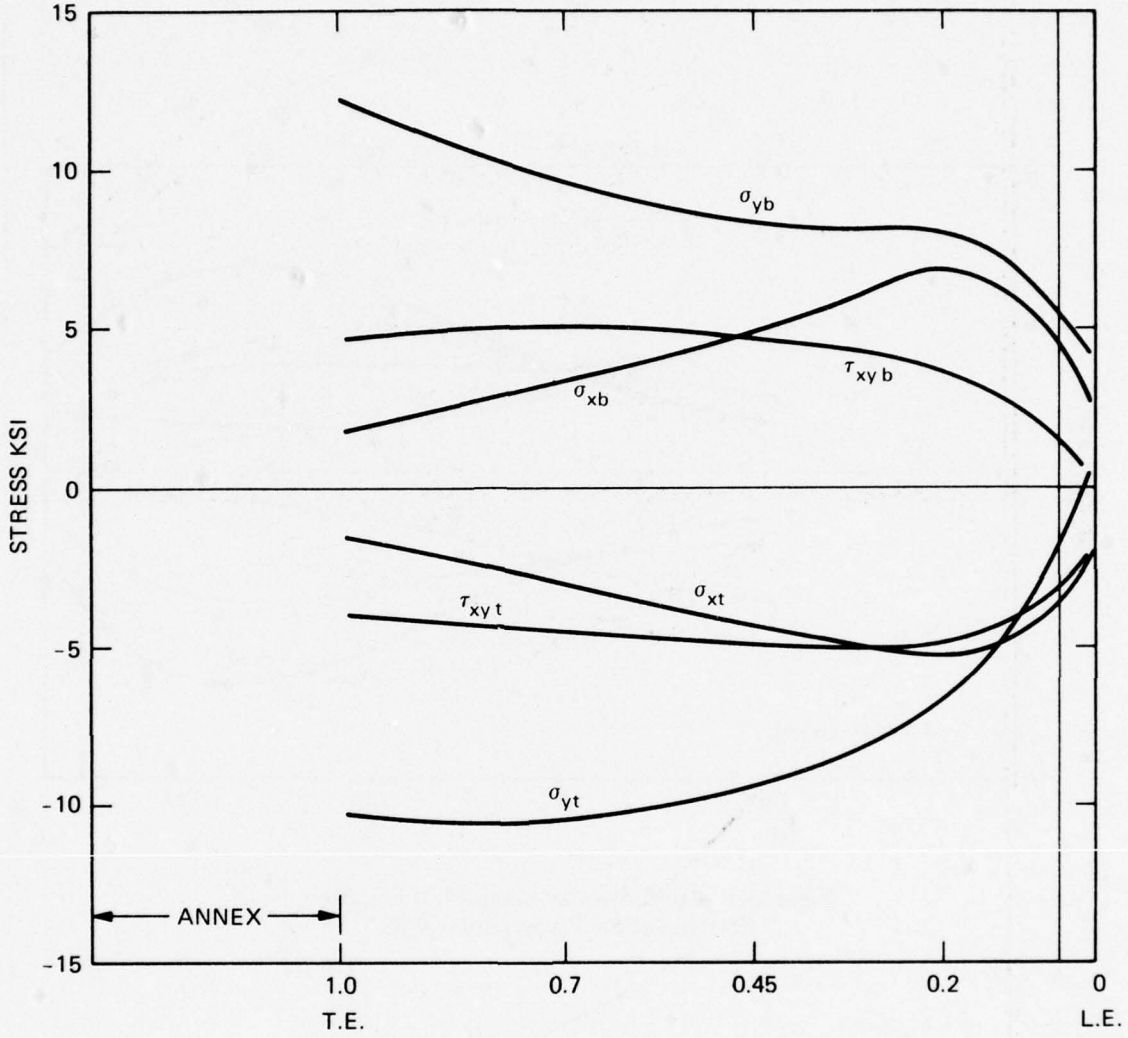

Figure 40 – Foil Stresses along Chord Section, 51 Percent Semispan (Solid Foil)

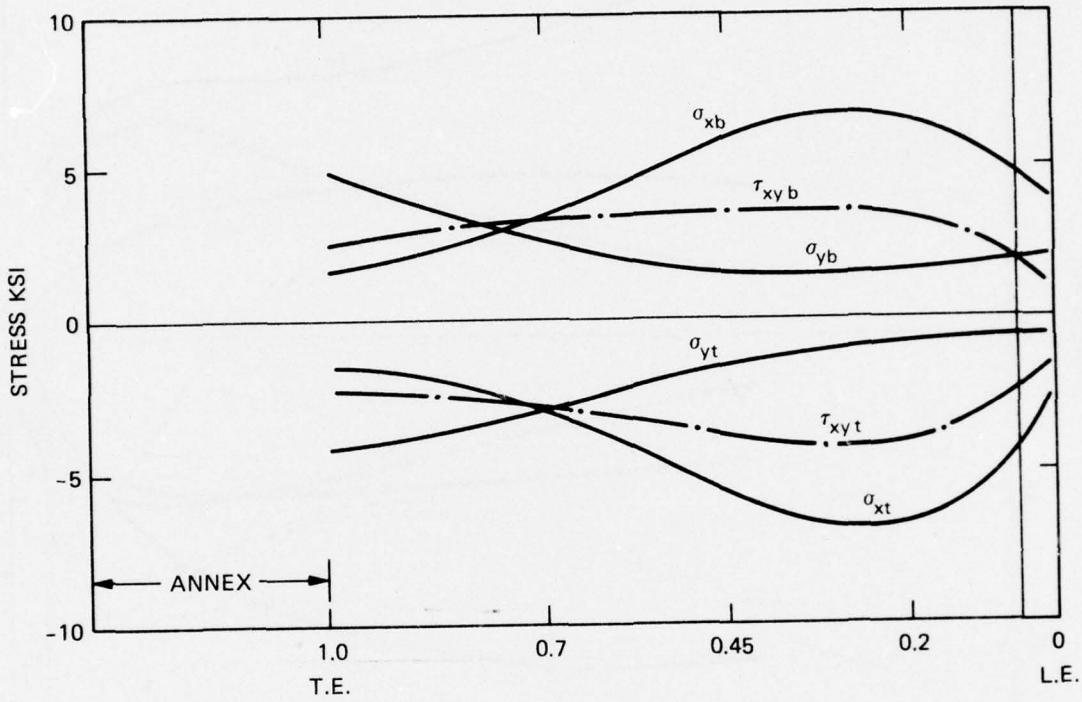

Figure 41 – Foil Stresses along Chord Section, 80 Percent Semispan (Solid Foil)

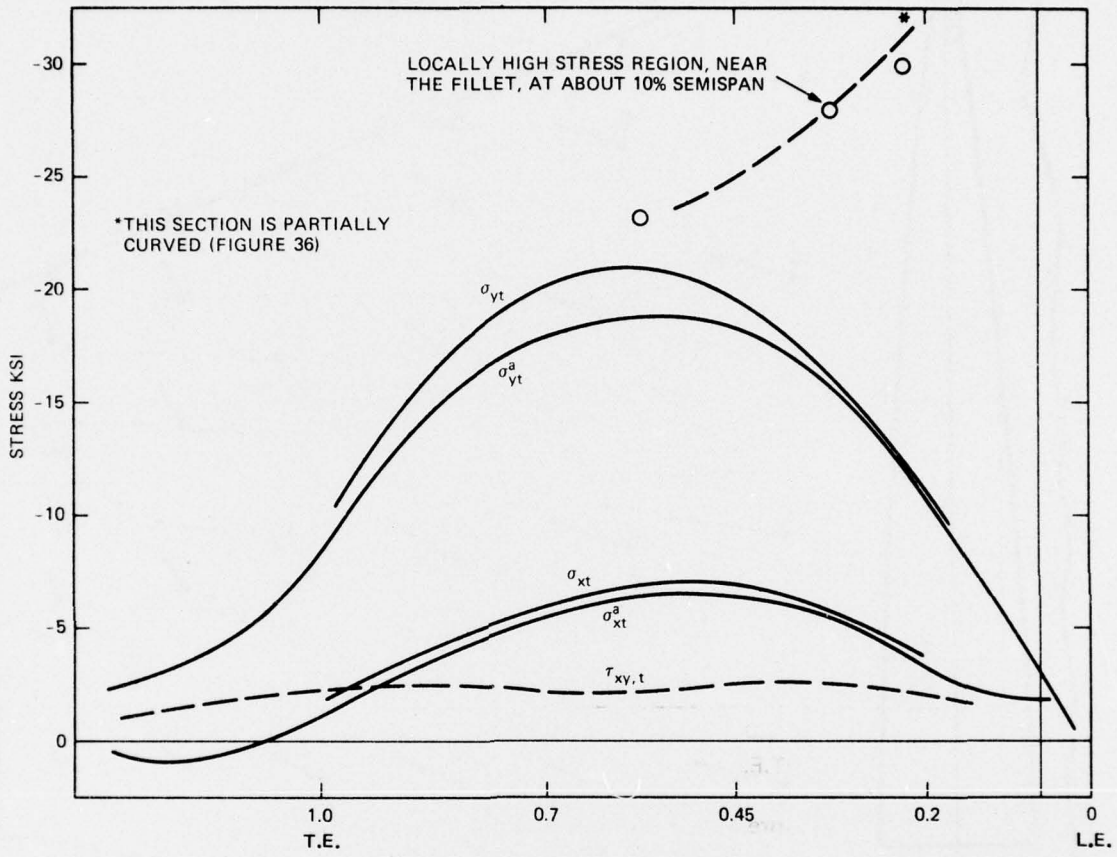

Figure 42 – Foil Stresses along Chord Section, 16 Percent Semispan, Top Face (Solid Foil)

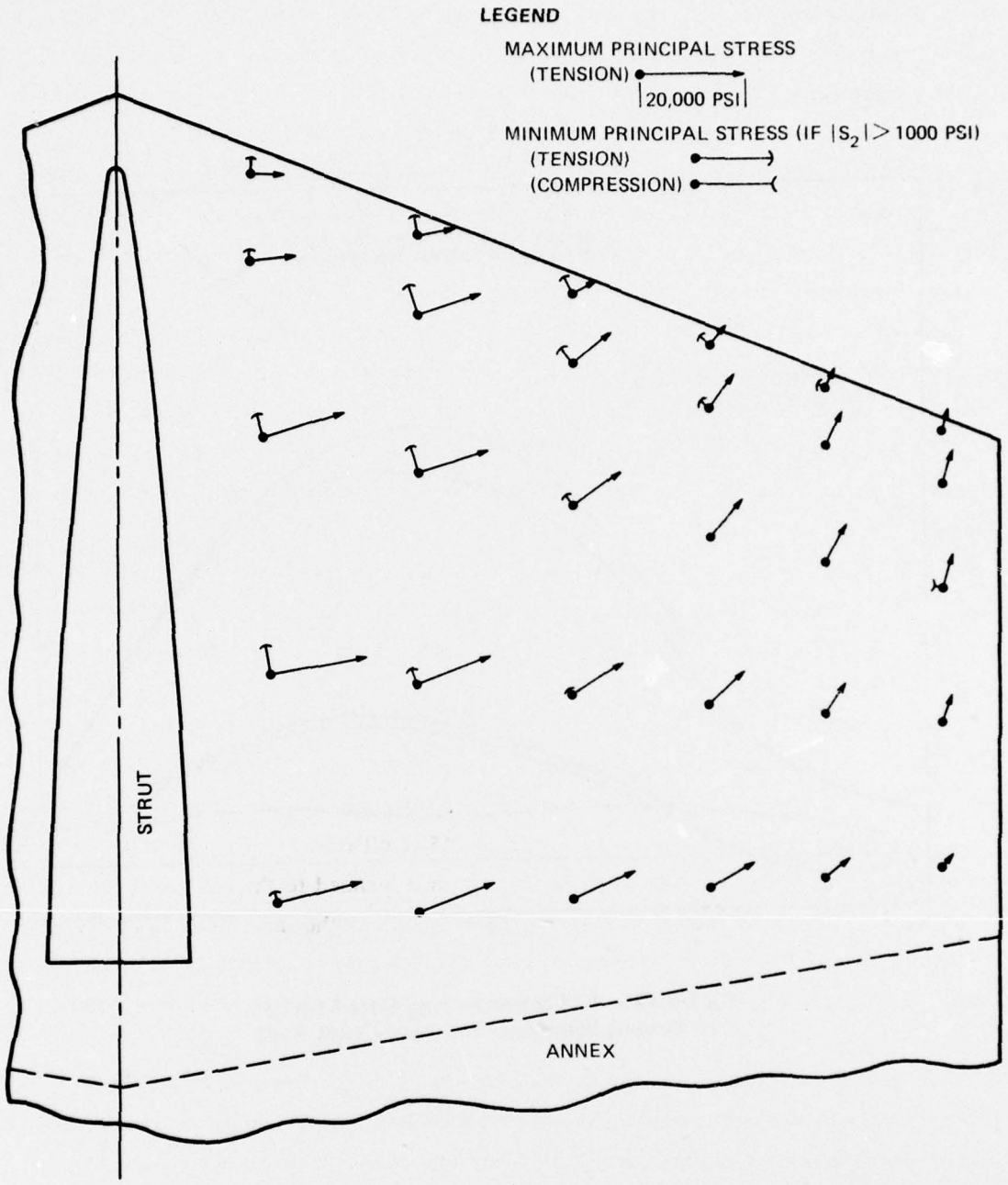

Figure 43 – Bottom Surface Principal Stresses, Design Condition I

COMPARISON OF FINITE ELEMENT AND SIMPLE BEAM STRESSES

Because of the common use of simple bending theory to provide estimates of required structural proportions, a comparison has been made of the more exact finite element stresses available here with those estimated by this simplified approach. The comparison has been made for leading edge and for foil root bending stresses. In the case of the leading edge stress, the inherent redundancy in bending strength has been eliminated by assuming the leading edge cut into chordwise strips which causes hydrodynamic loads to be carried in the chordwise direction only. For spanwise root bending stresses, the foil has been treated as a simple cantilever beam supported along the centerline of the foil.

Results of the finite element analysis include stresses* in the top and bottom foil surfaces in directions perpendicular to constant percent-of-chord lines. These are shown in Figure 44 as a function of the percent of the semispan. Since the bending moments shown in Figure 33, are proportional to the square of the chord and since the section modulus is also proportional to the square of the chord, the cantilever bending stress is constant along lines of constant percent-of-chord.

It is evident from Figure 44 that the stresses calculated by simple bending theory are larger than those derived from the finite element analysis. The simple bending theory thus gives an increasingly conservative estimate of the stress away from the leading edge of the foil.

An important consideration in the structural design of the foil is its bending strength as a cantilever beam extending spanwise from the supporting strut. Stresses have again been calculated by simple bending theory for a section approximately 16 percent of the semispan out from the strut. The stresses shown in Figure 45 result from bending about the centroidal principal axis of minimum moment of inertia, which is inclined to the foil chord plane at an angle of -2.13 degrees. The applied loading is that used for the finite element stress analysis which consists of the pressure distribution of Design Condition I applied to the foil lower surface without regard to the flap. Bending about the second principal axis was found to produce negligible stresses.

Spanwise stresses, σ_y, from the finite element analysis are shown in Figure 45 for comparison with the simple bending stresses. It is evident that the simple bending theory exaggerates the stresses at the trailing edge where the section thickness is greatest. On the other hand the maximum stresses obtained by the two approaches are relatively close.

*These stresses are marked as σ_r.

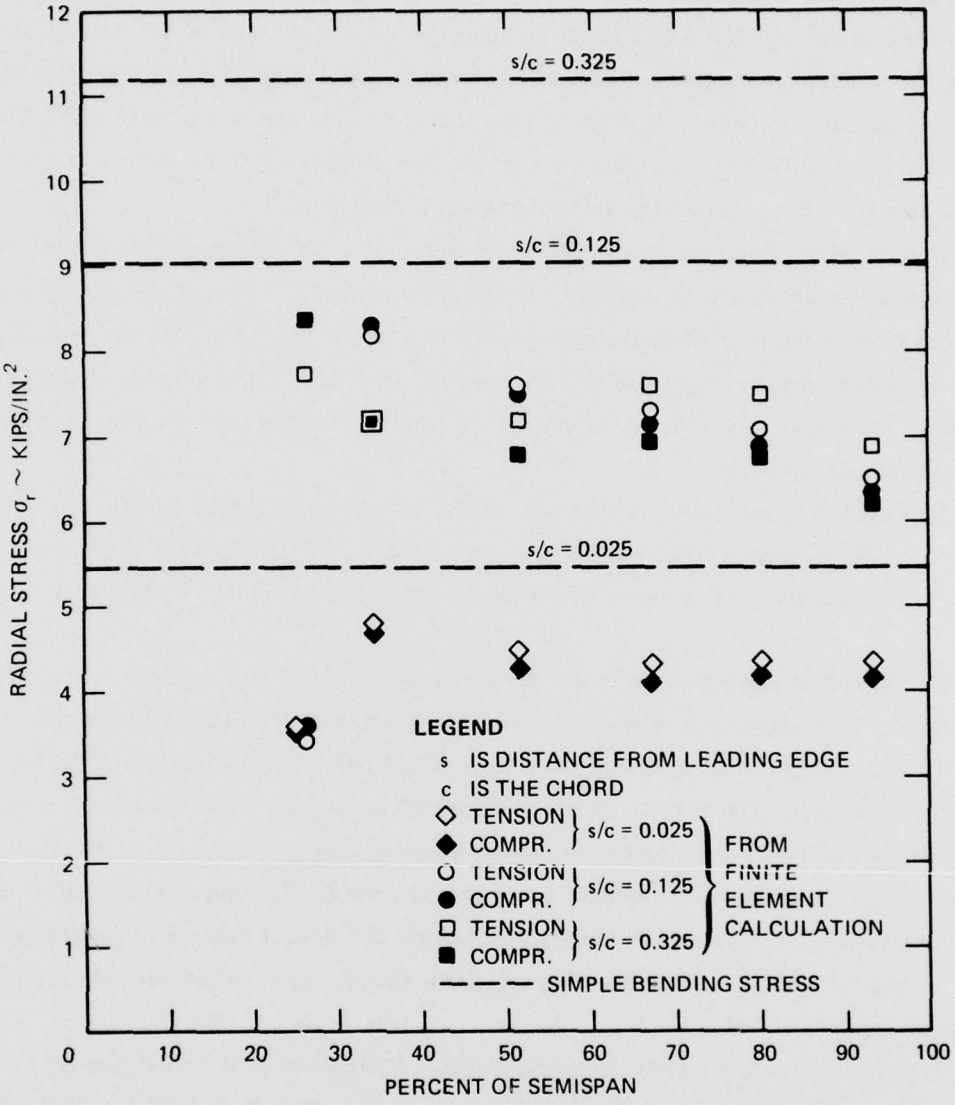

Figure 44 – Foil Chordwise Bending Stresses, Design Condition I

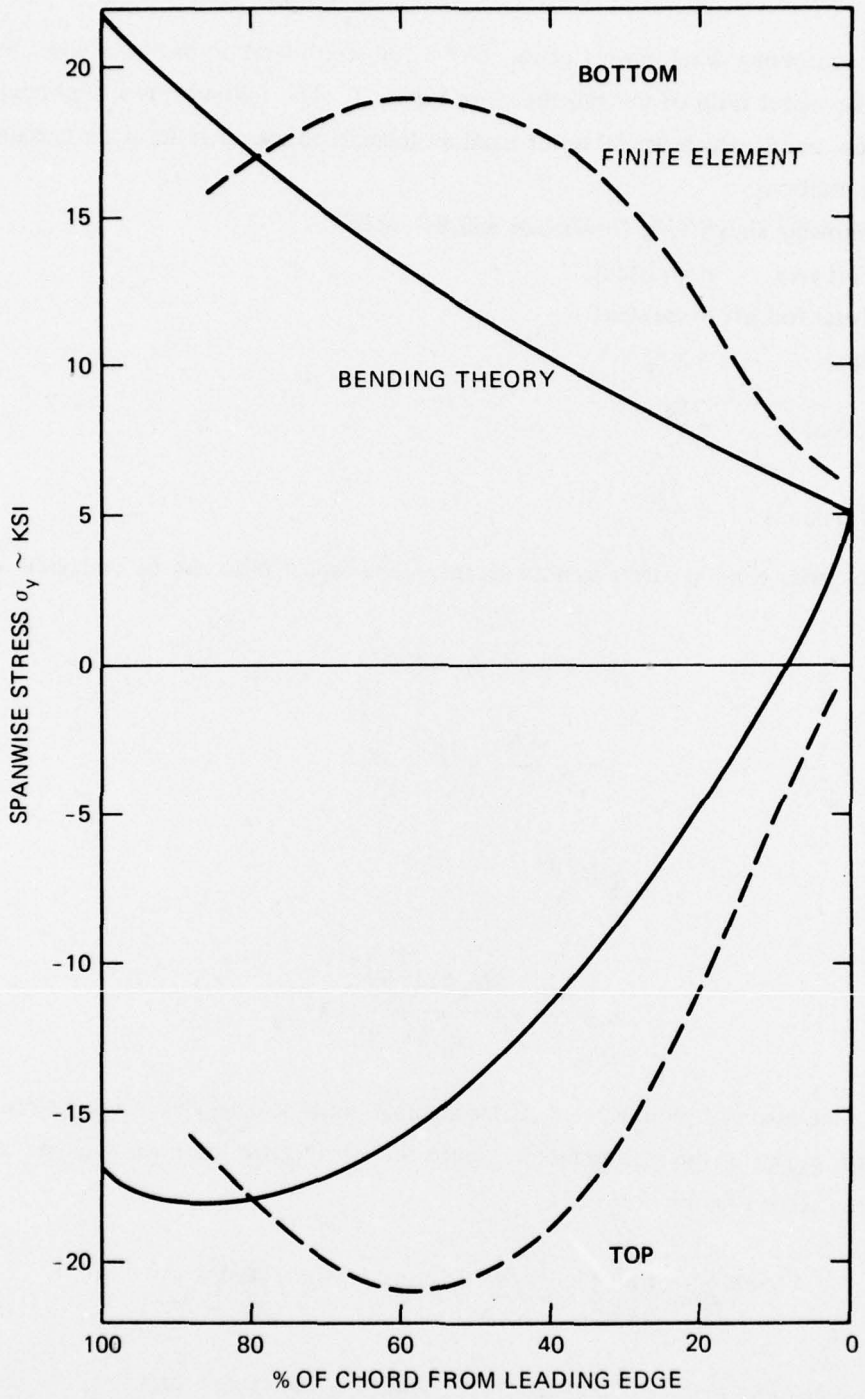

Figure 45 – Foil Spanwise Bending Stress, 16 Percent Span

FOIL BENDING STRESS TRENDS WITH ASPECT RATIO

In the continuing development of the TAP-1 foil, consideration has been given to increasing the aspect ratio of the foil shown in Figure 1. The following is a brief analysis of bending stress trends which would result from an increase in aspect ratio under certain simplified conditions.

The following simplifying constraints will be applied:

Foil area = constant

Total foil lift = constant

Span $= \lambda b_o$

Chord $= \dfrac{c_o}{\lambda}$

Thickness $= \dfrac{2\zeta_o}{\lambda}$

The spanwise bending stress trend with increasing aspect ratio can be evaluated as follows:

$$M = L \times \lambda k_1 b_o = \lambda M_o$$

$$I = \Sigma \frac{\Delta A_o}{\lambda^2} \times \frac{\zeta_o^2}{\lambda^2} = \frac{I_o}{\lambda^4}$$

$$\zeta = \frac{\zeta_o}{\lambda}$$

Then

$$\sigma = \frac{M\zeta}{I} = \frac{(M_o \lambda)\left(\frac{\zeta_o}{\lambda}\right)}{I_o/\lambda^4} = \lambda^4 \sigma_o$$

Thus under the assumed ground rules of linear dimensional scaling, the bending stress increases as the fourth power of the scaling factor. Since the aspect ratio itself will increase as the square of the scaling factor

$$\left(AR = \frac{b^2}{AREA} = \frac{\lambda^2 b_o^2}{AREA} = \lambda^2 AR_o \; ; \; \sigma = \left(\frac{AR}{AR_o}\right)^2 \sigma_o\right)$$

the spanwise bending stress will increase as the square of the aspect ratio.

The chordwise bending stress will be considered with the following additional nomenclature.

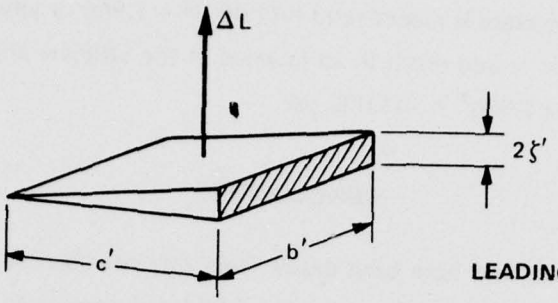

LEADING EDGE ELEMENT

The leading edge element has been assumed to be cut along chordwise vertical planes such that the applied bending moment is carried entirely by the cross hatched section. Again

$$\Delta L = \text{CONSTANT}$$

$$b' = \lambda\, b'_o$$

$$c' = \frac{c'_o}{\lambda}$$

$$M = \Delta L \times k_2 \times \frac{c'_o}{\lambda} = \frac{M_o}{\lambda}$$

$$I = b' \frac{(2\zeta')^3}{12} = (\lambda\, b'_o)\left(\frac{2}{3}\right)\left(\frac{\zeta'_o}{\lambda}\right)^3 = \frac{I_o}{\lambda^2}$$

$$\zeta' = \frac{\zeta'_o}{\lambda}$$

Then

$$\sigma = \frac{M\zeta'}{I} = \left(\frac{M_o}{\lambda}\right)\left(\frac{\zeta'_o}{\lambda}\right)\left(\frac{\lambda^2}{I_o}\right) = \sigma_o$$

The chordwise bending stress will therefore not change with increased aspect ratio under the above ground rules.

For the solid TAP-1 foil investigated in the finite element analysis discussed above an upper limit for foil aspect ratio based upon the stated scaling assumptions can be estimated. Referring to the spanwise bending stress data of Figure 45, an effective foil root stress of approximately 25,000 psi will be assumed under limit load. The ultimate allowable stress is 145,000 psi (see Reference 1). The permissible scale factor is then $\sqrt[4]{\frac{145{,}000}{37{,}500}} = 1.402$

and the corresponding increase is aspect ratio = $(1.402)^2 = 1.966$ or approximately 2.0. Thus a doubling of aspect ratio would result in an increase in the ultimate applied bending stress from 37,500 to $37,500 \times 1.966^2 = 145,000$ psi.

CONCLUSIONS

The following conclusions have been drawn from this investigation:

1. The conceptual design developed for the TAP-1 foil appears to be feasible from a structural point of view. The most significant difficulty encountered in design was associated with the recessed flap which presented problems in structural continuity both within the flap and within the foil.

2. In order to avoid design of the foil for structural loadings associated with full control surface deflections at all speeds, as in the case of subcavitating foils, it was assumed (as one alternative) that hinge moment limiting would be employed to preclude full flap deflection at the maximum design speed. With regard to strut design, the drag loads associated with the TAP-1 supercavitating foil are higher than normally encountered with a subcavitating foil of the same lift capability.

3. Under the critical limit load stress analysis of the solid foil, by finite element methods, indicates maximum stresses about 1/3 of the allowable stress. The stresses are a maximum in the fillet at the strut/foil juncture and decrease progressively toward the foil tip. These circumstances suggest, in general, that appreciable weight can be saved by hollowing the structure.

4. Calculation of spanwise bending stresses by simple beam bending theory yields maximum values in substantial agreement with the results of the finite element analysis for the solid section foil. The chordwise location of the maximum stresses is somewhat different, however, near the root of the foil.

5. Calculation of chordwise bending stresses near the leading edge of the foil, by simple beam bending theory, yields stresses higher than those given by the finite element analysis especially beyond about 15 percent of the chord. Thus the simple bending analysis may be conservatively applied for preliminary design.

6. The aspect ratio of the solid TAP-1 foil stress analyzed by the finite element technique could be increased by a factor of approximately 2.0 without exceeding the assumed ultimate allowable stress of 145,000 psi.

RECOMMENDATIONS

The following recommendations are offered as a result of this investigation:

1. More hydrodynamic data should be obtained for structural design purposes under conditions of maximum lift and drag. This applies to both pressure distribution and gross load (C_L, C_D, C_m, C_{M_F}, etc.) data.

2. In the conceptual design of any future supercavitating foil emphasis should be placed on the impact of flap installation requirements early in design.

3. Since no flutter checks were made during this investigation, it is advisable to have such analyses performed to assure adequate rigidity of the conceptual design developed herein.

ACKNOWLEDGEMENTS

The authors wish to express their appreciation to Mr. Albert P. Clark for his development of the conceptual design of the TAP-1 foil and to Dr. Young T. Shen for his over-all direction of the study.

REFERENCES

1. Clark, Albert P., *"Structural Design Concept of TAP-1 Hydrofoil,"* DTNSRDC Central Instrumentation Department Evaluation Reprot No. CID-29-48 (April 1975).

2. Waid, Robert L., *"Experimental Investigation of the BUSHIPS Parent Hydrofoil Model - Lockheed Underwater Missile Facility,"* Final Report, Lockheed Missiles and Space Company, Report LMSC/805568 (DB # U 1354) (Dec 1965).

3. Dobay, Gabor F., *"Hydrofoils Designed for Surface Ventilation - An Experimental Analysis,"* SNAME Hydrofoil Symposium Spring Meeting (1965).

4. Scherer, J.O., and Auslaender, J., *"Experimental Investigation of the 5-inch Chord Model of the BUSHIPS Parent Supercavitating Hydrofoil,"* Hydronautics, Inc., Technical Report 343-1 (March 1964).

5. Spangler, Peter K., *"Performance and Correlation Studies of the BUSHIPS Parent Hydrofoil at Speeds from 40 to 50 Knots,"* DTMB Report 2353 (December 1966).

6. Conolly, A.C., *"Experimental Investigation of Supercavitating Hydrofoils with Flaps,"* General Dynamics/Convair Report GD/C-63-210 (December 1963) (DB # U 1205).

7. Auslaender, J., *"The Behavior of Supercavitating Foils with Flaps Operating at High Speed Near a Free Surface,"* Hydronautics, Inc., T.R. 001-2 (1 July 1969).

8. Rothblum, R.S., Mayer, D.A., and Wilburn, G.M., *"Ventilation, Cavitation and Other Characteristics of High Speed Surface-Piercing Struts,"* DTNSRDC Report 3023 (July 1969).

9. Dailey, Nils P., *"Experimental Investigation of the Ventilation Force Characteristics of One NACA - 16 and Two Blunt-Based Parabolic Surface-Piercing Struts,"* DTNSRDC Evaluation Report SPD-479-H-07 (Nov 1973).

10. Dailey, Nils P., *"Determination of Selected Strut Force and Ventilation Characteristics Using the Rotating Arm Facility,"* DTNSRDC Evaluation Report SPD-479-06 (Dec 1973).

11. Kramer, R.L., *"An Experimental Study of the Ventilation of Blunt-Based Surface-Piercing Struts,"* Lockheed Missiles and Space Company Report No. LMSC/D311609 (Nov 1972).

12. DeYoung, John, and Charles W. Harper, *"Theoretical Symmetric Span Loading at Subsonic Speeds for Wings Having Arbitrary Plan Form,"* NACA Report 921 (1948).

13. Hoyt, E.D., *"Design Criteria for Detail Foil Design (Fully Submerged, Subcavitating Foils),"* Robert Taggart Incorporated, Report No. RT-303(01)01 (Jan 1971) p. III-36.

14. Hoerner, S.F., *"Fluid-Dynamic Drag,"* Published by the author in Midland Park, N.J. (1958).

15. Harrison, Z., and D.P. Wang, *"Evaluation of Pressure Distribution on a Cavitating Hydrofoil with Flap,"* California Institute of Technology Report No. E-133.1 (1965); also, Journal of Ship Research, Vol. 11, No. 2 (June 1967).

16. Meijer, M.C., *"Pressure Measurement on Flapped Hydrofoils in Cavity Flows and Wake Flows,"* California Institute of Technology Hydrodynamics Laboratory Report No. E-133.2 (October 1965).

17. McCarthy, J.H., and J.S. Brock, *"Static Stresses in Wide-Bladed Propeller,"* DTNSRDC Report 3182 (Sept 1967).

18. Westervelt, W.W., and A.S. Dale, *"Expanded Computer Program for Structural Analysis of Marine Propellers,"* Hamilton Standard Division of United Aircraft Corp. Final Technical Report HSER 6174-I (Dec 1972) (For Official Use Only).

19. Ma, J.H., *"Strength Analysis of Propellers Using Finite Element Methods, Part II, Supercavitating Blade,"* presented to Code PM 1731 (21 Mar 1973).

20. Ma, J.H., *"Stresses in Marine Propellers,"* Journal of Ship Research, Vol. 18 (Dec 1974).

21. Ma, J.H., *"Stress Analysis of Complex Ship Components by a Numerical Procedure Using Curved Finite Elements,"* DTNSRDC Report 4057 (July 1973).

22. Wermter, R., and Y.T. Shen, *"A Summary Report of High-Speed Struts and Foils,"* DTNSRDC Report 4779 (1976).

INITIAL DISTRIBUTION

Copies	
1	WES/Library
2	CNO
	1 OP 971
	1 OP 098
2	CHONR
	1 438/R. Cooper
	1 463
1	NRL 2627/Library
11	NAVMAT
	10 MAT 0333/Mr. R.V. Vittucci
	1 Library
7	NAVSEA
	1 SEA 0303
	1 SEA 03221/L. Benen
	1 SEA 031
	1 SEA 03412
	1 SEA 03413
	1 SEA 03423
	1 SEA 03512/Dr. T. Peirce
1	NAVOCEANO 1640
1	USNA/Library
11	NAVSEC
	1 SEC 6034B
	1 SEC 6110
	1 SEC 6114D
	1 SEC 6120
	1 SEC 6128
	1 SEC 6129
	1 SEC 6132
	1 SEC 6136
	1 SEC 6137
	1 SEC 6140B
	1 SEC 6148
2	NOSC
	1 6005/Fabula
	1 2501/Hoyt
9	NAVSHIPYD
	1 CHASN/Library
	1 MARE/Library
	1 PEARL/Library
	1 PHILA/240
	1 PTMSH/Library
	1 BREM/Library
	1 NORVA/Library

Copies	
12	DDC
1	AFFDL/FYS/Olsen
1	LC/SCI & TECH DIV
1	COGUARD/MECH MARINE SAFETY
1	MARD
1	MMA/Library
1	NASA LANGLEY RES CENTER/Library
1	NSF ENGR DIV/Library
1	U BRIDGEPORT/Uram
1	U CAL BERKELEY/Dept Name
1	U CAL Name/Paulling
1	U CAL Name/Wehausen
3	CIT
	1 Acosta
	1 Plesset
	1 Wu
1	COLORADO STATE U/Albertson
1	U CONNECTICUT/Scottron
2	CORNELL U
	1 Sears
	1 Aero Lab Appl Mech
1	HARVARD U/Birkhoff
2	U ILLINOIS
	1 Robertson
	1 College of Engr/Library
2	U IOWA OJR
	1 Kennedy
	1 Landweber
1	KANSAS ST U ENGR EXP/Nesmith
1	LEHIGH U FRITZ ENGR LAB/Library
1	U MARYLAND/Cunniff
4	MIT OCEAN ENGR
	1 Abkowitz
	1 Kerwin
	1 Leehey
	1 Mandel
1	MIT PARSONS LAB

Copies

3 U MICHIGAN NAME
- 1 Benford
- 1 Couch
- 1 Ogilvie

4 U MINNESOTA SAFHL
- 1 Song
- 1 Library
- 1 Wetzel
- 1 Silberman

1 NOTRE DAME/Standhagen

2 PENN STATE U
- 1 ARL
- 1 B. Parkin

1 ST JOHNS U Library

3 SWRI
- 1 Abramson
- 1 Bass III
- 1 Applied Mech Review

3 STANFORD U DEPT CIV ENGR
- 1 Perry
- 1 Street
- 1 Ashely

1 STANFORD RES INST LIB

3 SIT DAVIDSON LAB
- 1 Breslin
- 1 Tsakonas
- 1 Library

1 UTAH STATE U/Jeppson

2 WEBB INST
- 1 E. Lewis
- 1 L. Ward

1 VPI/G. Ryland

1 WPI ALDEN HYDR LAB LIB

1 SNAME

1 AEROJETGENERAL/Beckwith

1 BETHLEHEM STEEL
SPARROWS/A. Haff

Copies

12 BOEING AEROSPACE GROUP
- 1 H. Longfelder
- 1 R. Barbar
- 1 H. French
- 1 R. Hatte
- 1 R. Hubard
- 1 T. Marving
- 1 C. Ray
- 1 W. Rowe
- 1 F. Watson
- 1 D. Stark
- 1 D. Round

1 C LAB/F. Lane

1 DOUGLAS AIRCRAFT/Hess

1 GEN DYN ELEC BOAT/Boatwright

1 GIBBS & COX

4 GRUMMAN AEROSPACE
- 1 C. Pieroth
- 1 W. Carl
- 1 Wright
- 1 D. Postupack

3 HYDRONAUTICS
- 1 P. Eisenberg
- 1 M. Tulin
- 1 I.V. Johnson

4 LOCKHEED MISS & SPACE
- 1 R. Kramer
- 1 R. Lacy
- 1 R. Perkins
- 1 Waid

1 NEWPORT NEWS SHIPBUILDING LIB

1 OCEANICS/Kaplan

2 TETRA TECH, INC.
- 1 Dr. R. Wade
- 1 Dr. O. Furuya

2 WHEELER INDUSTRIES
- 1 E. Hoyt
- 1 J. Monk

CENTER DISTRIBUTION

Copies	Code	
1	11	W.M. Ellsworth
1	115	R.J. Johnson
1	1151	W.C. O'Neill
1	1152.1	D. White
1	1154	HYSTU
1	1103	V.K. Jones
1	15	W.E. Cummins
1	1500	J.B. Hadler
1	1502	V.J. Monacella
1	1505	S.F. Crump
1	1506	M.K. Ochi
1	1507	D. Cieslowski
20	152	R. Wermter
1	1521	P.C. Pien
1	1524	W.C. Lin
20	1524	Y.T. Shen
1	1532	G.F. Dobay
1	1532	H. Holling
1	1532	D. Gregory
1	154	W.B. Morgan
1	1542	B. Yim
1	1552	J.H. McCarthy, Jr.
1	1556	G.L. Santore
1	1556	P.K. Besh
1	1556	E. Rood, Jr.
1	1556	R. Rothblum
1	1562	M. Martin
1	1572	M. Ochi
1	1572	E. Zarnick
1	1572	C.M. Lee
1	156	G.R. Hagen
1	16	H.R. Chaplin
1	17	W.W. Murray
1	173	A. Stavovy
1	1730.3	W.H. Buckley
1	1730.5	J. Ma
1	1730.3	P. Yarnall
1	1730.3	D. Gill
1	18	G.H. Gleissnir
1	1966	Y.N. Liu
1	274	L.J. Argiro
1	2803	J.J. Kelly
1	2940	E. Screen
1	2940	A.P. Clark
30	5214.1	Reports Distribution
1	522.1	Library (C)
1	522.2	Library (A)

*U.S. GOVERNMENT PRINTING OFFICE: 1977 261-250/268 1-3

DTNSRDC ISSUES THREE TYPES OF REPORTS

1. DTNSRDC REPORTS, A FORMAL SERIES, CONTAIN INFORMATION OF PERMANENT TECHNICAL VALUE. THEY CARRY A CONSECUTIVE NUMERICAL IDENTIFICATION REGARDLESS OF THEIR CLASSIFICATION OR THE ORIGINATING DEPARTMENT.

2. DEPARTMENTAL REPORTS, A SEMIFORMAL SERIES, CONTAIN INFORMATION OF A PRELIMINARY, TEMPORARY, OR PROPRIETARY NATURE OR OF LIMITED INTEREST OR SIGNIFICANCE. THEY CARRY A DEPARTMENTAL ALPHANUMERICAL IDENTIFICATION.

3. TECHNICAL MEMORANDA, AN INFORMAL SERIES, CONTAIN TECHNICAL DOCUMENTATION OF LIMITED USE AND INTEREST. THEY ARE PRIMARILY WORKING PAPERS INTENDED FOR INTERNAL USE. THEY CARRY AN IDENTIFYING NUMBER WHICH INDICATES THEIR TYPE AND THE NUMERICAL CODE OF THE ORIGINATING DEPARTMENT. ANY DISTRIBUTION OUTSIDE DTNSRDC MUST BE APPROVED BY THE HEAD OF THE ORIGINATING DEPARTMENT ON A CASE-BY-CASE BASIS.